ESPOO 2003 VTT SYMPOSIUM 230

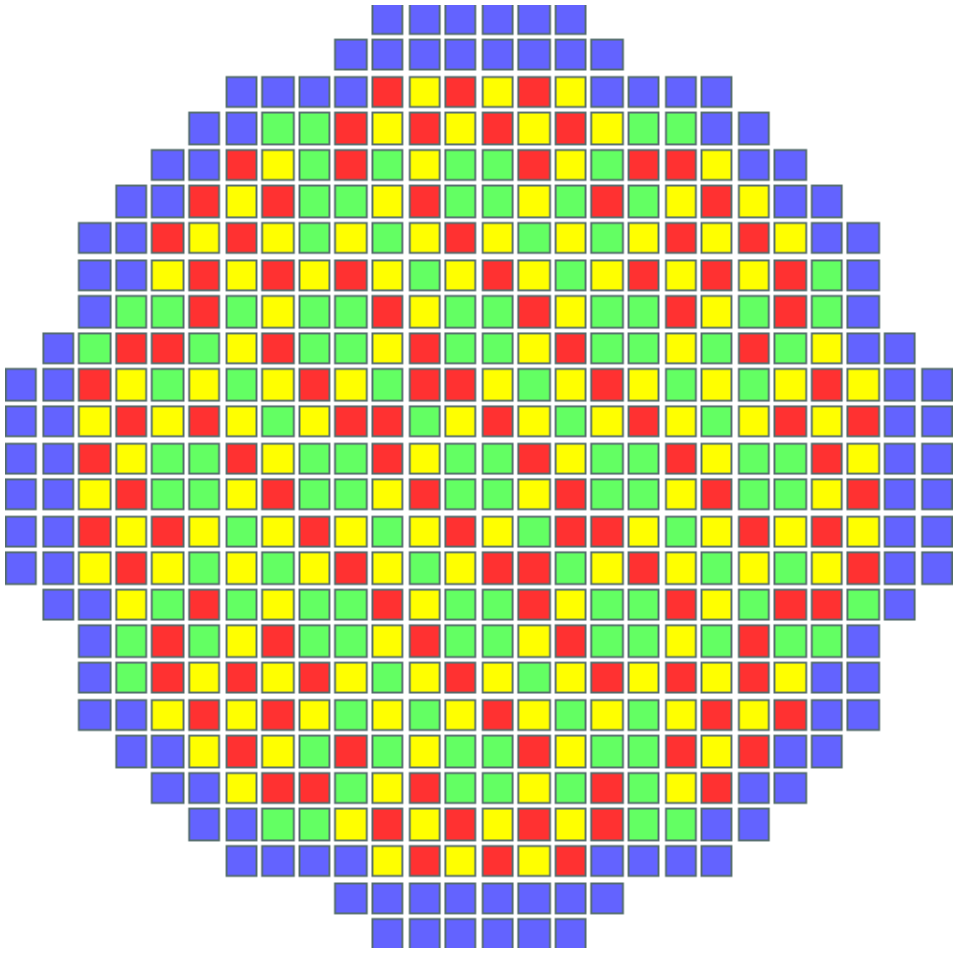

Reactor physics calculations in the Nordic countries

VTT SYMPOSIUM 230

Keywords:
nuclear waste transmutation, nuclear power safety,
reactor analyses, nuclear fuels, calculational methods

Reactor physics calculations in the Nordic countries

Proceedings of the 11th Nordic Reactor Physics Meeting

Helsinki, April 9–10, 2003

Edited by

Randolph Höglund

Organised by

VTT Processes

ISBN 951–38–6286–0 (URL:http://www.vtt.fi/inf/pdf/)
ISSN 1455–0873 (URL: http://www.vtt.fi/inf/pdf/)

JULKAISIJA – UTGIVARE – PUBLISHER

VTT, Vuorimiehentie 5, PL 2000, 02044 VTT
puh. vaihde (09) 4561, faksi 456 4374

VTT, Bergsmansvägen 5, PB 2000, 02044 VTT
tel. växel (09) 4561, fax 456 4374

VTT Technical Research Centre of Finland
Vuorimiehentie 5, P.O.Box 2000, FIN–02044 VTT, Finland
phone internat. + 358 9 4561, fax + 358 9 456 4374

VTT Prosessit, Tekniikantie 4 C, PL 1604, 02044 VTT
puh. vaihde (09) 4561, faksi (09) 456 5000

VTT Processer, Teknikvägen 4 C, PB 1604, 02044 VTT
tel. växel (09) 4561, fax (09) 456 5000

VTT Processes, Tekniikantie 4 C, P.O.Box 1604, FIN–02044 VTT, Finland
phone internat. + 358 9 4561, fax + 358 9 456 5000

Text preparing Arja Grahn

Otamedia Oy, Espoo 2003

Preface

The eleventh biennial meeting on reactor physics calculations in the Nordic countries was arranged by VTT Processes in Otaniemi, Espoo and on board Tallink's m/s Romantika on April 9–10, 2003. The previous meetings in this series were held in Göteborg 1983, Roskilde 1985, Espoo 1987, Oslo 1989, Stockholm 1991, Roskilde 1993, Espoo 1995, Kjeller 1997, Göteborg 1999 and Roskilde 2001. 18 technical papers on very different subjects in the field of reactor physics were presented by the 46 participants of 8 nationalities representing 13 organizations in 6 countries: research establishments, technical universities, utilities, consultants and suppliers. Thus, some participants from outside the Nordic countries were also present this time. Additionally, VTT's activities in the nuclear field and the "Finland-5" project were described.

General reactor physics, calculational methods, a code system adapted for RBMK reactor analyses, and transmutation of nuclear waste were presented by representatives of universities and programme developers (Royal Institute of Technology, Chalmers University of Technology, Studsvik Scandpower).

Computer programmes are the most important tools of reactor physics and new versions of old ones as well as entirely new ones based upon better and more accurate, alternatively faster and more efficient, methods and models are still evolving. At the meeting there were presentations of VTT Processes' new deterministic 3-dimensional radiation transport code MultiTrans and BWR simulator ARES based upon the AFEN (Analytic Function Expansion Nodal) model, and also of new features in internationally wellknown codes like CASMO-4E and POLCA (POLCA-T) together with results obtained by these programmes. A code for PWR loading pattern search, called LP-fun (Loading Patterns – for user´s need) is being developed by Westinghouse and others.

Experiments and measurements are necessary for the validation of the computer codes. Measurements on SVEA-96+ fuel bundles in the PROTEUS facility had been analyzed with the PHOENIX4 code, reactor scram experiments in the Loviisa and Mochovce VVER reactors using CASMO-4, MCNP4B and HEXTRAN, results of gamma scanning on fuel bundles by the PHOENIX4/POLCA7 combination. Some difficulties in predicting the power distribution in the reactor core with sufficiently good accuracy using any of the available code systems were reported by OKG.

The importance of direct heating, i.e. transfer of fission energy to non-fuel regions by gamma radiation and neutrons had been investigated using the HELIOS lattice code. Calculational results for heat deposition from gamma radiation in the moderator tank of the Forsmark-1 reactor were reported by Risø. Measurements and calculations of the pressure vessel exposure to neutrons have been performed by VTT during the whole life of the Loviisa reactors.

New and more efficient nuclear fuels are continuously being developed. Successful introduction of a new fuel type requires extensive numerical analyses as well as experimental measurements and feedback from users' experiences. Framatome ANP and Westinghouse described the development and characteristics of the SVEA-96 Optima and ATRIUM 10 fuels.

The twelfth meeting in the series is preliminary scheduled to be arranged by Institutt for energiteknikk and Studsvik Scandpower AS in Norway in 2005.

Randolph Höglund

Contents

On the average chord length

N. G. Sjöstrand
Department of Reactor Physics
Chalmers University of Technology
SE–41296 Göteborg, Sweden
Email: nils@nephy.chalmers.se Fax: +46 31 772 3079

Abstract

A recent discussion on the definition of the average chord length in a convex body is summarized. It is shown that an unclear formulation in the early derivation of it may lead to misunderstandings.

On the average chord length

The average chord length in a convex body is a fundamental concept in reactor physics. It gives an estimate of how long distances particles travel in the body. Over the years it has been used in many connections, e.g. in collision theory and in the evaluation of detector disturbances. The concept is closely related to the escape probability of a particle from a body. Recently, it came up in the interpretation of measurements of localized absorbers, see Drozdowicz *et al.* (2001 a and b).

It is customary to use a beautiful general formula by Dirac (1943), which gives the average chord length, R_{av}, of a convex body as

$$R_{av} = \frac{4V}{S} \tag{1}$$

where V is the volume and S the surface of the body. From it follows that the average chord length for a sphere with radius a is $4a/3$ and for an infinite slab with thickness d is $2d$. A derivation of the formula has been given by Case *et al.* (1953). In this deviation it is assumed that the number of chords in a given direction is proportional to the cosine of the angle, θ, between the inner surface normal and the chord direction. No motivation for this assumption is given. Also in a dozen other references (see Sjöstrand, 2002) there is no discussion of the background of Eq. (1). This gave the author the idea not to weight with a cosine in the calculation of the average chord length. With this assumption the average chord length for a sphere is equal to its radius, a, which is in contrast to the result $4a/3$ from Eq. (1). Since the shorter average chord length seemed to agree better with some experiments, a note was published on this (Sjöstrand, 2002).

However, Kruijf and Klosterman (2003) soon claimed that Eq. (1) is indeed correct. It seems that all depends on what is assumed regarding the incoming particles. We will illustrate this in the case of a sphere.

Consider a point source on the surface of the sphere with radius *a*, see Fig. 1. We assume that the particle flux is isotropic, i.e. that all chords within a certain solid angle dΩ at the angle θ with a fixed diameter are equally probable. The length of a chord is

$$s = 2a \cos \theta \tag{2}$$

The solid angle is

$$d\Omega = \frac{2\pi s \sin \theta \, s \, d\theta}{s^2} = 2\pi \sin \theta \, d\theta \tag{3}$$

The average chord length is then

$$R_{av} = \frac{\int_0^{\pi/2} s \, 2\pi \sin \theta \, d\theta}{\int_0^{\pi/2} 2\pi \sin \theta \, d\theta} = a \tag{4}$$

This does not agree with Eq. (1). However, we may like to normalize the number of incoming particles to those passing through a surface element. Then we use the particle current, which is obtained from the flux by multiplication with cos θ. In that case the average chord length will be

$$R_{av} = \frac{\int_0^{\pi/2} s \, 2\pi \sin \theta \cos \theta \, d\theta}{\int_0^{\pi/2} 2\pi \sin \theta \cos \theta \, d\theta} = \frac{4a}{3} \tag{5}$$

Thus, with normalization of the incoming particle current we obtain a result which agrees with Eq. (1). In a similar way it is easy to show that Eq. (1) is valid also for an infinite slab. This normalization is probably realistic in most cases. However, it is always necessary to know the assumptions underlying Eq. (1). In some special applications they may not be fulfilled.

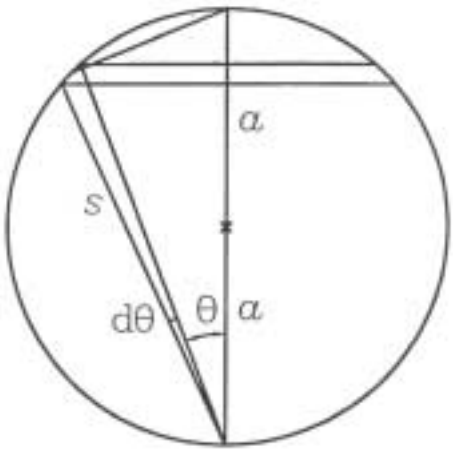

Figure 1. Notations for calculation of average chord length in sphere.

Acknowledgements

Discussion on this problem with Drs. K. Drozdowicz, I. Pázsit, D. C. Sahni and U. Woźnicka are gratefully acknowledged.

References

Case, K. M., de Hoffman, F. & Placzek, G. (1953). Introduction to the Theory of Neutron Diffusion. Los Alamos. P. 21.

Dirac, P. A. M. (1943). Approximate Rate of Neutron Multiplication for a Solid of Arbitrary Shape and Uniform Density. British Report MS-D-5, Part I.

Drozdowicz, K., Gabańska, B., Igielski, A., Krynicka, E. & Woźnicka, U. (2001a). A Pulsed Measurement of the Effective Thermal Neutron Absorption Cross-Section of a Heterogeneous Medium. Ann. Nucl. En. 28, 519.

Drozdowicz, K., Gabańska, B., Krynicka, E. & Woźnicka, U. (2001b). Influence of the Grain Size on the Effective Absorption Cross-Section of Thermal Neutrons in a Medium Containing Highly Absorbing Centres. Ann. Nucl. En. 28, 1485.

Kruijf, W. J. M. de & Klosterman, J. L. (2003). On the Average Chord Length in Reactor Physics. Ann. Nucl. En. 30, 549.

Sjöstrand, N. G. (2002). What is the Average Chord Length? Ann. Nucl. En. 29, 1607.

Reactor physics calculations and core analysis at the Nuclear Power Safety Division, KTH

Audrius Jasiulevicius
Nuclear Power Safety Division
Royal Institute of Technology
Stockholm, Sweden

Abstract

This paper provides a short overview of the recent research, carried out in the field of the reactor physics calculations and core analysis at the Nuclear Power Safety Division (NPS) of the Royal Institute of Technology in Stockholm, Sweden. The core analysis efforts presented here were directed towards the research of the RBMK-1500 type reactors, the research topic that was pursued at the NPS for the last several years under a contract with the Swedish International Projects. At the present the project is in the final stages of the development and the main achievements and results are the topic of this Paper.

1. Introduction

The RBMK reactors are channel type, water-cooled and graphite moderated reactors. The first RBMK type electricity production reactor was put on-line in 1973. Currently there are 13 operating reactors of this type. Two of the RBMK-1500 reactors are at the Ignalina NPP in Lithuania.

The aim of the project at NPS was to develop an independent RBMK-1500 core calculation methodology and tools. First of all, the neutron cross section data was generated using HELIOS code. The cross section data was verified during the Critical Experiment calculations. Later on, the 3-D neutronics calculations of the RBMK-1500 reactor core were carried out using the CORETRAN code with both new HELIOS code generated cross section library and previously used library, generated with WIMS-D4 code. The CORETRAN calculation results were benchmarked against the results of the Russian code STEPAN, which is commonly used in routine RBMK-1500 calculations. The CORETRAN results were also verified against the available experimental results for hot and cold zero power reactor conditions. The final stage of the development was to integrate thermal hydraulics calculations, carried out with 6-equation thermal hydraulic code VIPRE02 into the CORETRAN code. Additional CHF correlations were implemented into the VIPRE02 code in order to provide the correct CHF predictions for RBMK-1500 reactor fuel assembly.

2. Description of methodology

2.1. Overview of RBMK-1500 reactor neutron dynamics calculation methodologies

The RBMK reactor physics calculations, performed in Russia are similar to those performed for light water reactors (LWR's) in the West. The two group neutron cross section libraries are generated with the WIMS-D4 code, where the various cross sections are represented as a function of fuel and graphite temperatures, fuel burn up, Xenon-135 concentration and coolant density. A homogenized cell model is used, having reflecting boundary conditions for a many group one – dimensional or two – dimensional neutron transport equation solution. The spectrum obtained is then employed to collapse the many group cross-sections to 2 group cross sections. The more recent calculations are also carried out employing Monte Carlo codes MCNP and MCU calculations.

For reactor core calculations there are two Russian codes available. The Kurchatov Institute (KI) uses the STEPAN code. The STEPAN code solves two-energy group diffusion equation in two or three – dimensional geometry. The equations are solved by either the finite-difference scheme or by using nodal approximation. The STEPAN code is coupled with KOBRA thermal hydraulic code to obtain the transient thermal hydraulic feedback or with KONTUR code for the steady state thermal hydraulic feedback. The Russian Research and Development Institute of Power Engineering (RDIPE) has developed the SADCO code, which is similar to the STEPAN code, and it also employs the 2 group cross section libraries generated with the WIMS code.

The combinations of both the STEPAN – WIMS and the SADCO – WIMS codes in general are not able to predict accurately the measured radial power distribution in the INPP. Modifications are made in the cross sections to obtain better fits to the measured power distributions. The STEPAN code changes the thermal cross sections for some assemblies while the SADCO code changes the assembly burnups, which change the cross sections for both groups, and also the axial positions of control rods. The correction procedures employed by these two codes, are not documented and lack transparency.

Some Western codes, e.g. German QUABOX/CUBBOX 3D neutronics code coupled with ATHLET thermal – hydraulic codes are also used for the RBMK reactor analysis. WIMS code generated cross section data are employed for the QUABOX/CUBBOX calculations. Recently, RELAP-3D code is also employed for RBMK reactor calculations.

2.2. Methodology developed at NPS

An independent methodology is recently being developed at Royal Institute of Technology, Division of Nuclear Power Safety (NPS). The methodology employs Western computer codes for the RBMK reactor calculations. The two group neutron cross sections are

calculated using the HELIOS code, where exact geometry of the various assemblies is employed. The core neutron dynamics calculations are performed using the CORETRAN code, which employs neutron cross sections generated with HELIOS code. No corrections are made to the two group cross sections generated with the HELIOS code.

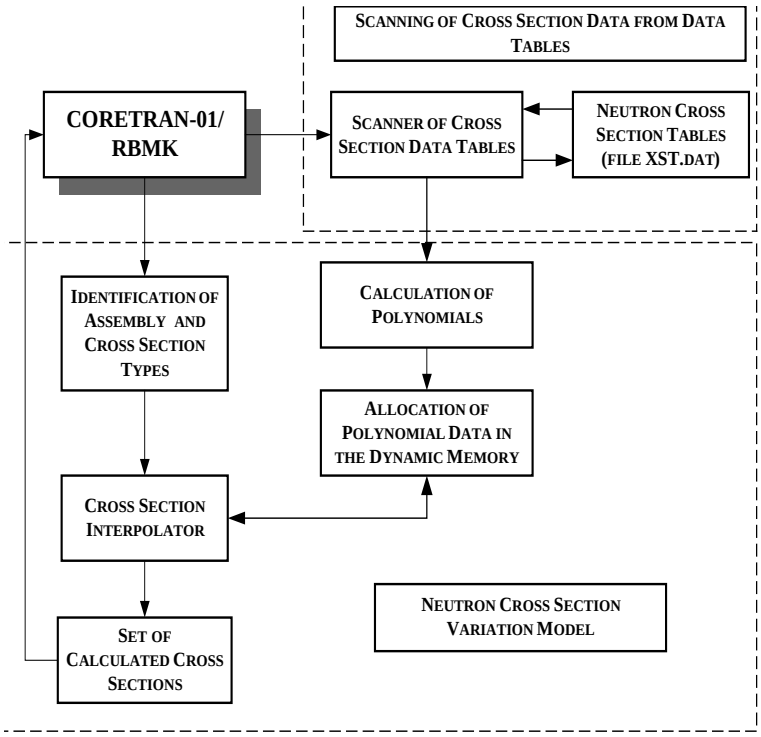

Figure 1. Cross section variation model for RBMK assemblies.

The neutron cross-section variation model for the RBMK applications is based on the logic shown in the Figure 1. The CORETRAN code reads a file with HELIOS code calculated 2 group neutron cross-section data, recorded in the form of tables and performs computation of 2D polynomial coefficients. The coefficients are allocated in the dynamic computer memory during the time of CORETRAN calculations and are directly accessed each time when a recalculation of each cross section is performed during the transient computations. The polynomial coefficients define 2D functions for each cross - section (XS) of each assembly type. These 2D functions are used to calculate basic components in the XS variation model. The basic components are calculated by running special interpolation procedure, which performs interpolation by using polynomial coefficients. The thermal-hydraulic parameters computed in a respective calculation node by the CORETRAN code are considered as the reference points for the calculation of the time dependent cross sections. The basic components are summed up and the final change in cross sections is obtained.

3. HELIOS code calculations

Two types of models were developed for HELIOS calculations. The first model represents the fuel cell. During the calculation of cross sections the fuel cell is treated as a stand-alone cell with mirror boundary conditions. The different sets of cross sections are obtained by varying coolant density, fuel temperature and graphite temperature. A second model is developed to facilitate calculation of the cross sections for the non-fuel assemblies. The non-fuel cells do not contain source of neutrons; therefore, these cells have to be surrounded by 8 fuel cells (sources of neutrons). The macroscopic cross sections for non-fuel assemblies are calculated by extracting the non-fuel area and using neutron flux spectrum generated by surrounding fuel cells. Required collections of cross-sections are obtained by varying coolant density in the surrounding fuel channels, graphite temperature, and coolant density in the non-fuel channel. It should be noted that the graphite temperature is assumed to be uniform in the whole macro-cell and fuel burn up is fixed at 10MWd/kg.

The recent reactor units in the INPP are loaded with two main fuel types: 2.00% U-235 enriched fuel and 2.40% U-235 enriched fuel with 0.41% erbium as a burnable poison. Er is introduced to reduce the positive void reactivity coefficient, which is a specific feature of the RBMK reactors. In a near future there are plans to introduce 2.6% U-235 enriched fuel with additional 0.5 % of Er. This would help to reach even lower positive void reactivity coefficients and will allow increased burn up of the fuel in the reactor. The HELIOS neutron cross sections were generated for all of the types of fuel assemblies, which are present in the reactor. The HELIOS calculation results, presented in this paper were compared against those calculated using WIMS-D_4 code as well as the critical facility experiment calculations.

The main conclusions of the cross section data validation and verification are:

1. There is an acceptable level of agreement with the experimental data for the CORETRAN calculations, performed using HELIOS cross sections for criticality state calculations, control rod reactivity worths, fuel assembly reactivity worths, channel pipe efficiency, fuel channel and control rod imitators filling with coolant effects (for separate assemblies) and radial and axial neutron flux distribution measurements.

2. In the case of core voiding, system voiding, additional absorber channels voiding and control rod voiding experiments, the CORETRAN calculated effects with both HELIOS and WIMS cross section, are almost two times lower, than the experimental values. However, even for this case, calculations with HELIOS cross section sets provide a slightly better agreement. During the calculations, according to the recommendations in the experiment description, static reactivity calculations were carried out (i.e. reactivity was calculated as a difference between initial and final states of the experiment). The use of inverse point-kinetics in the reactivity

calculations may provide closer agreement with the measurements. However, the differences are too large to disappear.

3. In the general, cross section libraries prepared with the HELIOS provide a better 3D neutronics calculations results as compared to those with WIMS code; even though the WIMS cross sections have already been ‘corrected’ to better fit the experimental results.

4. The methodology, employed in the WIMS cross section library for the ‘cold’ reactor conditions provide large differences for the fuel and graphite temperature reactivity coefficients from the ‘hot’ reactor state calculations.

5. The ARROTA calculations (ARROTA code was CORETRAN code successor), performed using CASMO-4 generated cross sections for fuel cells and WIMS cross sections for where the biggest error between experimental and calculation results was noticed (e.g. for the various voiding effects) with cross sections generated from HELIOS and WIMS-D4 codes. Thus, no conclusion about suitability of the CASMO-4 code to generate adequate cross section sets can be drawn. Also, there is no possibility to generate cross sections for non-fuel cells, which is the main drawback of the CASMO-4 code.

4. CORETRAN code verification against RBMK-1500 experiments

The RBMK-1500 reactor calculations were carried out for cold and hot reactor conditions. Both series of steady state and transient calculations were carried out in order to assess the CORETRAN model for the wide range of the RBMK-1500 conditions. Two sets of neutron cross section data were used: neutron cross sections, calculated using HELIOS code and WIMS-D4 code generated cross sections. The HELIOS code generated data for RBMK-1500 were previously compared with WIMS-D4 generated data and validated against experimental results.

4.1. Cold reactor states

Some of the measurements of the RBMK reactor safety parameters are carried out during the reactor maintenance period, under the cold reactor conditions. One of the most important measurements in this phase is the reactor subcriticality under cold reactor conditions, after Xenon transient (i.e. about 120 hours after the reactor shutdown). These measurements are carried out on all RBMK type reactors at least once a year. The main safety requirement for these conditions is that the minimal reactor subcriticality remains

under 1% (or under 2% during the reactor outage). During these measurements, the control rod efficiency is measured also.

These cases were calculated with CORETRAN code using both HELIOS and WIMS-D4 code generated cross section data in order to compare the results of the calculation with the actual plant data.

4.2. Hot reactor states

A series of validation calculations were carried out in order to assess CORETRAN code calculation results for the hot reactor states (i.e. under parameters, similar to reactor operational conditions). The results of the calculations were compared to the data, recorded in the Ignalina NPP reactor database (recorded data for the reactor state for each day is available, where the sensor readings allow calculating actual radial and axial power distribution in the operating reactor. This data allows testing the existing model under operating reactor conditions). Also, CORETRAN code provided more realistic representation of the axial flux distribution (the double-humped shape of the curve), as well radial and axial peaking factors, as well as average deviations of the calculated results from the database data are provided.

Also, during the operation of the Ignalina NPP, at periodic intervals measurements of some important operational parameters, e.g. steam void coefficients are performed. A series of such calculations were performed at RIT, comparing results obtained with the CORETRAN code against data from both reactors at the Ignalina NPP (INPP-1 and INPP-2). The calculations using new HELIOS neutron cross section library were also compared against the same 3-D neutron kinetics calculations, but using cross section library, generated using WIMS-D4 code, which is already widely used in RBMK reactor applications, and against STEPAN code results. In most cases, the calculations, performed with new HELIOS cross-section library, give a better agreement with the experiment data. Here $\alpha_\varphi, \alpha_w, \alpha_t, \alpha_C, \Delta\rho_{MCC}, \Delta\rho_{CPS}$ are respectively the void coefficient, the power coefficient, the Doppler coefficient, the graphite temperature coefficient, the MMC voiding effect and the CPS voiding effect.

4.3. Transient calculations

Two examples of transient calculations are presented in this paper: spontaneous withdrawal of a control rod and Control and Protection System LOCA (loss of coolant accident). These transients represent two types of hypothetical accidents, which have to be analyzed also in the scope of the Safety Analysis Report (SAR) for the RBMK-1500 type reactor.

The RBMK-1500 Control and Protection System (CPS) is divided into 12 local zones. In each local zone, there are one automatic regulator (LAR) and two Emergency Shutdown

Rods (LAZ) rods. About 350 groups of detectors are in the reactor. Each group comprises of the 2 to 7 detectors.

Besides these detector groups, there are 3 groups of the out-of-core detectors, which monitor total reactor power. These detectors generate full reactor scram signal when the total change of the reactor power exceeds ~10 %. The control logic for the RBMK-1500 reactor control and protection system operation was coded into the CORETRAN. The spontaneous single control rod withdrawal transient allows us to evaluate the performance of the coded logic.

We have analyzed a spontaneous withdrawal of one control rod at the periphery of the core. For the reactor database, the core state of January 29, 2001 of the Ignalina NPP Unit-1 was chosen. The reactor was operating at 4156 MWth. The description of the calculated transient:

According to Figure 2, the control rod was fully withdrawn after about 15 seconds from the beginning of the transient. At approximately 7th second of the transient, AZ-3 control and protection signal was generated. This signal enables the 50% reduction of the reactor power. After about 37 seconds, new power level at 50% of the initial power was reached, and the further movement of the control rods stabilized the reactor at this level.

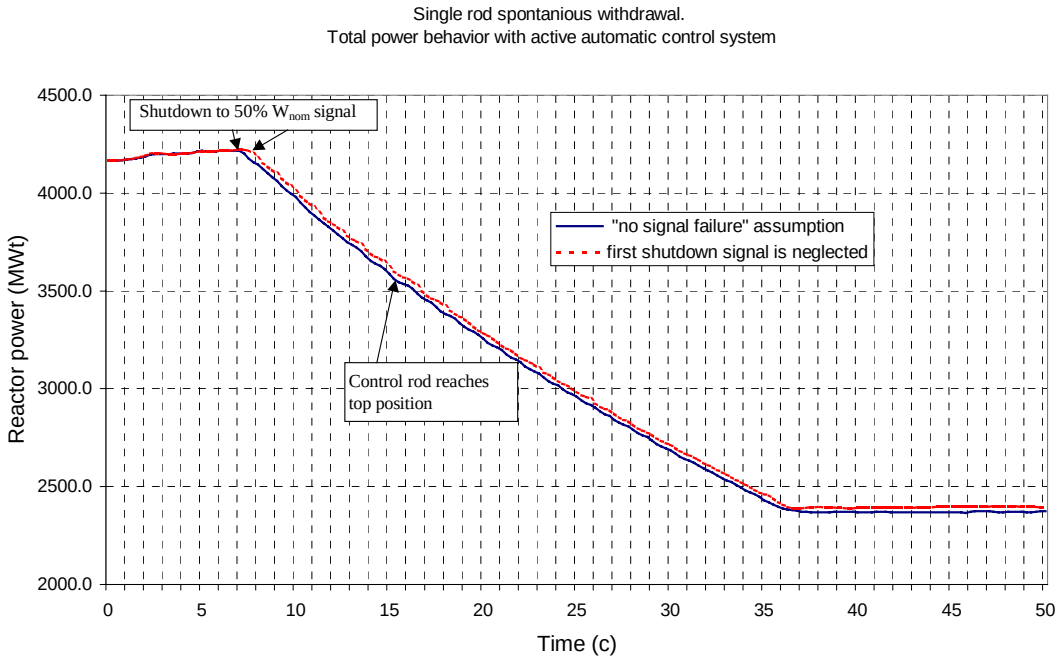

Figure 2. Reactor power behavior during CORETRAN calculation of spontaneous single control rod withdrawal.

All the process was calculated automatically, i.e. according the CPS logic, implemented into CORETRAN. CPS system ensured the stabilization of the reactor power at the new level of 50% (set-point values for the automatic regulation were automatically adjusted by the code for the new power level).

The calculations were repeated assuming ATWS (anticipated transient without scram) conditions. For this case, first shutdown signal, generated by the control and protection system was neglected. This led to the generation of a second CPS signal 0.5 sec later (Figure 2, red line). After the delay, the transient proceeded in a similar way as during the first case: the reactor power was reduced by 50% and stabilized at the new power level.

The Control and Protection System Loss of Coolant Accident (CPS LOCA) transient is considered to have the most positive reactivity input in the RBMK type reactors. Although the exact time, during which all the coolant is removed from the CPS system, is not defined, it is usually assumed that the CPS system water level reaches the bottom of the RBMK reactor core in about 45 seconds (assuming that at the time zero the CPS coolant was at the core top level in the control and protection system). However, no precise data about the exact duration of the transient and the conditions (e.g. the distribution of the flow rates in various parts of the core) are available.

During the CORETRAN calculations, the following assumptions were made:

- All CPS channels lose coolant at the same rate (i.e. the coolant level reduces with the same rate in all regions of the core)

- Technological set points, according to which the reactor scram signal is generated are neglected. The transient starts at time zero, i.e. the moment when coolant level in the CPS system reaches the top of the reactor core.

- LAC – LEP system is operating.

The CORETRAN calculation results are presented in the Figure 3.

The CORETRAN calculations were conducted using two sets of neutron cross section libraries: generated with HELIOS and generated with WIMS-D4 codes. During the transient, at about 17 second AZ-3 control and protection signal is generated. This signal empowers the reduction of the reactor power by 50% of the initial value. At about 50 seconds of the transient, the reactor power is stabilized at the new level. Further movement of control rods keeps the new reactor power level constant.

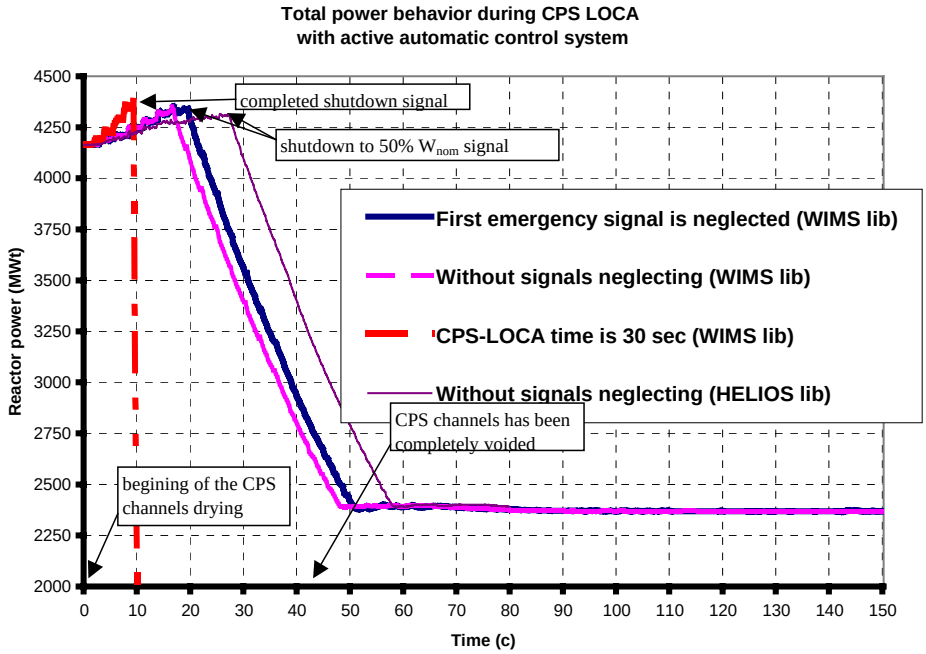

Figure 3. CORETRAN calculated reactor power during CPS LOCA transient.

The calculated case implies, that the control and protection system of the RBMK-1500 reactor is capable of handling even the transient with the most positive reactivity addition without having to scram the reactor. I.e. LAR and LAZ systems ensure the operation of the reactor at the reduced power level even after the coolant is no longer present in the control and protection system circuit.

The CORETRAN calculations were repeated employing both HELIOS and WIMS-D4 cross section data, assuming shorter loss of coolant time for the CPS circuit. It was assumed that the water level reaches the bottom of the reactor core at 30 seconds after the beginning of the transient (Figure 3). For this case, CORETARN calculations with WIMS cross section data predicted the occurrence of AZ-1 (full reactor scram signal) at about 10 seconds after the beginning of the transient, due to the CPS signal, initiated by the increase of the reactor power by more than 10%. The use of the HELIOS cross section date led to the delay in the generation of the emergency protection signal. This could be explained by the difference in the cross section data, generated with HELIOS and WIMS-D4 codes: HELIOS code predicts higher absorption cross sections for the control rods, which leads to higher ‘weights’ of the rods.

Analogous to the first transient, analyzed in this paper, the ATWS case for the CPS LOCA accident was also investigated. First signal, generated by the control and protection system was neglected during the CORETRAN calculations (Figure 3). This led to the delay of the system response by 2 seconds. Otherwise, the reactor power was stabilized at the new level of 50% initial power.

The main conclusion of the CORERTRAN code validation work are: As for the transient calculations, spontaneous withdrawal of one control rod and Control and Protection System Loss of Coolant Accident were simulated. The calculations were carried out using HELIOS and WIMS-D4 code generated neutron cross section libraries.

The cold and hot steady state calculations allowed carrying out the validation of the CORETRAN model for the RBMK-1500 reactor against the experimental reactor data. In general, CORETRAN code provides good agreement with the experimental results (and with STEPAN code calculations). CORETRAN code provides closer to experimental, values for the power coefficient, compared to the STEPAN code results.

Transient calculations showed, higher, than expected, level of performance of the RBMK-1500 reactor Control and Protection System: during both spontaneous withdrawal of one control rod and the CPS LOCA transient, the LAC and LEP control rods of the reactor proved to be capable of controlling these reactivity transients and reducing the power level to 50% in an orderly fashion. No full reactor shutdown was predicted.

5. Development of VIPRE02 code

VIPRE02 thermal hydraulic code is a part of CORETRAN-01 package. CORETRAN-01 is a detailed 3D core simulation program, capable of performing both core depletion and reactivity transient calculations. VIPRE02 code, incorporated in the CORETRAN-01, for thermal hydraulic analysis and the thermal hydraulic feed back to the neutronic analysis, contains 6 liquid and vapour equations for mass, energy and momentum variables. Homogeneous Equilibrium Model (HEM) could be used if desired. Method of Characteristics (MOC) numerics could also be employed as an option for e.g. BWR stability analysis. Both HEM and two-fluid models can be employed in the 3-D rod bundle subchannel analysis with estimation of cross flow across the lateral contact between subchannels.

Several CHF and CPR correlations are available in the VIPRE02 library. The CHF correlations include major vendor correlations published in 1970s-1980splus several correlations, which span over the wide range of both BWR and PWR operating parameters. Among these are Babcock & Wilcox, Westinghouse, Bowring, EPRI and other correlations. Also a capability is provided to incorporate into the code user – defined correlations into VIPRE02.

Additional CHF correlations, relevant to RBMK-1500 reactor geometry and parameters, were implemented into the VIPRE-02 code at the Nuclear Power Safety Division, Royal Institute of Technology. In total, four different correlations were added to the standard code version: Osmachkin correlation for lower assembly, which is a modification of the Mac Beth formula; RRC KI correlation for the upper assembly was included to take into account additional flow intensifiers, which are present in the upper fuel assembly; Khabenski

correlation, which was derived for the low mass fluxes in RBMK and VVER reactors. In addition to the four correlations above, a modification for the Osmachkin correlation was implemented in order to perform CHF calculations for cases, when the axial power distribution does not vary along the axis of the fuel assembly. In this case the use of the standard Osmachkin correlation results in zero value. The correlation was modified to allow the Osmachkin correlation predictions also for this case.

In order to facilitate the subchannel analysis, the experimental RBMK fuel channel was modeled as a set of 30 triangular and square subchannels with lateral connections (Figure 4). Flow intensifiers and fuel rod spacer grids were modeled at their axial locations in the RBMK-1500 fuel assemblies.

The implemented VIPRE02 model allows modeling of the lateral cross flows between subchannels, which take place in the fuel channel. This model is more sophisticated than the 1-D representation of the fuel channel used in most codes. The 3-D subchannel model allows predicting the non-uniformities of the fuel rod wall temperatures in the various locations of the channel.

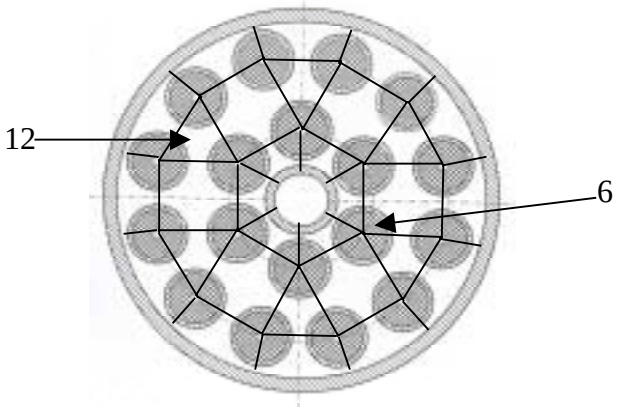

Figure 4. Cross section of the RBMK-1500 fuel channel model with VIPRE02.

The VIPRE02 code calculation results were compared to the experimental data from a single tube CHF experiments, performed at KTH (Sweden) and E-108 (Russia) test facilities and with the RBMK-1500 rod bundle CHF experiments, carried out at RRC KI (Russia).

The main conclusions are: EPRI CHF correlation, although provides erroneous results for single channel experiments (E-108 and RIT, Jasiulevicius and Sehgal, 2002), provides satisfactory agreement for the CHF for the multichannel fuel bundle model (RRC KI experiments). This correlation is recommended when performing RBMK-1000 thermal hydraulic analysis and also when performing CHF evaluation for the lower assemblies of RBMK-1500 fuel channels. For upper fuel assemblies of the RBMK-1500 RRC KI

correlation gives a good prediction for the critical heat flux. The accuracy of the correlation decreases with increasing liquid subcooling at the entrance of the fuel channel. Bowring CHF correlation, implemented in the standard VIPRE02 version, also provides a close agreement with the experimental results for the CHF for upper assemblies of RBMK-1500; the best agreement is obtained at higher values of the liquid subcooling at the entrance. For the nominal operational parameters (nominal inlet temperature), the Bowring correlation underpredicts (slightly) the values of CHF. Khabenski CHF correlation provides good estimation for the CHF only for low mass flow rates (up to about 1100 kg/m^2s).

6. Summary

A short overview of code development, validation and verification work, which has been carried out at the Nuclear Power Safety Division of the Royal Institute of Technology in Stockholm, Sweden, is given in the paper. The main conclusions obtained during the neutron cross section model development and validation, as well as 3-D reactor dynamics and thermal hydraulics analysis for RBMK-1500 reactor are also presented in this paper.

Comprehensive rehomogenisation

Sten-Örjan Lindahl
Studsvik Scandpower

Conventional core calculations and its shortcomings

Step 1: 2D Single Assy calc. => Σ_{α}^{Homog}, f_{side}

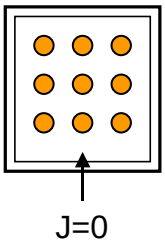

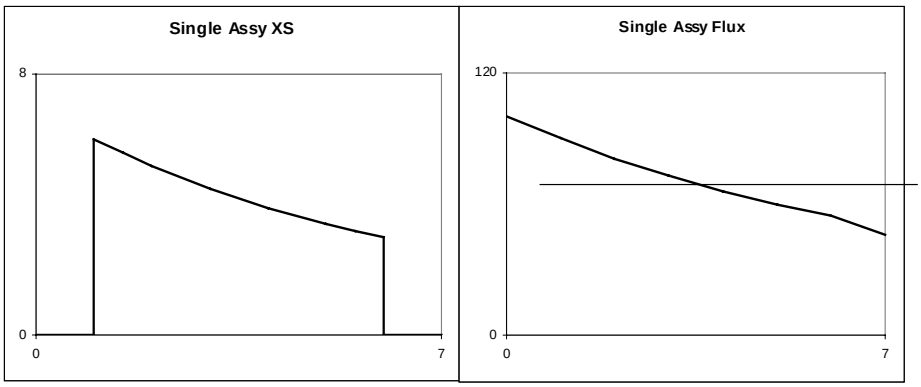

Homogenised cross sections: $$\Sigma_{\alpha}^{Homog} = \frac{\frac{1}{V}\int \Sigma_{\alpha}(r)\cdot\phi(r)\,dV}{\frac{1}{V}\int \phi(r)\,dV}$$

Discontinuity factors: $$f_{side} = \frac{\phi_{side}}{\varphi_{side}^{Homog.}}$$

Step 2: 3D Core Calculation – Perturbed XS distribution + Perturbed flux
Should give modified homogenised XS and disc. factors

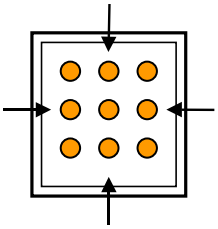

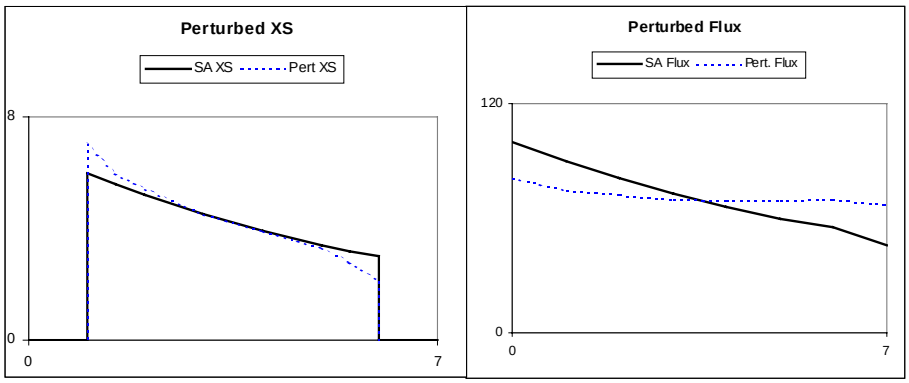

How is the problem handled today?

- Once $\Delta\Sigma_\alpha(r)$ is estimated =>

$$\Delta\Sigma_\alpha^{REHOM-1} = \frac{\int \Delta\Sigma_\alpha(r)\cdot\phi^{Hom}(r)dV}{\int \phi^{Hom}(r)dV}$$

- Once $\Delta\phi(r)$ is estimated =>

$$\Delta\Sigma_\alpha^{REHOM-2} = \frac{\int \Sigma_\alpha(r)\cdot\Delta\phi(r)dV}{\int \phi^{Hom}(r)dV}$$

- Discontinuity factors – Essentially never corrected

Proposed remedy

In 3D core calculations, recompute Σ^{Hom}, f based on known $J^{\mathrm{side}}(s)$ and $\Sigma(r) = \Sigma^{SA}(r) + \Delta\Sigma(r)$.

Step 1: Input from XS generator:

$$\Sigma_{\alpha}^{SA}(r) = \sum_{m=0}^{L}\sum_{n=0}^{L}\Sigma_{mn}^{SA}P_m(x)P_n(y)$$

Step 2: Input from 3D simulator:

$$\Delta\Sigma_{\alpha}(r) = \sum_{m=0}^{L}\sum_{n=0}^{L}\Delta\Sigma_{mn}P_m(x)P_n(y)$$

$$J^{Side}(s) = \sum_{m=0}^{L}J_m^{Side}P_m(s)$$

Step 3: Solve diffusion eqn using a variational method to estimate changes in flux caused by changes in cross sections and non-zero side net currents.

Step 4: Output to 3D simulator: Σ^{Rehom}, f^{Rehom}
Pin form functions

Test case BWR:

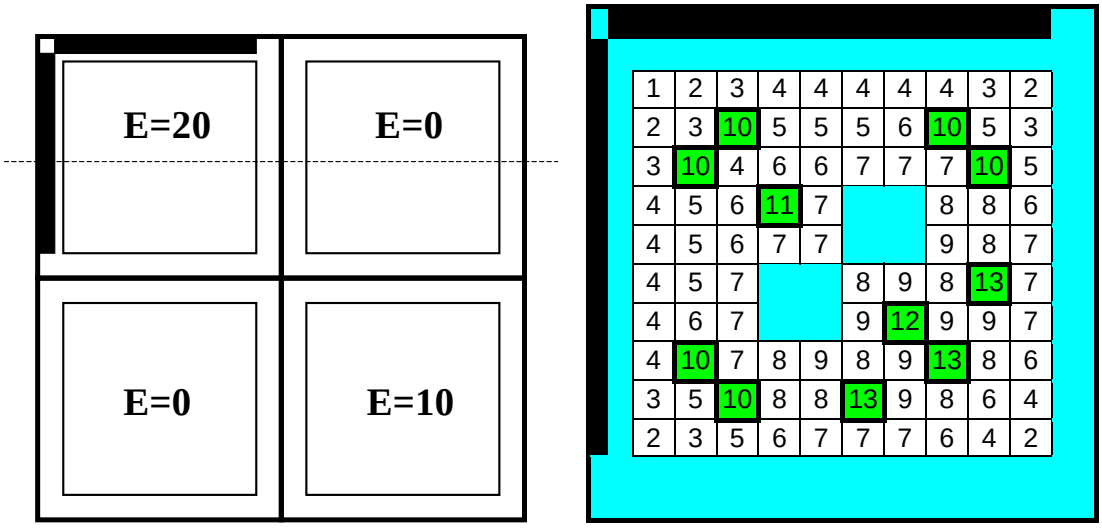

$\Delta\Sigma_{a2}(x,0)$

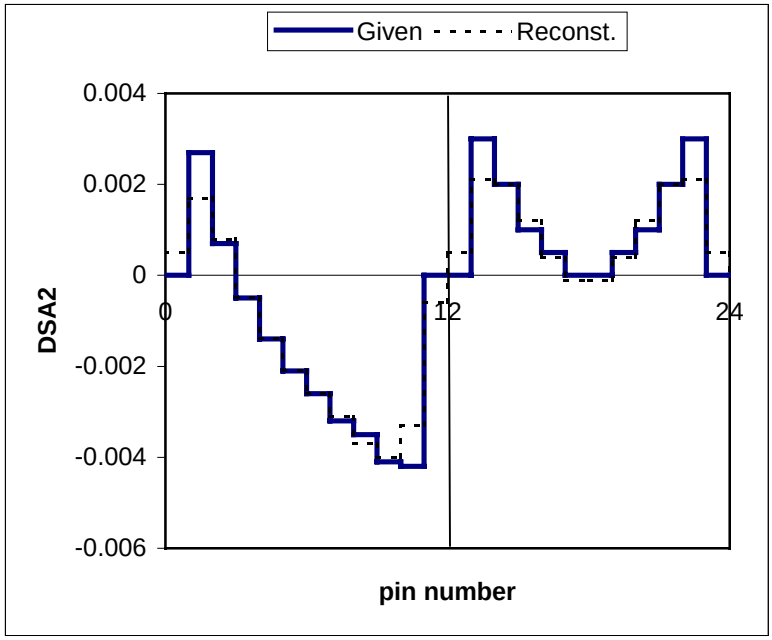

Test case PWR:

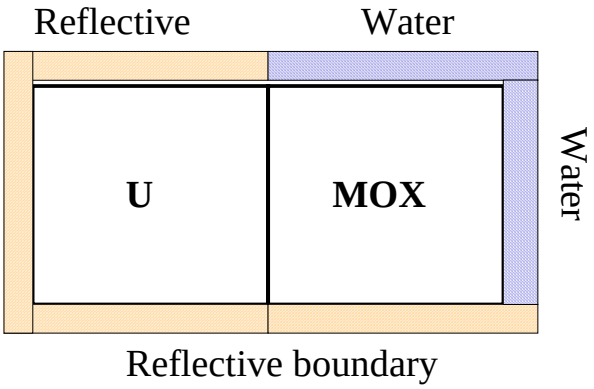

$\Delta\Sigma_{a2}(x,0)$

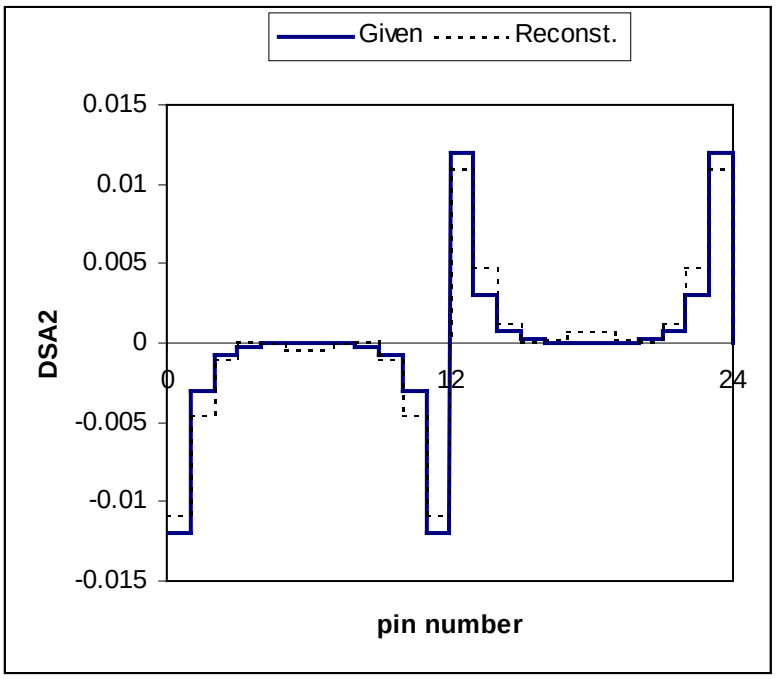

Test case calculations

Calculations are performed within the framework of 2-group diffusion theory

Reference solution generated by a high order diffusion code (LABAN)

Three sets of cases have been investigated:

1. Clean boundary condition perturb. ($J^{side} \neq 0, \quad \Delta\Sigma_\alpha = 0$)
2. Clean cross section perturbation ($J^{side} = 0, \quad \Delta\Sigma_\alpha \neq 0$)
3. Combined perturbations ($J^{side} \neq 0, \quad \Delta\Sigma_\alpha \neq 0$)

To be checked:

1. Error in k_{inf}
2. Max error for four sides of fast discontinuity factors
3. Max error for four sides of thermal discontinuity factors

BWR case – Accuracy as a function of expansion order L

Clean boundary condition perturbation

NW node	L	Dkinf pcm	DF1 max	DF2 max
	Uncorr.	-446	0.02	0.15
	2	-66	0.01	0.02
	3	-64	0.00	0.02
	4	95	0.00	0.01
	5	14	0.00	0.00
	6	-13	0.00	0.00

NE node	L	Dkinf pcm	DF1 max	DF2 max
	Uncorr.	-133	0.01	0.02
	2	38	0.00	0.07
	3	45	0.00	0.04
	4	59	0.00	0.01
	5	61	0.00	0.01
	6	10	0.00	0.00

Clean cross section perturbation

NW node	L	Dkinf pcm	DF1 max	DF2 max
	Uncorr.	-847	0.00	0.01
	2	383	0.00	0.01
	3	-35	0.00	0.00
	4	9	0.00	0.00
	5	10	0.00	0.00
	6	18	0.00	0.00

NE node	L	Dkinf pcm	DF1 max	DF2 max
	Uncorr.	-283	0.00	0.01
	2	-155	0.00	0.01
	3	-158	0.00	0.01
	4	36	0.00	0.00
	5	32	0.00	0.00
	6	23	0.00	0.00

Combined perturbations

NW node	L	Dkinf pcm	DF1 max	DF2 max
	Uncorr.	-1246	0.02	0.12
	2	366	0.01	0.02
	3	-114	0.00	0.01
	4	124	0.00	0.00
	5	19	0.00	0.00
	6	10	0.00	0.00

PWR case – Accuracy as a function of expansion order L

Clean boundary condition perturbation

East node	L	Dkinf pcm	DF1 max	DF2 max
	Uncorr.	-353	0.03	0.05
	2	-189	0.01	0.04
	3	-158	0.01	0.04
	4	-13	0.01	0.03
	5	-2	0.01	0.03
	6	-15	0.01	0.01

Clean cross section perturbation

West node	L	Dkinf pcm	DF1 max	DF2 max
	Uncorr.	-700	0.04	0.16
	2	-90	0.00	0.02
	3	-57	0.00	0.00
	4	-45	0.00	0.00
	5	-26	0.00	0.00
	6	-18	0.00	0.00

Accuracy of traditional homogenisation of cross sections

This conventional approach (based on the homogenised flux) is compared with the comprehensive method of this report.

Clean cross section perturbation.
Expansion order L=4.

BWR case

Node:	Uncorr. pcm	Conv. homog.	This report
NW	-847	-313	9
NE	-283	-195	36
SE	282	340	32

PWR case

Node:	Uncorr. pcm	Conv. homog.	This report
West	-700	-52	-45
East	-524	-360	-51

CASMO-4E and fuel storage rack calculations

Joel Rhodes, Nicholas Gheorghiu, Kord Smith & Malte Edenius

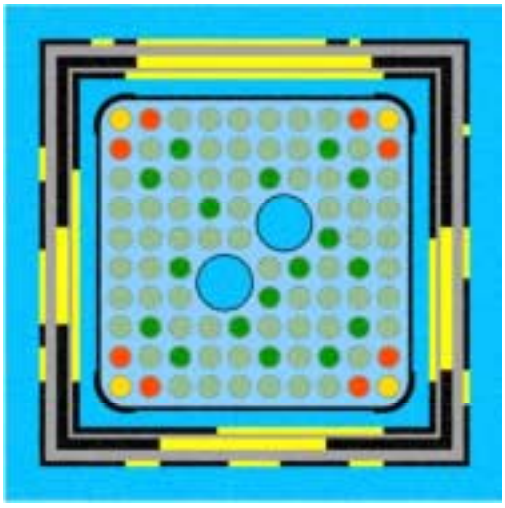

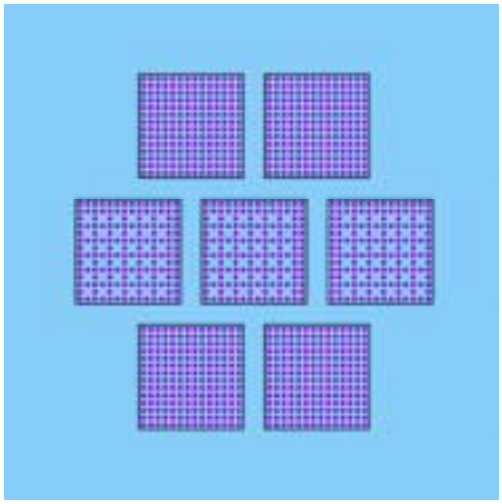

Outline

- Brief CASMO-4 / CASMO-4E overview
- Fuel storage rack benchmarking against critical and subcritical measurements

CASMO-4

Lattice Analysis

- Any BWR / PWR lattice design
  - Gd/B_4C/Pyrex/WABA/IFBA/Erbia
  - MOX, REU
  - Detailed heterogeneous 2D calculation
  - Simple fuel storage rack geometries
- Automated data bank generation

CASMO Experience

Country	Companies	BWRs	PWRs
England	1	0	0
Finland	3	2	0
Germany	5	6	13
Japan	9	21	18
Korea	1	0	12
Spain	2	1	2
Sweden	2	8	3
Switzerland	2	1	2
Taiwan	3	4	2
USA	23	32	51
Total	**51**	**75**	**103**
Cycles		**> 1500**	**> 2000**

CASMO-4E

Extended CASMO-4

- Libraries
  - JEF-2.2 and ENDF/B-6
  - 325 nuclides
  - Extended depletion chains
    200 fission products
    45 heavy nuclides
    Thorium depletion
- Geometric flexibility
  - Multi-assembly / **Full core calculations**
  - Extended fuel rack geometry
  - Hexagonal lattices
  - Cluster / Magnox / AGR
  - Azimuthal pin depletion
  - Fuel rod shuffling in between burnt assemblies

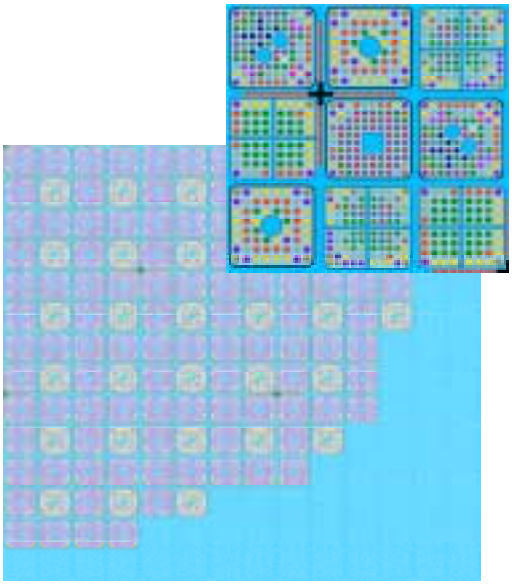

¼-Core BWR Geometry

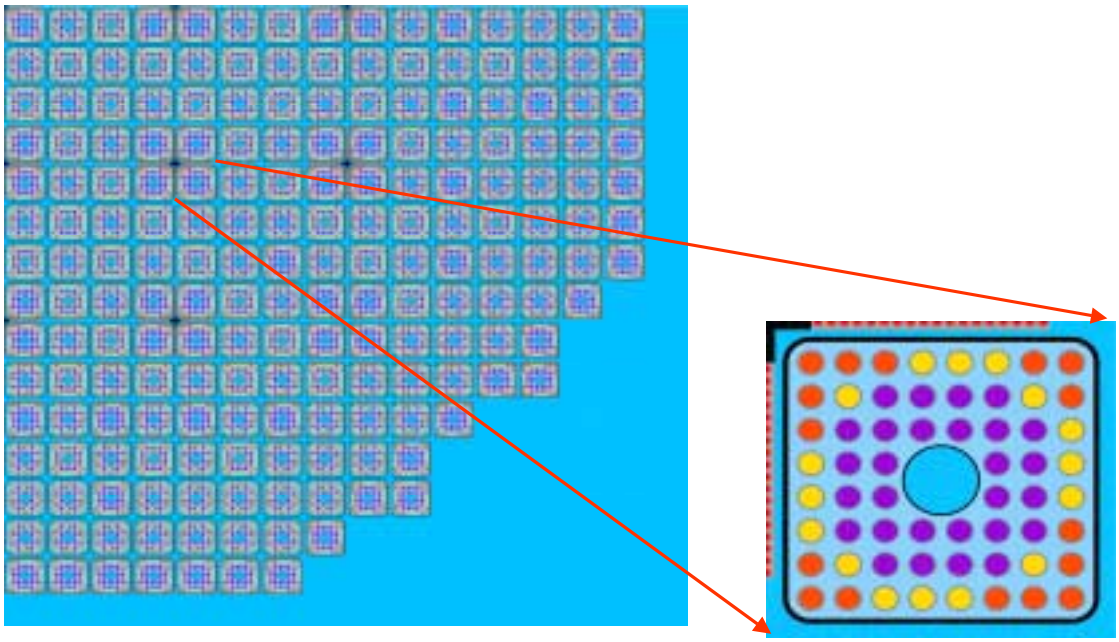

Physical to Computational Transformation

Physical geometry

Flat-flux geometry

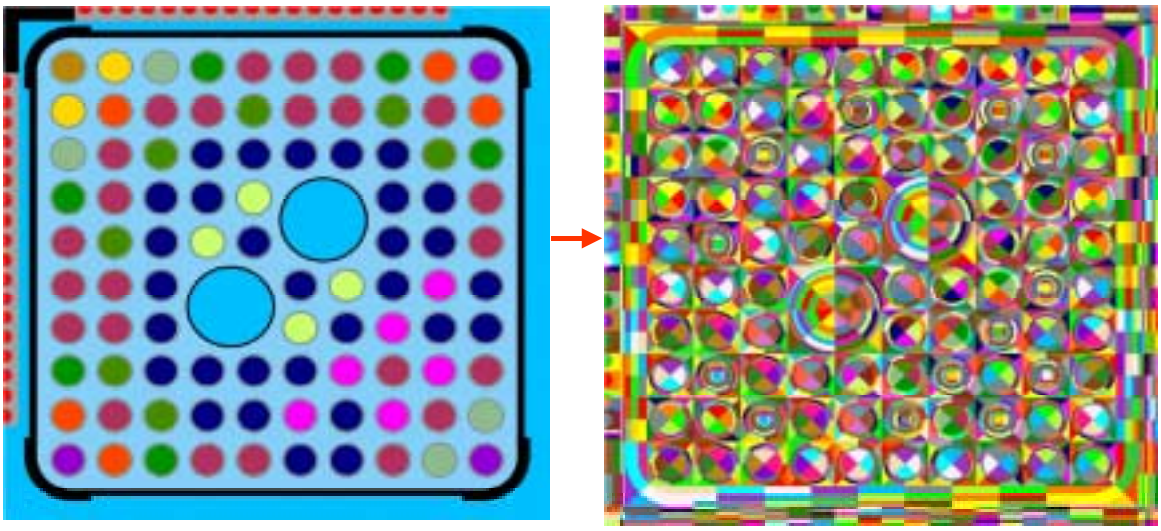

- Typical spatial resolution:
  - 1000 fuel assembly, reflector, and vessels volumes
  - 5000 scalar flux regions per assembly
- Typical angular resolution:
  - 64 azimuthal angles
  - 3 polar angles
- Typical energy resolution:
  - 16 energy groups
- Total angular flux unknowns: ~ 15 Billion (1.5×10^{10})

Features of CASMO-4E Rack Model

- Arbitrary number of slabs on each side of the segment
  Slabs subdivided into arbitrary lengths with unique compositions

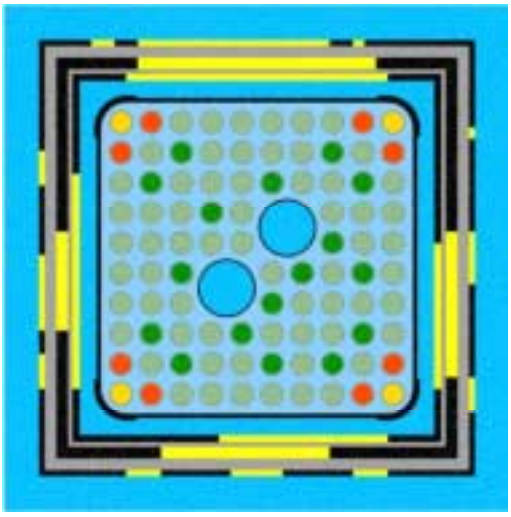

- Together with the CASMO-4E multi-segment (MxN) option, large complex geometries may be modeled in full spatial detail

- The 2D transport characteristics solution runs in:
  - Typically 40 energy groups
  - Fine spatial mesh both in flat source discretization and ray-spacing
  - Typically 25–80 million tracks

Rack Benchmarking

- Rack benchmarking against:
  - B&W Close-packed Storage Experiments (BAW-1484-7)
  - Critical experiments with Subcritical Clusters (PNL-3314)
  - Criticality experiments with Neutron Flux Traps (PNL-6205)
  - Fuel rods in Shipping Cask Geometry (PNL-6838)

- Three cross section libraries
  - J2 from JEF 2.2
  - E6 from ENDF/B-6, rev 5
  - L ENDF/B-4 based ‘production’ library

Babcock &Wilcox Close-packed Storage Experiments (BAW-1484-7)

16 critical experiments

Core I
Cylindrical array of 438 fuel pins

Cores II through X
Nine 14x14 assemblies in a 3 by 3 array with assemblies spaced varying distances apart

Cores XI through XXI
Stainless Steel or Boron-Aluminum sheets between assemblies

2.46% U-235 enriched UO_2, Pin pitch =1.636 cm,
Pellet radius = 0.515 cm, Fuel pin outer radius = 0.603 cm

Core I

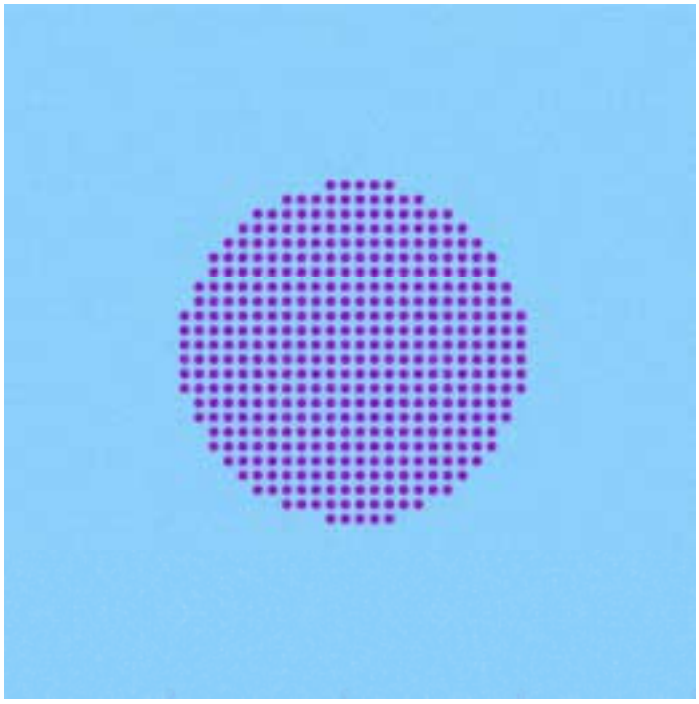

Cores III, IX and X (Various gaps)

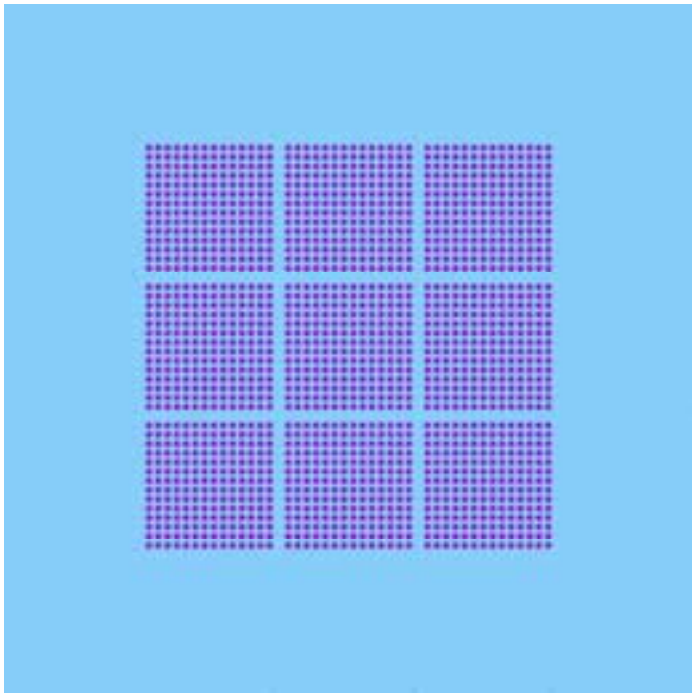

Cores XI through XXI (Various gaps)

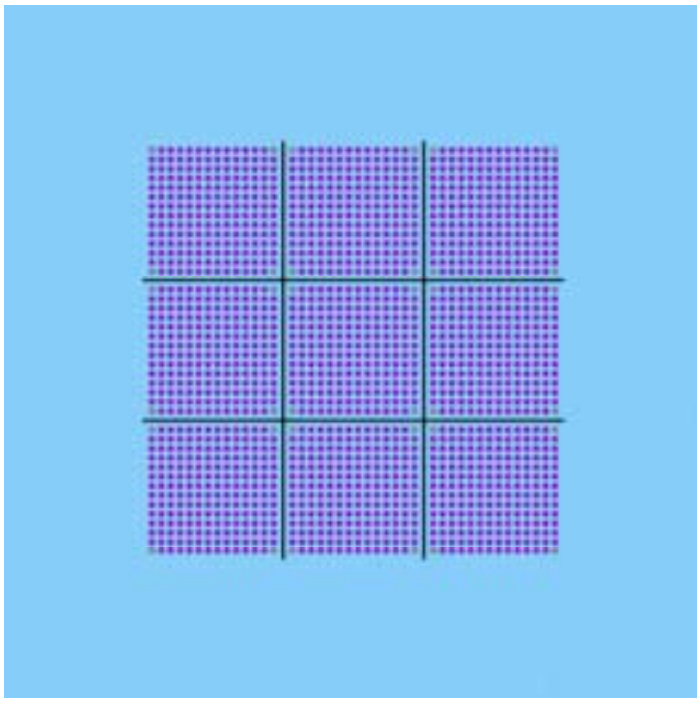

K-eff for B&W Criticals

Core	Boron (ppm)	Gap (cm)	Absorber Slab	KENO	C4E J2	C4E E6	C4E L
I	0	-	-	0.998	1.00441	1.00247	1.00124
II	1037	0	-	1.007	1.00398	1.00313	1.00128
III	764	1.63	-	0.999	1.00409	1.00328	1.00064
IX	0	6.52	-	0.987	1.00504	1.00403	1.00106
X	143	4.89	-	0.988	1.00510	1.00396	1.00100
XI	514	1.63	SS	1.015	1.00468	1.00396	1.00141
XII	217	3.26	SS	0.991	1.00413	1.00331	1.00064
XIII	15	1.63	1.614/Al	1.008	1.00186	1.00065	0.99895
XIV	92	1.63	1.257/Al	1.003	0.99848	0.99729	0.99553
XV	395	1.63	.401/Al	0.995	0.99468	0.99343	0.99138
XVI	121	3.26	.401/Al	0.990	0.99523	0.99530	0.99158
XVII	487	1.63	.242/Al	0.993	0.99873	0.99918	0.99526
XVIII	197	3.26	.242/Al	1.005	0.99858	0.99854	0.99475
XIX	634	1.63	.100/Al	0.991	1.00087	1.00150	0.99719
XX	320	3.26	.100/Al	0.997	1.00058	1.00059	0.99654
XXI	72	4.89	.100/Al	0.981	0.99934	0.99746	0.99507
			AVERAGE	0.997	1.00124	1.00004	0.99772
			STDEV	0.009	0.00346	0.00359	0.00352
			AVERAGE *)	0.997	1.00213	1.00096	0.99861
			STDEV *)	0.009	0.00263	0.00277	0.00272

*) Excluding cores XV and XVI

Critical Experiments with Clusters
(PNL-3314)

12 Critical Experiments

4.31% U-235 enriched UO_2 rods in water simulating LWR fuel shipping and storage configurations

Separation plates: Boron-Aluminum with various Boron loadings, Boroflex, Cadmium, Copper

Pin pitch = 1.892 cm, Pellet radius = 0.632 cm,
Fuel pin outer radius = 0.707 cm

Core 56
(No separation plates)

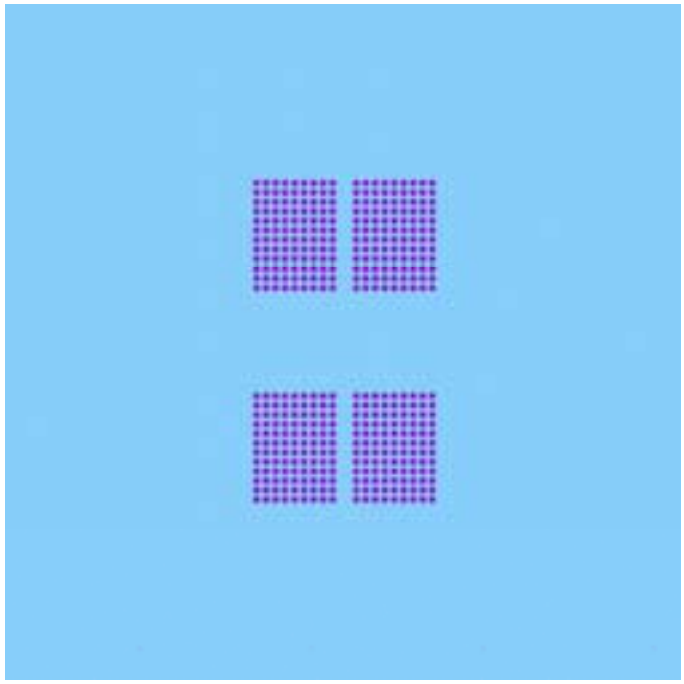

Cores 80 through 114

(Various spacing and number of fuel pins)

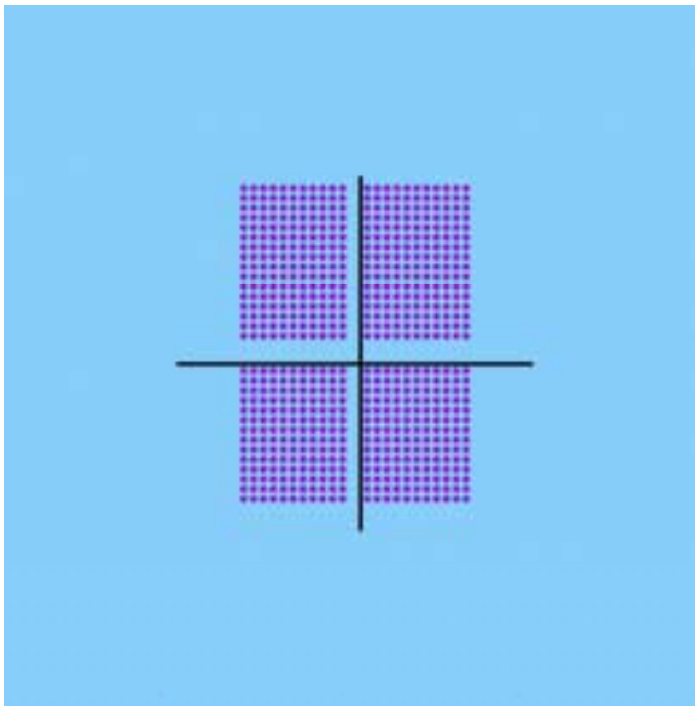

K-eff for PNL Criticals

Core	Sep. Plate	Gaps (cm) Xc / Yc	Fuel Rods Critical Size	C4E J2	C4E E6	C4E L
056	NONE	2.83 / 19.81	432	1.00569	1.00261	1.00089
080	Boral 28.7	2.83 / 4.80	660	1.00381	1.00072	0.99957
086	Boral 30.4	2.83 / 5.24	638	1.00206	0.99898	0.99792
088	Boral 30.4	2.83 / 3.17	616	1.00442	1.00145	1.00030
092	Boral 31.9	2.83 / 3.53	616	1.00423	1.00125	1.00014
096	Boroflex	2.83 / 3.60	616	1.00637	1.00339	1.00218
102	Cadmium	2.83 / 6.43	616	1.00504	1.00201	1.00113
103	Cadmium	2.83 / 5.30	594	1.00385	1.00087	0.99996
106	Boroflex	2.83 / 4.94	660	1.00582	1.00273	1.00153
109	Copper	2.83 / 10.21	468	1.00071	0.99855	0.99642
113	Copper	2.83 / 2.67	306	0.99749	0.99596	0.99260
114	Copper	2.83 / 3.47	324	0.99722	0.99579	0.99228
			AVERAGE	1.00306	1.00036	0.99874
			STDEV	0.00310	0.00253	0.00333
			AVERAGE *)	1.00459	1.00156	1.00040
			STDEV *)	0.00131	0.00132	0.00124

*) Excluding cores 109, 113 and 114

Criticality Experiments with Neutron Flux Traps (PNL-6205)

6 critical experiments

4.31% U-235 enriched UO_2 rods
Four clusters with max 256 rods in 16 x 16 arrays

Boron-Aluminum separation plates with different Boron loadings in the centre of the 4 fuel clusters

Pin pitch = 1.891 cm, Pellet radius = 0.632 cm,
Fuel pin outer radius = 0.707 cm

Cores with Neutron Flux Traps

Cores 226 and 227

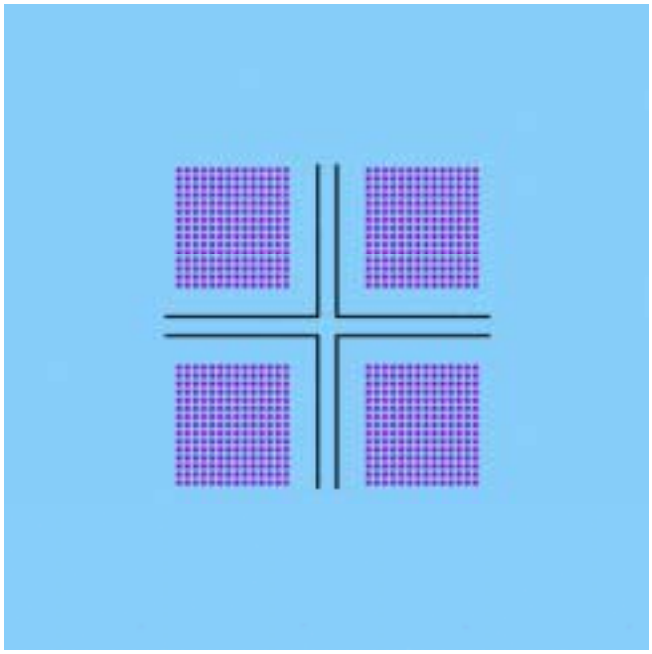

Cores with Neutron Flux Traps

Core 228

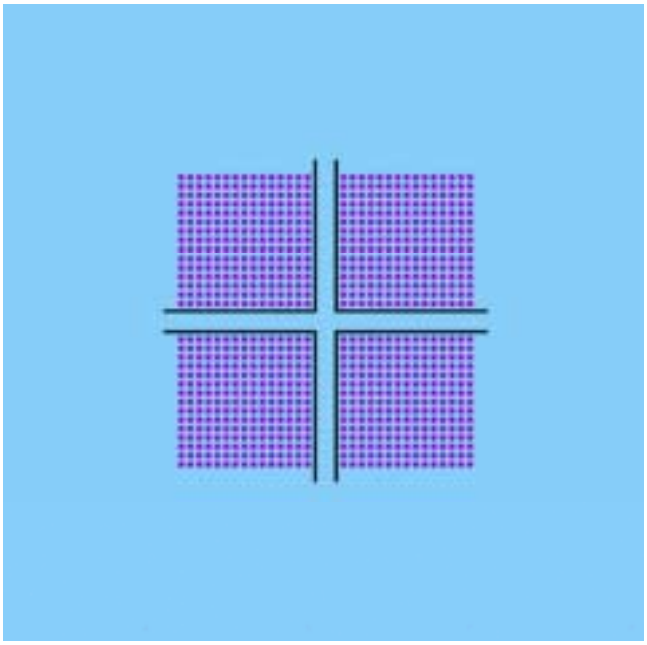

K-eff for Flux Trap Criticals

Core	Absorber Sheet	Trap Width (cm)	Fuel Rods	C3/S3	C4E J2	C4E E6	C4E L
226	Boral .45	3.71	840	0.99303	1.00522	1.00153	1.00094
227	Boral .13	3.76	840	0.99309	1.00580	1.00211	1.00152
228	Boral .13	3.76	900	1.00227	1.00245	0.99882	0.99851
229	Al	3.81	306	-	0.99253	0.98900	0.98619
230	Boral .05	3.75	855	1.00669	1.00563	1.00204	1.00164
231	Boral .45	3.71	960	1.00836	1.00784	1.00419	1.00376
			AVERAGE	-	1.00325	0.99961	0.99876
			STDEV	-	0.00553	0.00548	0.00638
			AVERAGE *)	1.00069	1.00539	1.00174	1.00127
			STDEV *)	0.00731	0.00193	0.00192	0.00188

*) Excluding core 229

Fuel Rods In Shipping Cask Geometry

(PNL-6838)

3 subcritical configurations

4.31% U-235 enriched UO_2 rods arranged in shipping cask geometry
Various number of fuel rods in each cluster (maximum 196 fuel rods in 14 x 14 arrays)

Each fuel cluster enclosed in 0.384 cm thick Boron-Aluminum sleeves

Pin pitch = 1.891 cm, Pellet radius = 0.632 cm,
Fuel pin outer radius = 0.707 cm

Shipping Cask Core Geometry

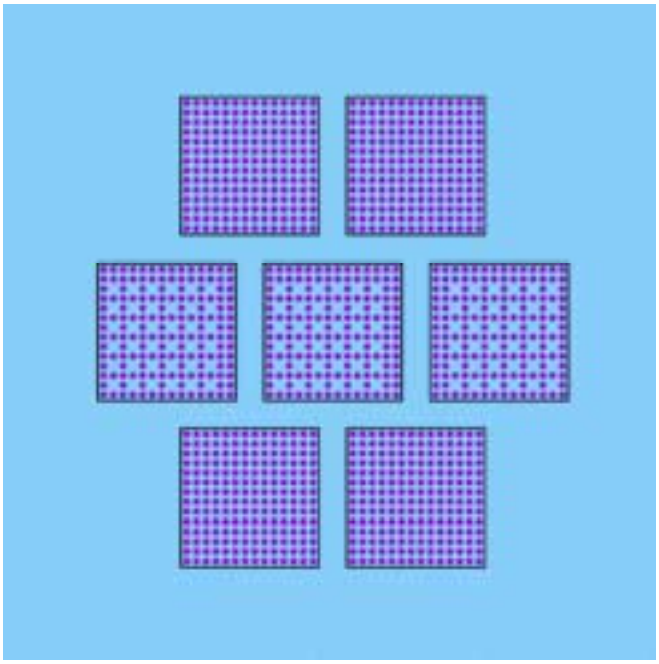

K-eff for Shipping Cask Subcriticals

Fuel Rods	C3/S3	C4E J2	C4E E6	C4E L	Measured GO	Measured GR
1264	0.888	0.90490	0.90154	0.90068	0.888	0.917
1329	0.883	0.89739	0.89384	0.89349	0.881	0.906
1372	0.867	0.87800	0.87399	0.87495	0.799	0.879

Measured GO: Gozani Method of Pulse Neutron Measurement
Measured GR: Gurelis-Russel Method of Pulse Neutron Measurement

Conclusions

- CASMO-4E extended rack model benchmarked against 37 experimental configurations
- k-eff shows good agreement with experiments
  No bias versus amount of absorber
  No bias versus gap widths between assemblies
- 8 and 40 group 2D solutions are very close
- All data libraries give approximately same accuracy

Development of the new deterministic 3-D radiation transport code MultiTrans

Petri Kotiluoto
VTT Processes
petri.kotiluoto@vtt.fi

MultiTrans

- A programme for radiation transport in arbitrary 3-D geometry.
- Based on the SP_3 approximation.
- Utilises efficient tree multigrid technique.
- The calculation grid is generated directly from stereolitography-files, offering an easy CAD-interface.

Tree multigrid (TMG) technique

- The multigrid method is *the most efficient way* to solve elliptic problems: the number of iterations required is directly comparable to the number of grid points *N*. The basic idea of the multigrid method is to approximate the problem on coarser grids, and to accelerate the iteration procedure by transferring data from coarser grids to finer grids, and backwards.
- In the tree multigrid technique, self adaptive features of the grid generating procedure are utilised. That is, the grid is *automatically refined* at material surfaces or from computational demand. In three dimensions the obtained tree multigrid is often called an *octree grid*.
- With the tree-structure, memory is saved and problems can be solved with even lower computational costs (number of grid points *N* is considerably smaller compared to uniform grids).

Octree grid generating routines with CAD interface

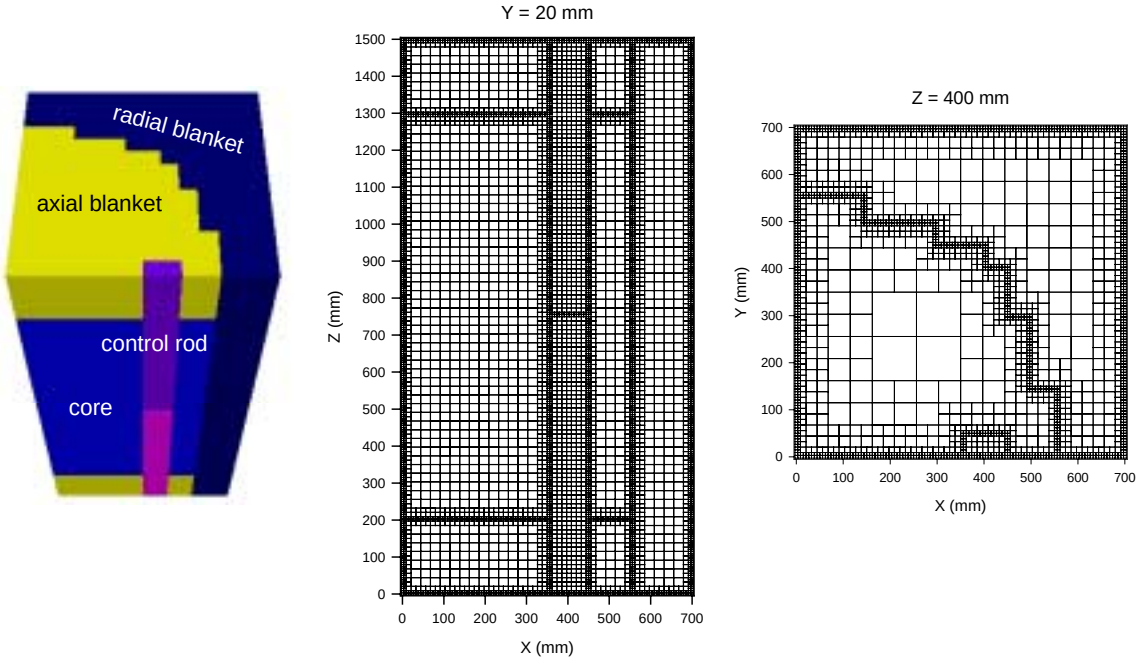

Octree grid generating routines with CT interface

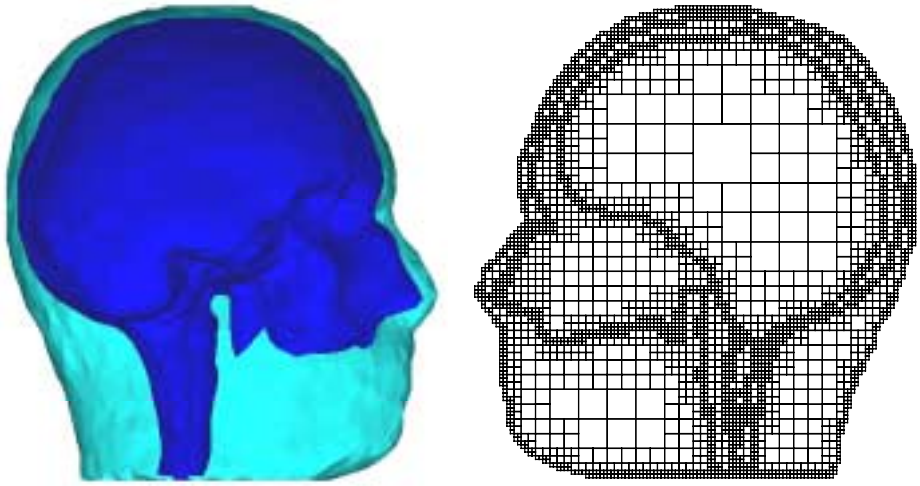

SP_3 approximation for radiation transport

- Simplified P_N (SP_N) approximations were first introduced by Gelbard in early 60's by simply replacing the derivative in one-dimensional P_N equations by a multi-dimensional Laplace operator. Despite the promising numerical results obtained by these SP_N approximations, equations did not gain popularity due to the lack of theoretical background.

- Only recently Brantley and Larsen (*Nucl. Sci. Eng.* **134**, 2000) derived the SP_3 approximation with boundary conditions from the variational principle for inhomogeneous medium with multi-group anisotropic scattering.

- For homogeneous medium, P_3 equations can be reduced to SP_3 equations. Also for inhomogeneous medium, SP_1 equations are congruent with P_1 diffusion theory.

Simplified P_3 (SP_3) equations

$$\hat{\Phi}_0(\vec{r}) \equiv \Phi_0(\vec{r}) + 2\Phi_2(\vec{r}) \;,\quad D_0^{i,g} = \frac{1}{3\sigma_{a1}^{i,g}} \;,\; D_2^{i,g} = \frac{9}{35\sigma_{a3}^{i,g}}$$

$$-D_0^{i,g}\nabla^2\hat{\Phi}_0^g(\vec{r}) + \sigma_{a0}^{i,g}\hat{\Phi}_0^g(\vec{r}) = 2\sigma_{a0}^{i,g}\Phi_2^g(\vec{r}) + S^i(\vec{r})$$

$$-D_2^{i,g}\nabla^2\Phi_2^g(\vec{r}) + \sigma_{a2}^{i,g}\Phi_2^g(\vec{r}) = \frac{2}{5}\left\{\sigma_{a0}^{i,g}\left[\hat{\Phi}_0^g(\vec{r}) - 2\Phi_2^g(\vec{r})\right] - S^i(\vec{r})\right\}$$

PMMA dosimetry benchmark, BNCT

Polymethyl-methacrylate
Diameter: 20 cm
Length: 24 cm

Beam aperture
diameter: 14 cm

^{55}Mn(n,γ) reaction rate in PMMA phantom

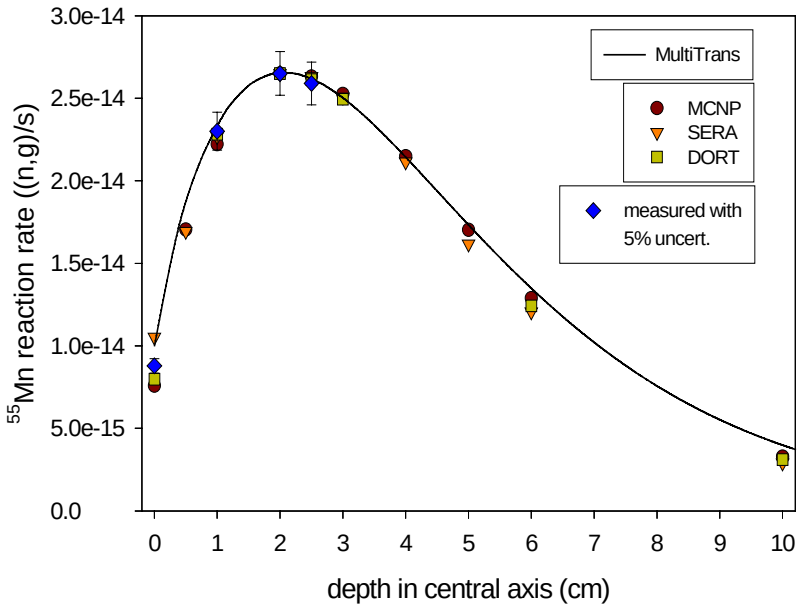

All the results have been scaled to measured ^{55}Mn(n,γ) reaction rate in 2 cm depth in central axis of the PMMA phantom.

The scaling factors for DORT, MCNP, SERA, and MultiTrans were 0.92, 1.00, 0.96, and 0.98, respectively.

^{197}Au(n,γ) reaction rate in PMMA phantom

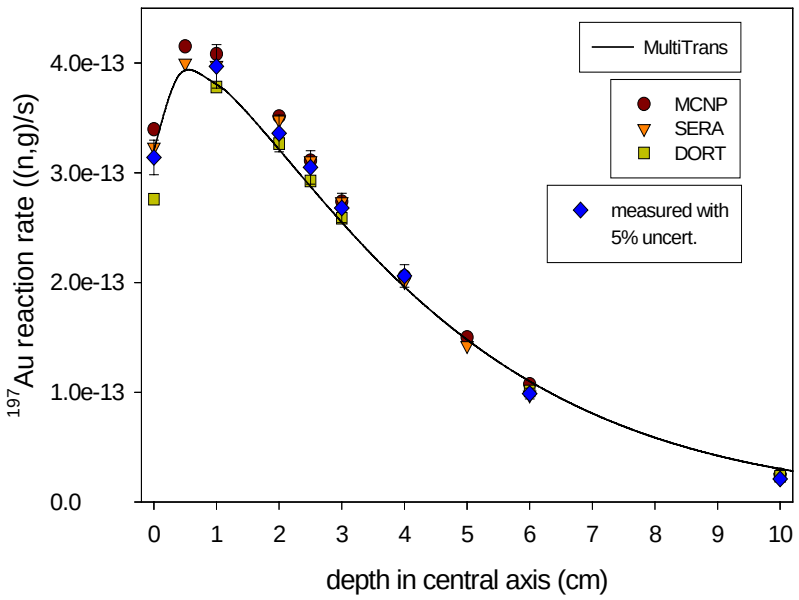

All the results have been scaled to measured ^{55}Mn(n,γ) reaction rate in 2 cm depth in central axis of the PMMA phantom.

The scaling factors for DORT, MCNP, SERA, and MultiTrans were 0.92, 1.00, 0.96, and 0.98, respectively.

Neutron spectrum in different depths in PMMA phantom

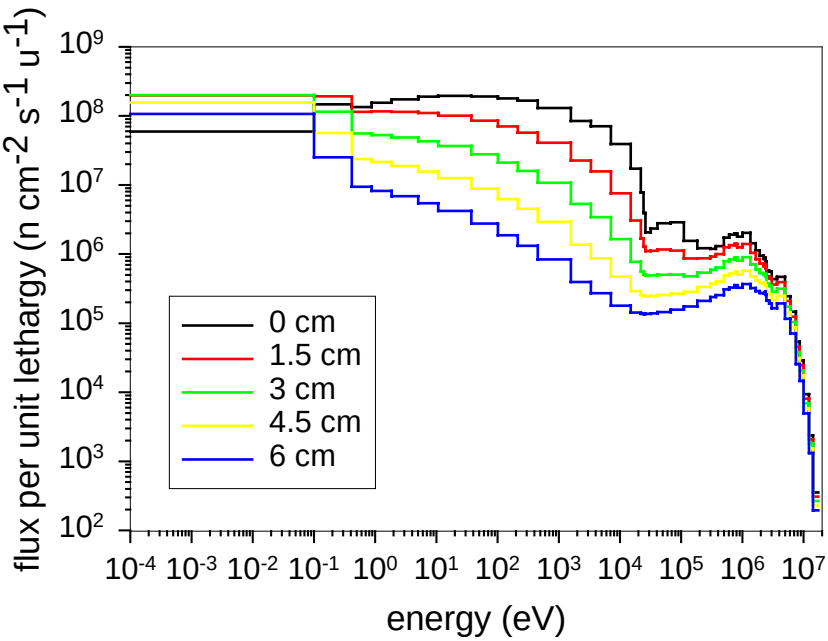

LWR benchmark

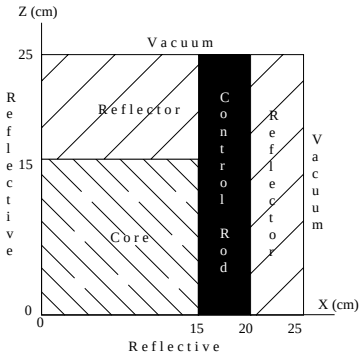

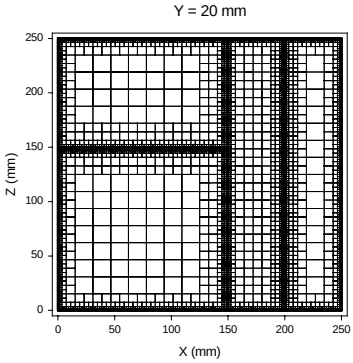

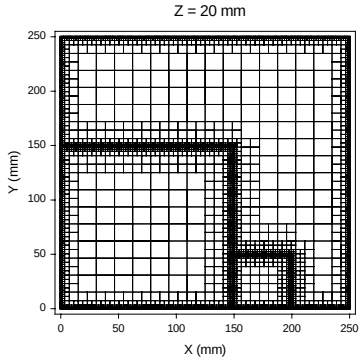

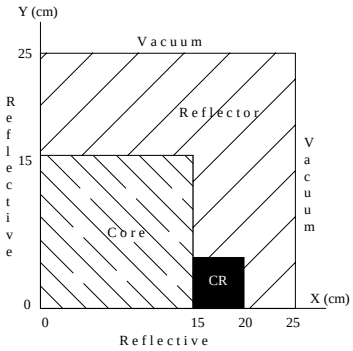

Method	Case1	Case2	Control Rod Worth
Exact Monte Carlo †	0.9780	0.9624	1.66×10^{-2}
MultiTrans SP_3	0.9521	0.9647	-1.37×10^{-2}

†Takeda & Ikeda, NEACRP-L-330 (1991)

FBR benchmark

Method	Case1	Case2	Control Rod Worth
Exact Monte Carlo †	0.9732	0.9594	1.47×10^{-2}
MultiTrans SP_3	0.9768	0.9625	1.52×10^{-2}

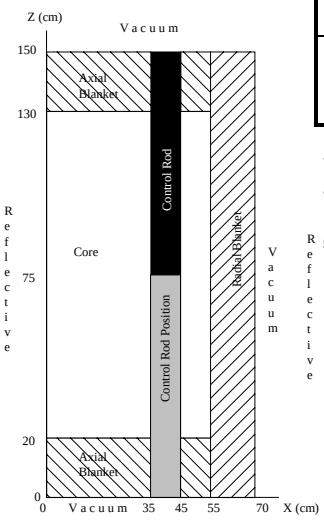

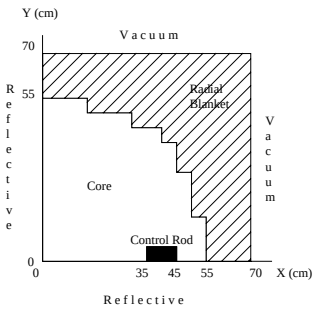

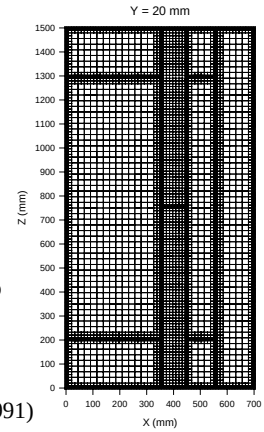

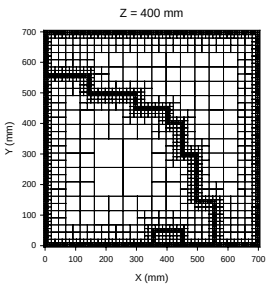

†Takeda & Ikeda, NEACRP-L-330 (1991)

CONCLUSIONS

- Tree multigrid technique offers a new promising deterministic solution method for 3-D radiation transport problems.

- The CAD interface allows easy construction and upgrading of the geometry, and make MultiTrans a flexible design tool.

- Void regions are problematic for the used SP_3 approximation (as seen for instance in the rod-out case of the previous LWR benchmark).

ARES – a New BWR Simulator

Riku Mattila
VTT Processes

Project Status

- Development started in 2000.
- Neutronics, thermalhydraulics, cross section and burnup modules written, testing in progress.
- Current version can be used in simplified reactor conditions, improved models needed for real cores (e.g. CR tips) in progress.
- First application: benchmarking of SIMULATE-3.

Stating Point for the Project

- Main goal was to evaluate international development of nodal methods in past two decades from two points of view:
  - to acquire understanding of the current state and limitations of nodal models
  - to improve the neutronics model of the TRAB-3D code
- The AFEN (Analytic Function Expansion Nodal) model, initially developed in South Korea in mid-1990:s was chosen as the basis for further analysis.
  - the model was expanded from 2 dimensions to a full non-separable 3D model at VTT

Main Results of the Project (1)

- It turned out possible to derive a full 38 component analytical form function based nodal model.
  - improved modelling of diagonal flux tilts within assemblies
  - improved accuracy near assembly corners => better pin power reconstruction capabilities
- The large amount of couplings (up to 150 per flux value) tends to make convergence extremely slow (up to 2000 iterations required).

- the problem was solved by using nodal rebalancing => number of required iterations down by factor of 20

Main Results of the Project (2)

- Instead of coupling the new neutronics model directly to the thermalhydraulics of TRAB-3D, a more sensible approach was to write an independent stationary-state thermalhydraulics model for the code.
  - re-evaluation of models and solutions used in existing generation of codes

- After adding a burnup module and a new cross section model, we can now present the first version of a new BWR simulator program, named ARES (for Afen REactor Simulator).
  - by changing the cross section model, analysis of rectangular-geometry PWR:s is, of course, also possible

Applications of the New Simulator (examples)

- Back up -calculations for commercial codes
  - reference tool for finding and evaluating problem areas, supplementary evaluation of safety margins

- Burnup calculations for transient analyses
  - independent code system for planning and safety evaluation

- Evaluation and testing of new models and ideas for core analysis.
  - dynamic re-evaluation of assembly discontinuity factors and detector response functions
  - models for taking into account inter-assembly currents in cross section calculation

Next Goals in the Code Development

- Series of test calculations for analyzing the four new models:
  - neutronics (AFEN), thermalhydraulics, cross section and burnup modules

- Integration of ARES into the code system of VTT:
  - straightforward transfer of burnup data to TRAB-3D for transient analyses

- Thorough documentation and code cleanup.
  - release 1.0 of ARES will be published during the first half of 2003, after completing the test calculations and making required modifications

ARES: Specific Features

- Eigenmode representation of two-group diffusion equation.
- Analytical form functions for the flux modes (19 per mode).
- Discontinuity factors for both boundary and edge fluxes (8 per group).
- Nodal rebalancing module to cut running times.
- 2100 point cross section model: history variables interpolated from arrays, momentary variables from polynomial fits.
- Four-equation thermalhydraulics model, 2. order discretization, multi-dimensional Newton iteration.
- Conventional predictor-corrector burnup module.

Result example (1): IAEA-3D benchmark

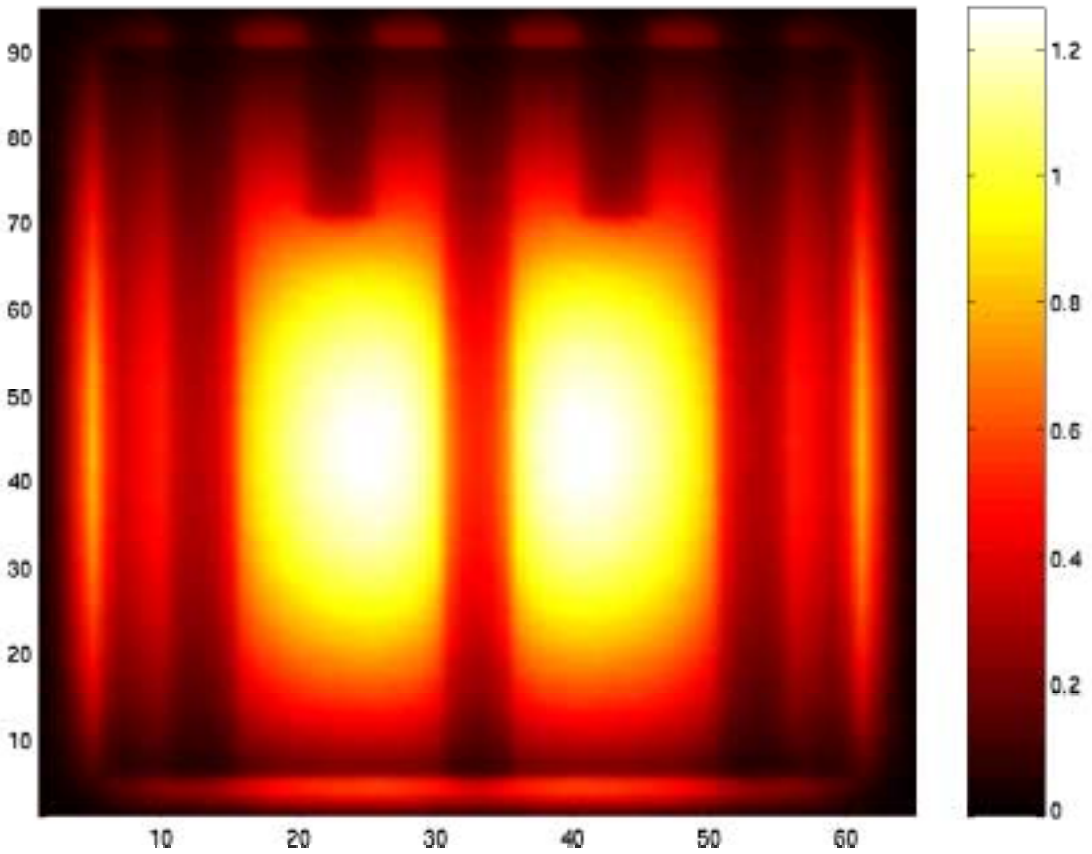

Result example (2): IAEA-3D benchmark

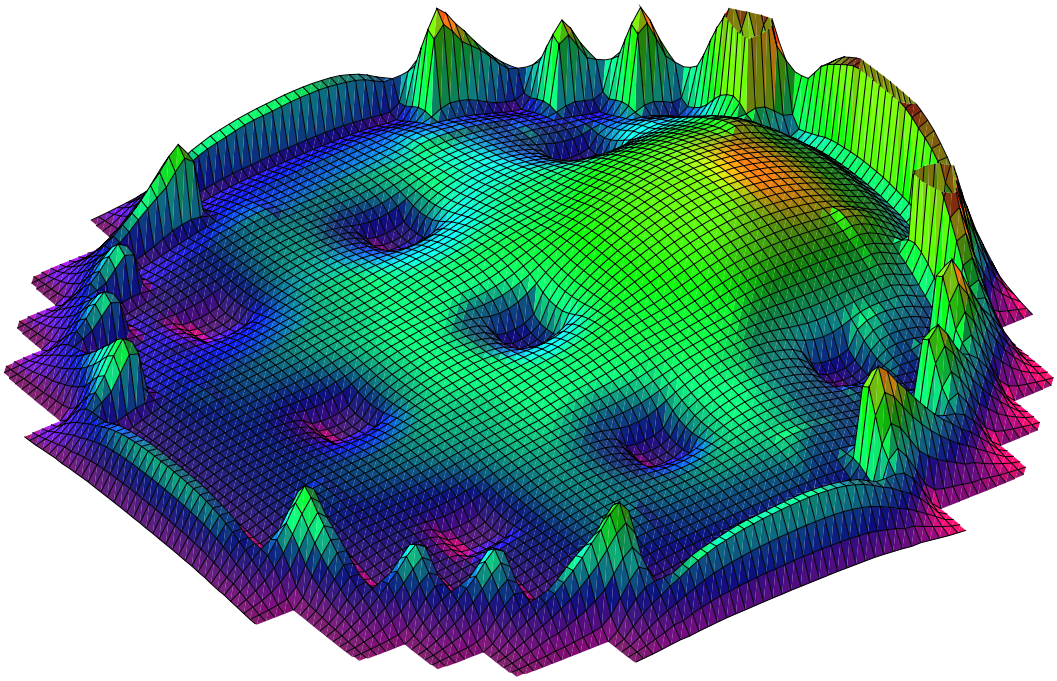

Result example (3): BWR test calculation

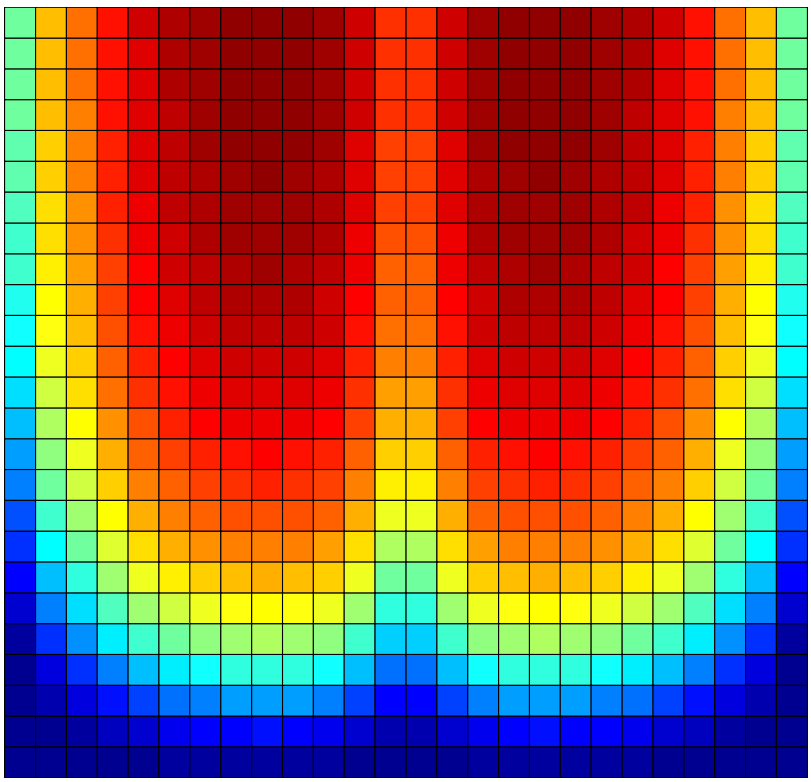

POLCA-T – 3D safety and core analysis tool

Lars Paulsson
BWR Services – Safety Analysis

Content

- Overview
  - What is POLCA-T?
  - Main features
  - Status and plans
- Applications
- Verification and Validation
  - Some examples
- Summary

What is POLCA-T?

- POLCA-T is a computer code for static and transient 3-D BWR safety analysis
  - Core design etc *(today POLCA)*
  - Stability analysis *(today RAMONA)*
  - Transient analysis *(today BISON, RAMONA etc)*
- …and also a powerful general t/h code
  - Hydraulic loads… *(today RELAP, GOBLIN…)*
- ...with extensibility for use in
  - LOCA analysis *(today GOBLIN)*
  - Containment analysis *(today COPTA)*
  - PWR analysis

POLCA-T main features

- Consistent modelling for static and transient applications
  - No interfaces
  - No transformation/condensation/normalization
  - Data entered once

- Input data highly reusable
  - POLCA-7 CM2 – applicable
  - BISON – SAFIR and PARA models can be reused
  - GOBLIN – GOBLIN reactor/system data can easily be reused for POLCA-T

- Powerful models and modern code structure
  - T/H five equation formulation
  - Staggered mesh – hydraulics (volume cells/flow junctions)
  - Finite difference – conduction
  - Topological input – Object oriented
  - Fortran 95 object oriented programmed

- CompaqTru64 UNIX and Linux environments supported

POLCA-T, Influences

The POLCA-T code is based in different extent on following codes:

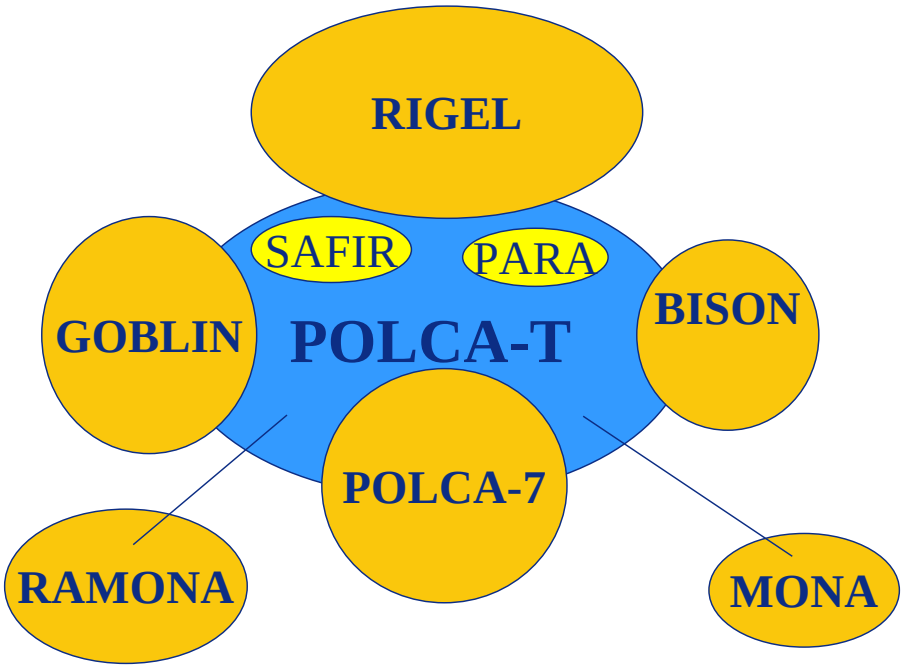

POLCA-T, Status and Plans, Summary

Project status:

- Released for production use (stability), version 1.0
  - Transition from RAMONA to POLCA-T for stability calculations started
- Already used for some specific applications

Preliminary time schedule:

- Release 2.0 for transient applications in Dec 2003
  - Final transient validation and some model improvements ongoing
- NRC Licensing planned for

POLCA-T, Some specific applications

POLCA-T has been used for some specific applications:

- Special studies of stability performance
  - Innovative fuel designs
- 3D transient methodology studies
  - Presented in NKS seminar 8 April
- Nuclear heating events in BWR
- Hydraulic loads in piping due to pipe break and valve closure
- Natural circulation in BWR90+ Core Catcher test facility

POLCA-T, Verification and Validation

Analytical solutions:

- Oscillations in U-tube
- Incompressible flow
- Compressible flow
- Gravity driven flow
- …

Separate effects:

- INEL jet pump tests
- Steam separator tests
- FRIGG void
- FRIGG pressure drop
- FRIGG stability
- FRIGG dryout
- F3 channel flow
- RIA SPERT III E-Core
- …

Integral tests, stability:

- Forsmark 2
- Oskarshamn 3
- Peach Bottom 2

- Ringhals 1
- KKL
- …

Integral tests, transients:

- Peach Bottom 2 TT
- OL 1 pump trip
- F3 pancake core
- …

Integral tests, static:

- Benchmark vs POLCA7
- OL 2 Start-up sequence
- OL 2 Core follow
- …

Examples of recent activities, some results:

- Separate effects
  - FRIGG void and two-phase pressure drop measurements
- Transient applications
  - Peach Bottom 2, EOC2, TT2 OECD/NRC benchmark
- Stability applications
  - Peach Bottom 2, EOC2, stability measurements
  - Forsmark 2 stability measurements

Summary

FEATURES

- Powerful tool for 3D transient and core analyis
- Consistence between static and transient calculations
- Existing models highly reusable (BISON, POLCA, GOBLIN)

STATUS

- Released for production use (stability), version 1.0
  - Transition from RAMONA to POLCA-T for stability calculations started
- Transient version 2.0 by the end 2003 – validation ongoing
- NRC licensing coming up
- Westinghouse standard tool for BWR Safety Analysis

Something cuckoo in the Oskarshamn 1 core model

Christer Netterbrant
OKG AB
SE-572 83 Oskarshamn, Sweden

Abstract

Oskarshamn unit 1 has always shown large TIP deviations. Simulating the core power with satisfactorily accuracy has always been an arduous task regardless of the computer code package used. Typical TIP deviations are shown and the reason for the faults is discussed.

Introduction

The Oskarshamn 1 core consists of 448 bundles and has a thermal energy of 1375 MW, giving it a very low power density of 35 MW/m^3 or 17 kW/kg uranium. Many different fuel types have been loaded over the years. The core now consists of Exxon 8x8, KWU 9x9, Svea-64, Svea-96 and Svea-96 Optima.

To simulate the core power, different codes have been used such as:
Casmo-4 / Simulate-3, Casmo-4 / Polca-4, Casmo-4 / Polca-7 and Phoenix / Polca-7. Common to all are the large TIP-deviations both axially and radially. In this report the focus has been on Casmo-4 / Simulate-3 being the official online and offline computer code at OKG.

The problems

- k-effective hot and cold is around 200 pcm higher than Oskarshamn 2 and 600 pcm higher than Oskarshamn 3 using the same computer code package.

- All simulator codes give large errors axially and radially. Some cycles look fairly good (4–5 % RMS), but quite a few have TIP errors of up to 10 % RMS.

- The power profile is often not bottom-peaked enough in the simulator, especially at the beginning of each cycle. It gets better near end of cycle.

- The radial deviations are high. At some TIPs, single TIP-channels deviate much, at others regions of the core deviate much.

- k-effective is not stable after temporary power reductions. Typically k-effective after reaching full power, decreases 100 pcm during about 15 hours and then slowly increases to its original value prior to the power reduction.

- There is a tendency to overpredict the axial power in the middle of the bundle.

- The power density is too low in the bottom of the core, at node 1 and 2.

- The simulator often overpredicts the power above partially inserted control rods.

- Cold criticals look normal, and as good as Oskarshamn 2 and 3.

Known Faults

The Fuel Temperature is probably too low in Simulate for high burnup fuel due to an old version of Interpin (v.2.16), the program which gives the fuel temperature as input to Simulate-3. Raising the temperature will broaden the resonance, giving lower power in high burnup fuel. The main effect of this is that k-effective will decrease 200 pcm. Lower power in high burnup fuel also leads to a somewhat more bottom-peaked power distribution as is evident from the picture below where the fuel temperature was increased 200 deg C in all cycles for fuel above 20 MWd/kgU in burnup.

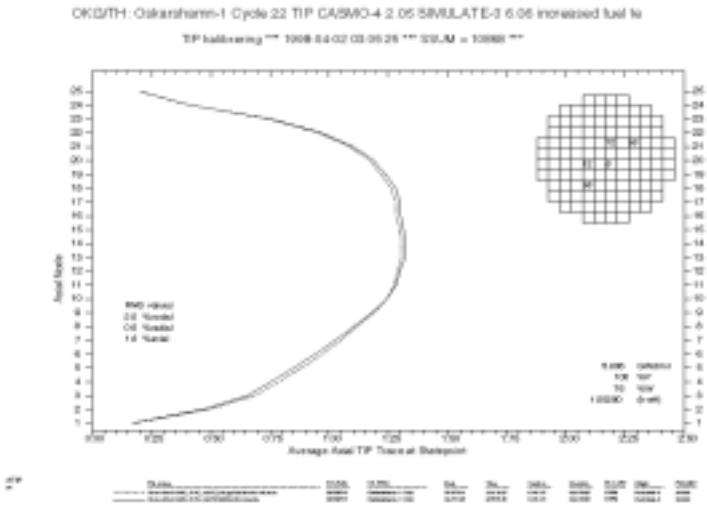

Figure 1. Effect of raising the fuel temp 22 deg C for fuel above 20 MWd/kgU in cycle 22. Solid line is before raising the temperature, broken line after.

An error in the recirculation flow measurement has been detected. The RC-flow input to Simulate was 200-800 kg/s too low for the last five cycles. Increasing the RC-flow will give a less bottom-peaked power profile, but the effect diminishes rapidly because of less burnup in the bottom of the core. The effect is so small it cannot be a major cause for the overall TIP deviations.

Discussion

The fact that k-effective is higher at Oskarshamn 1 than at Oskarshamn 2 and 3 using the same computer code may give a clue to what is wrong. No further conclusion is drawn at this point. The k-effective is quite unstable between cycles (Figure 2). A reason is probably the many short and long periods of shutdowns.

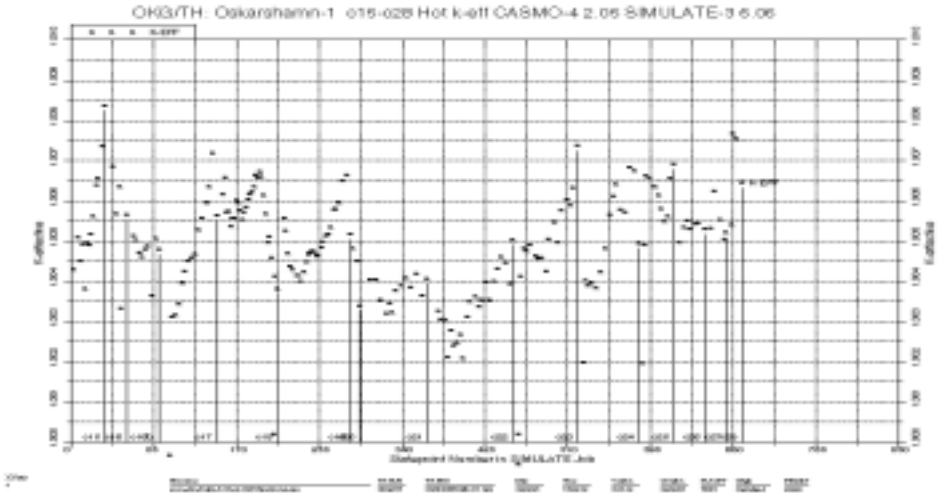

Figure 2. Hot k-effective at TIPs, cycle 15-28.

Since all used computer codes give large deviation axially and radially, it is unlikely that the major reason for the faults is in the computer codes themselves.

The fact that the power profile is not bottom-peaked enough could be due to too little reactivity in fresh and once burnt fuel. Another reason could be in the thermohydraulics, i.e. not enough void in the simulator.

Likely reasons for the high deviations in single TIP-channels (Figure 3) are channel bow and channel bulge. The statistics for measured channel bow at Oskarshamn 1 (Figure 4) show that the channels are known to bow somewhat away from the control rod, i.e. towards the TIP channel.

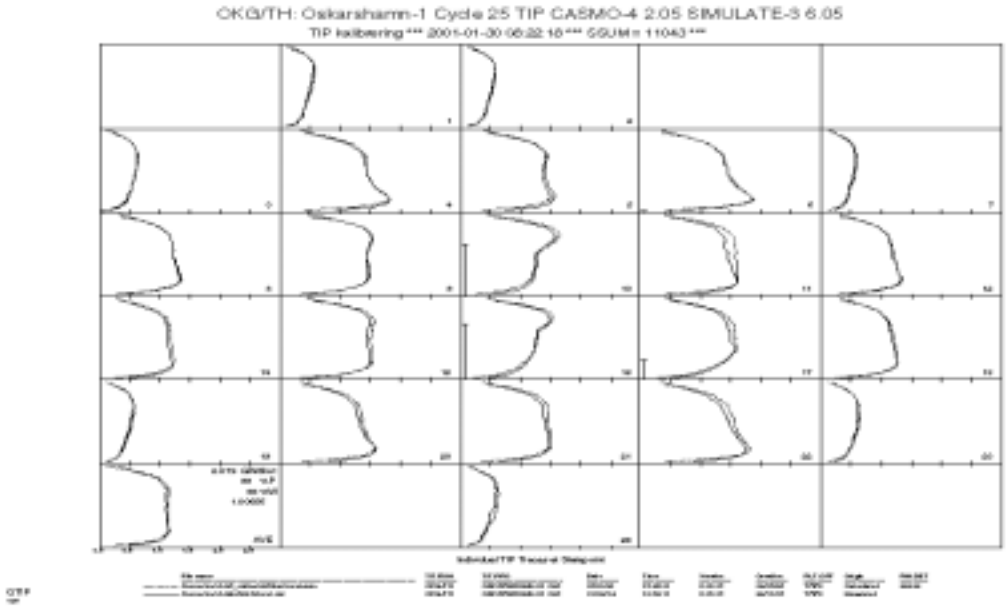

Figure 3. Individual TIP channel deviation. Broken line is Simulate-3.

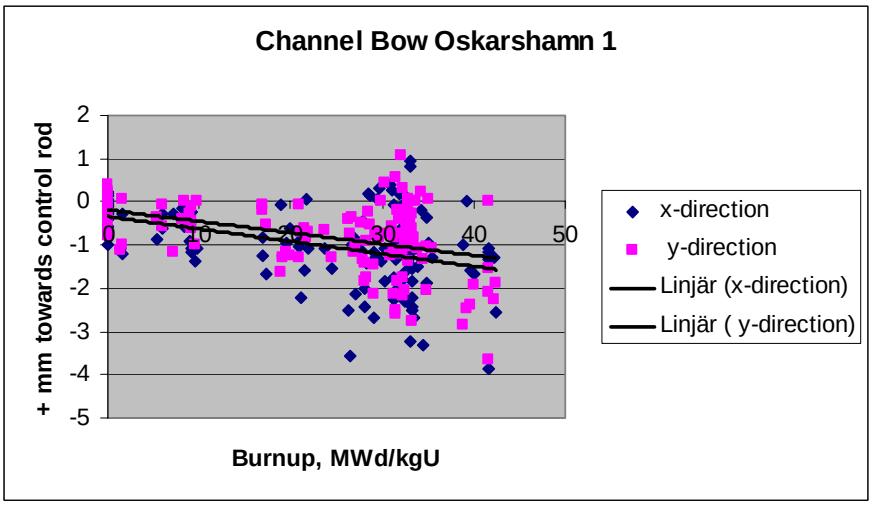

Figure 4. Measured channel bow at Oskarshamn 1.

This could also be the explanation for the somewhat overpredicted power midchannel, Figure 5, as is often the case for Oskarshamn 1.

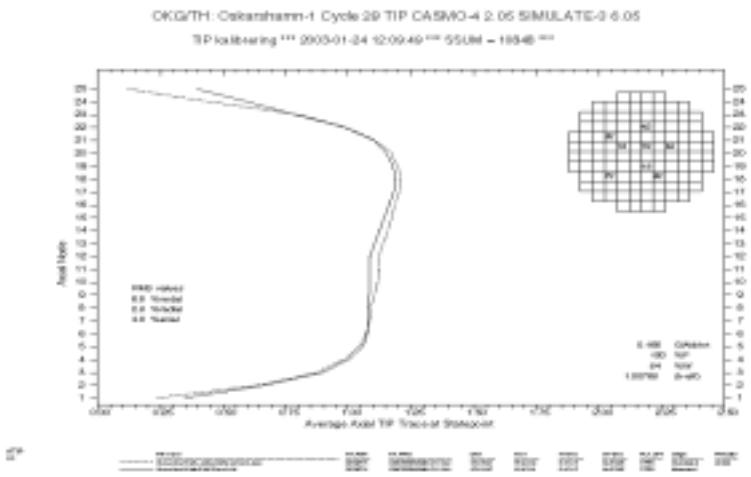

Figure 5. Typical TIP-curve with overprediction midchannel, underprediction in the bottom nodes.

The problem with an unstable k-effective after a power reduction is shown in Figure 6. The k-effective typically decreases 100–150 pcm during the first 15–20 hours after full power has been reached after which it stabilises at the previous level. The reason is not known, but it may have something to do with xenon and an axial shift in the power distribution. The effect is seen in both Polca-4 and Simulate-3. It can not be seen in neither Oskarshamn 2 and 3, nor in Ringhals 1, another low power density reactor.

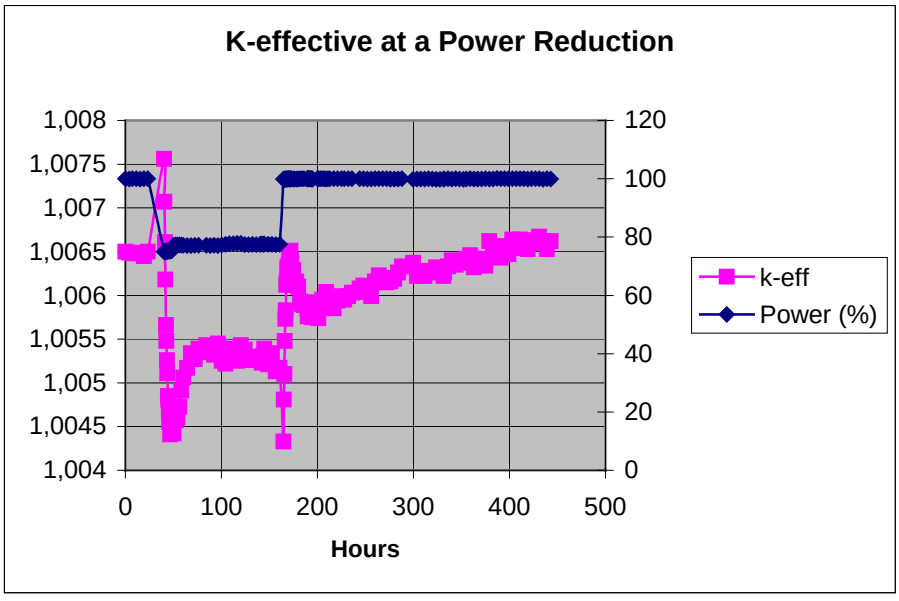

Figure 6. Typical behaviour of k-effective at a temporary power reduction.

Too low power in the bottom nodes, node 1 and 2, can be seen on virtually all Nordic Boiling Water Reactors and is not typical for Oskarshamn 1. A test was done to replace the bottom and top reflector with pure water, which gave negligible result for the axial power distribution. Plausible reasons for the deviation could be channel bow and/or the TIP-detector not being linear at very low gamma fluxes.

At the end of cycle 27 two TIP calibrations were made one week apart, the first with all control rods withdrawn and the second with every second control rod withdrawn 84 %. The result is shown in Figure 7. As is evident from the picture the simulator overpredicts the power above partially inserted control rods. The reason could be in the thermohydraulics (not enough void above the control rods) or in the difficulty of modelling the top of the control rods. The top is modelled using three different segments: the boron part of the rod, the hafnium part and the handle.

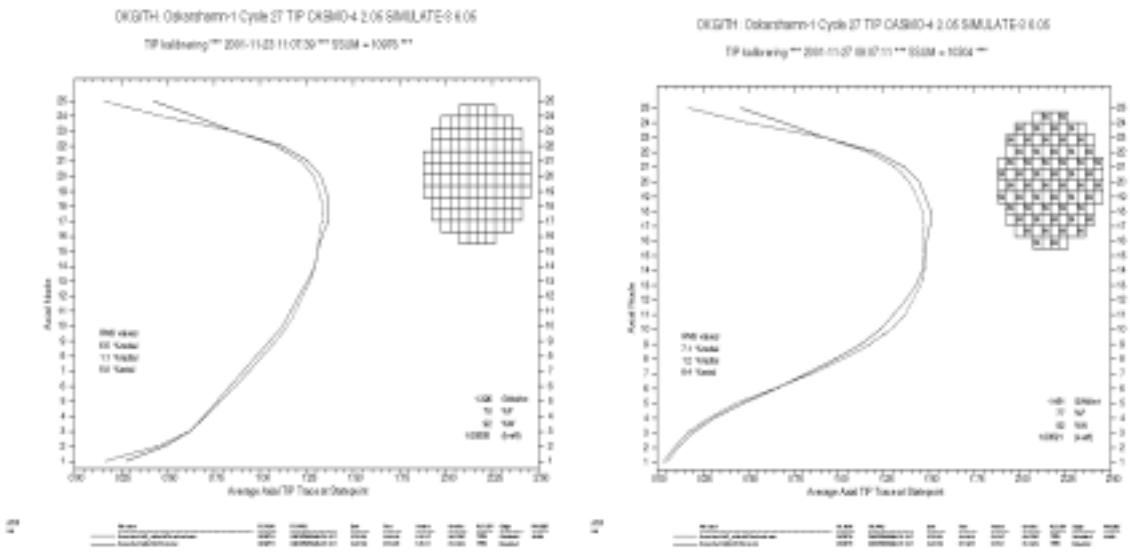

Figure 7. Two consecutive TIPs at the end of cycle 27, one with all control rods withdrawn, one with every second control rod withdrawn only to 84 %.

Excuses for the large deviations

Oskarshamn 1 has very low power density. It had a three year long shutdown between cycle 20 and 21, in which the shutdown cooling effect could have large impacts on the fuel. Oskarshamn 1 has had many shorter and longer shutdowns and many scrams. Some cycles have been very short and have had very small reload batches, giving the core large peaking factors, which gives hard-predicted power distributions. Lots of different fuel types with long residence times (up to 10 years) gives very hard-predictable cores.

Conclusions

The Oskarshamn 1 Core Model shows large errors at TIP calibrations both axially and radially.

No tried single parameter can explain the large deviations.

The fact that single TIP channels deviate much indicates that channel bow and channel bulge could be a major villain of the piece.

Loading pattern search by branching and bounding batch patterns enumerated under constraints

Brian Beebe

Background Information

- A new LP search code is jointly developed by Westinghouse, SNERDI and MHI
- The method used is called B3PEC:

  Branching and **B**ounding **B**atch **P**atterns **E**numerated under **C**onstraints
- The code is called LP-fun:

  Loading **P**atterns – **f**or **u**ser's **n**eed

Remarks on LP Search Methods

- LP search contains three steps:
  1. Generating patterns by shuffling
  2. Spatial flux/power calculation
  3. Evaluation for acceptance/rejection
- Step 2 is time consuming, Step 3 straightforward
- Step 1 is the most crucial, controlling the search space and the effectiveness of a method
- Most methods focus on Steps 2 and 3, and are stochastic (random) in Step 1
- The B3PEC method shifts the focus to Step 1

Unique Features

- B3PEC is a deterministic and comprehensive search process, not a stochastic one
- Using the enumeration technique and the B&B technique in integer programming
- It resembles but theorizes the practical search process of core design engineers
- It uses only the design code (ANC) for spatial flux and power calculation

The Search Process

- Defining a **B**atch **LP** (**BLP**):
  “containing batches of “identical” assemblies”
- Starting with ALL the (coarse) BLPs that satisfy the user specified loading constraints
- Through the search process, the coarse batches get split into finer batches, and end up with real LPs of distinct assemblies
- All allowable LPs are covered, and each assessed and visited (when necessary) only once

BPEC: Batch Pattern Enumeration under Constraints

- BPEC only uses logical and integer operations, efficiently generating each and all of allowed BLPs
-
- A variety of flexible loading constraints:

  arbitrary forbidden domain for each batch
  arbitrary forced loading domains for each batch (min < # < max)
  arbitrary forbidden domains for various kinds of clustering
  arbitrary forced domain for various kinds of adjacent constraint
  domains can overlap, and each can be topologically disconnected

- A user can repeatedly run BPEC to define the search problem and assess its solution space size before starting any spatial calculation

Branch and Bound

- Shuffling the “distinct” assemblies in a batch is an integer permutation problem (N! shuffles)
- If the distinct assemblies could be arbitrarily taken apart and reassembled in mixture, then this would become a continuous real variable problem
- The continuous problem can be quickly solved, and its best solution always bounds the best integer solution
- If the bounding solution is not acceptable, there is no need to perform any of the N! shuffles

The Basic Idea of B & B

- Repeated trials for the Integer Variable
- Direct differentiation for the Real Variable
- No acceptable R.V. minimum → no acceptable I.V. minimum (contrary is NOT true)
- Don’t bother with repeated I.V. trials. A whole “branch” is cut.

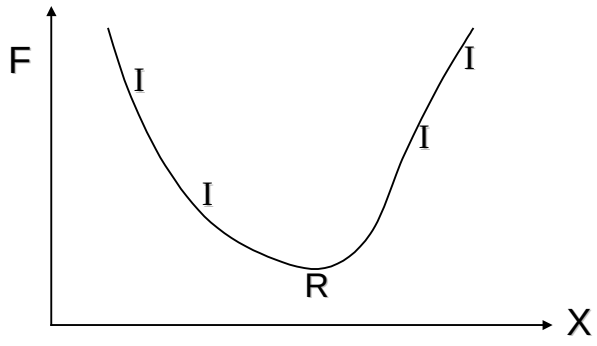

B3PEC Implementation in LP-fun

- ANC 3D to 2D collapsed depletion model (how?)
- ANC generated Sensitivity Matrix for BA adjustment and burnt fuel shuffling for each BLP (how?)
- S-matrix used to optimize BA loading and in-batch shuffling via B&B mixed integer linear programming
- Need more than one level of batch split to assure the validity of the S-matrices
- Solution space explored is immensely larger than that by methods used in other codes
- Final LPs can be directly put in ANC for designs

B3PEC Implementation in LP-fun

- The concept of B&B is used in setting the batch split hierarchy, and for optimum in-batch shuffle as well.
- A powerful commercial optimization code, CPLEX, is used for B&B mixed integer linear programming.
- Any design constraint or optimization objective can be implemented in CPLEX, if it can be expressed as a linear function of power distribution, FΔH distribution and PPM at any or all of the depletion steps (via the use of the S-matrix.)
- In addition to BPEC, loading position constraints can be imposed via CPLEX as well.

LP- for users' need

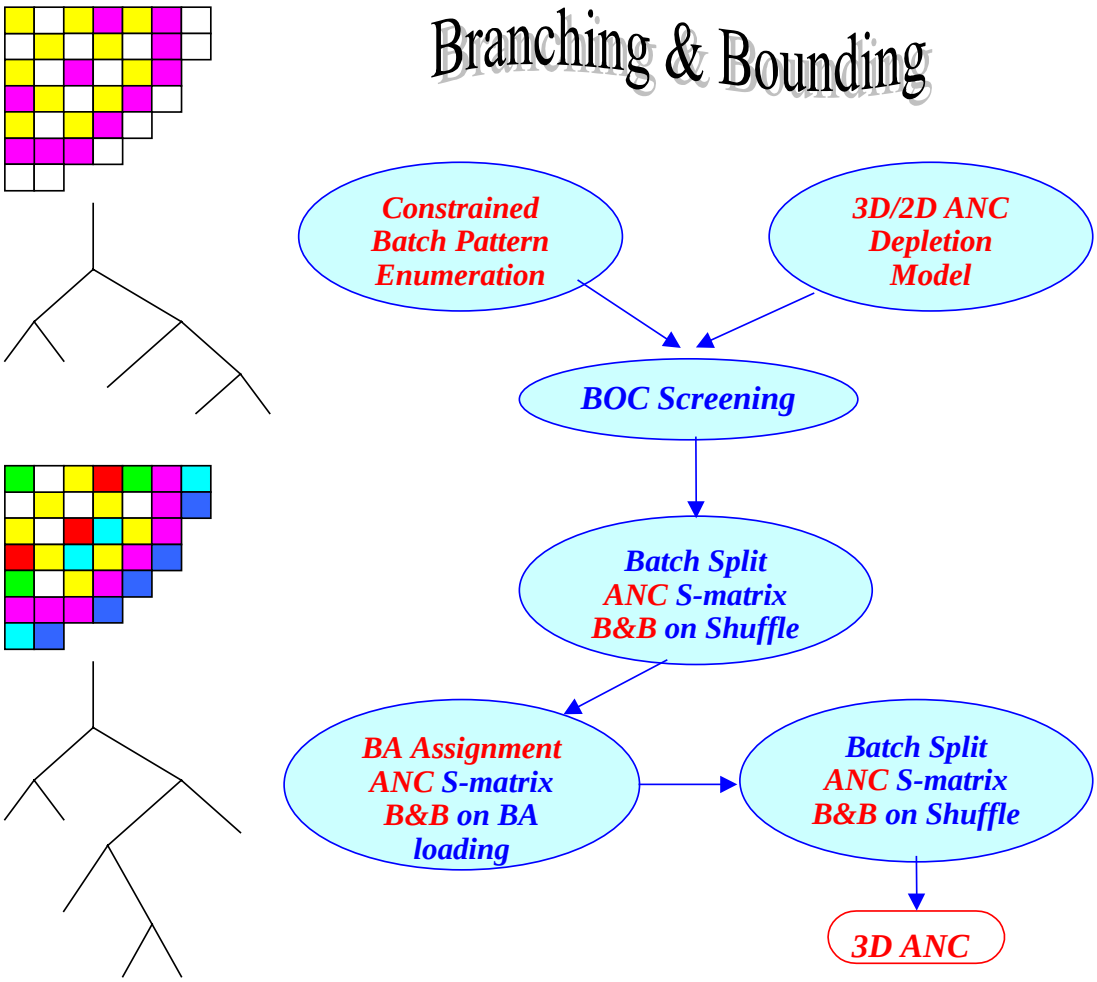

BPEC Example

3- Batch Checker-Board BLPs

Additional Constraints	2-Loop	3-Loop	4-Loop
none	*12,342*	*127,932*	*1,995,472*
no feeds in central region	*1,798*	*3,692*	*5,649*
(And) only feeds on edges	*4*	*31*	*41*

BPEC Example (continuing)

Peak Power for the 5,649 4-Loop BLPs
(no feeds in central region)

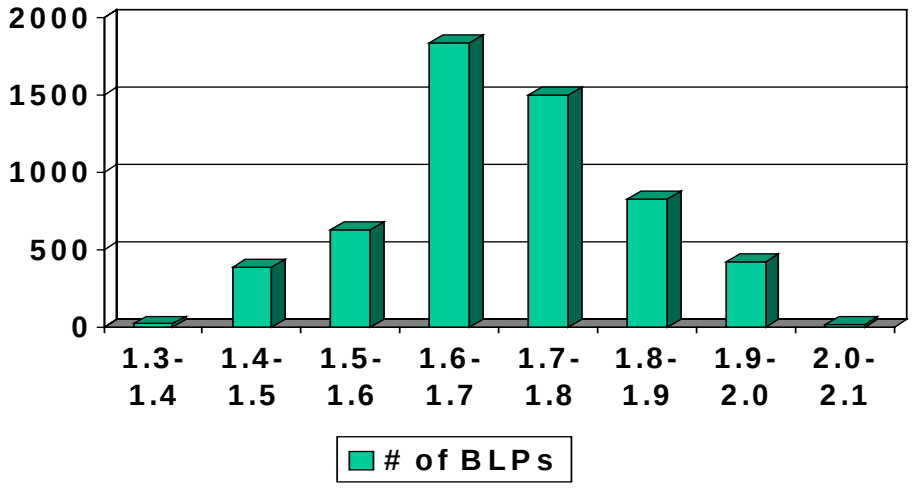

BPEC Example (continuing)

Peak Power for 4583 Improved 4-Loop BLPs
(inboard feeds adjacent to twice burnt)
(allow once burnt to cluster)

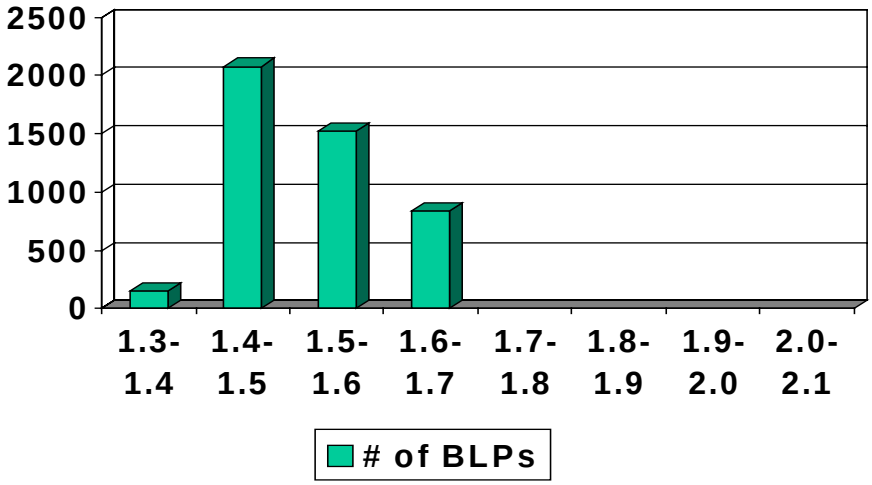

BPEC: Any Physics on How to Use the Constraints?

- The flux distribution in a uniform cylindrical core is a spherical Bessel function, which gives a peak power over 2.0 at the center.
- To reduce the power peak, the out-board reactivity must be raised → "a fire ring".
- "Minimum Critical Mass" study in early years showed via variational calculus that the theoretically ideal in-board reactivity distribution is flat.
- Load the most reactive ones first, then the least reactive ones, and the medium ones last, using position constraints to flatten the in-board reactivity.

Example 1 for a 4-loop Core

start with 4 batches

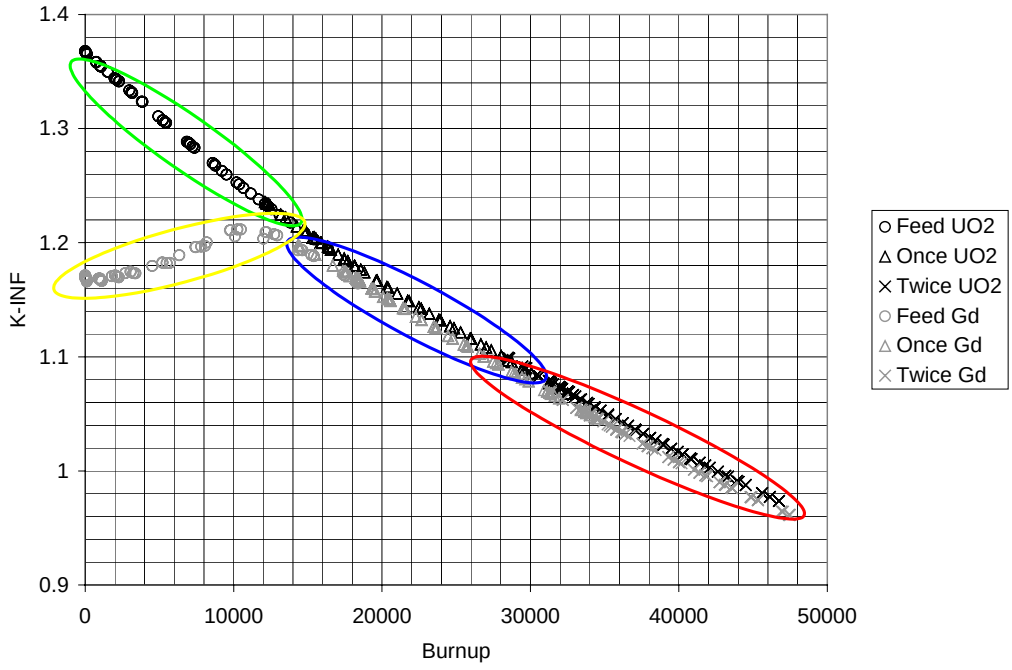

Example 1 for a 4-loop Core (continuing)
BOC results screening

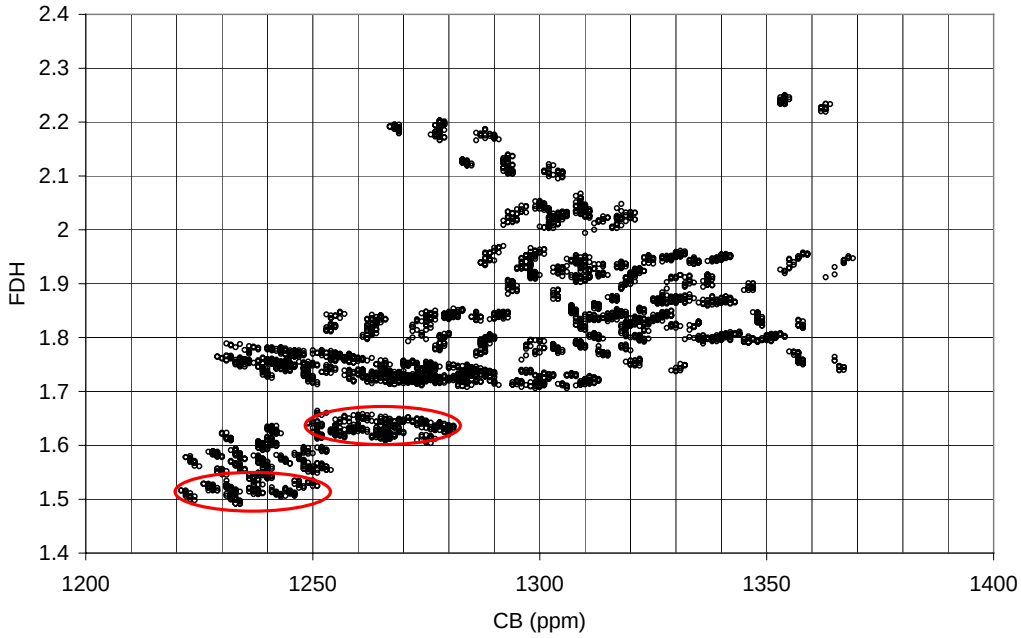

Example 1 for a 4-loop Core (continuing)
B&B results compared to ANC at BOC

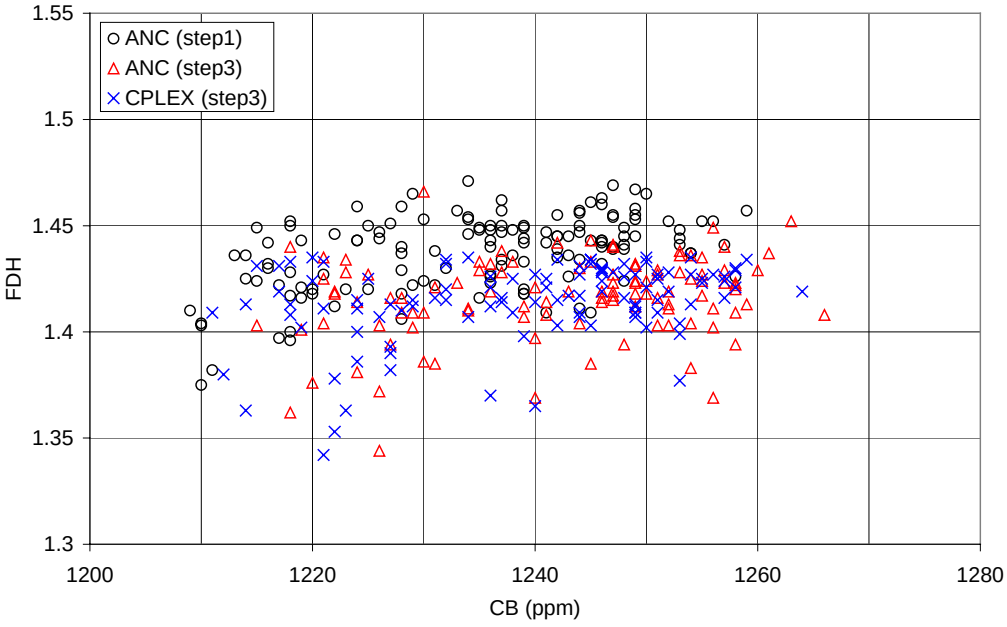

Example 1 for a 4-loop Core (continuing)

B&B results compared to ANC at EOC

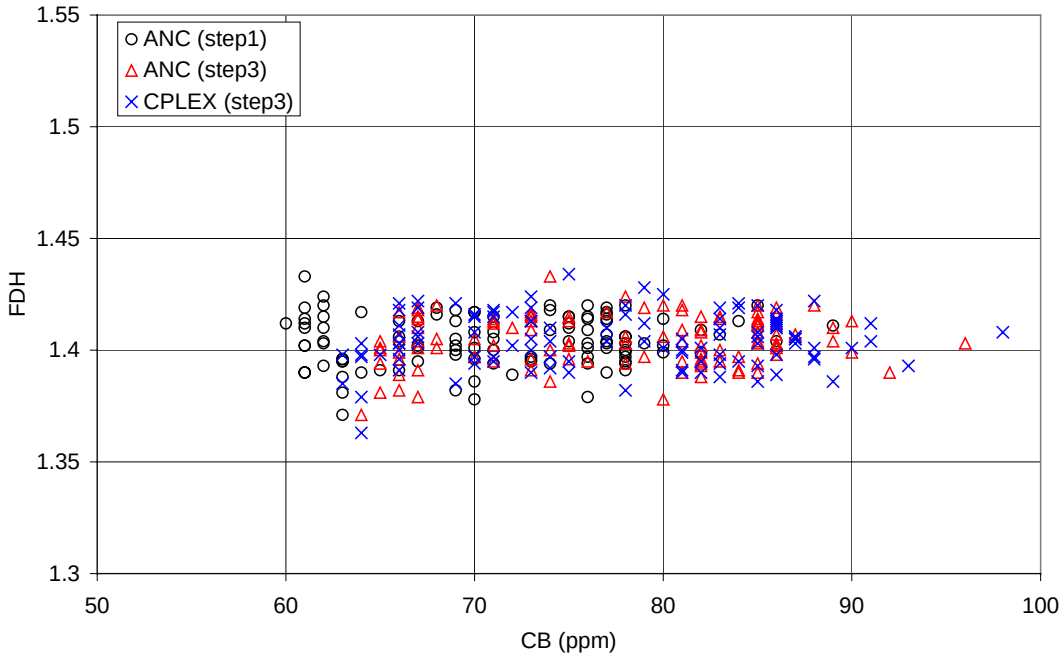

Example 1 for a 4-loop Core (continuing)

3D/2D ANC comparison for the final LPs

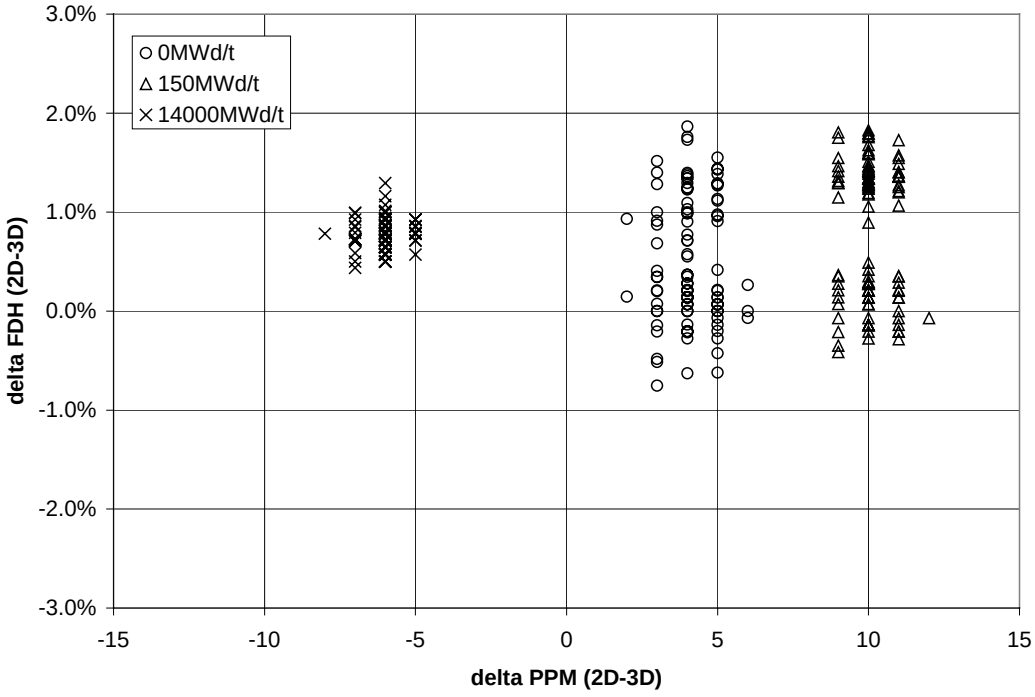

Example 2 for a 4-loop Core
start with 4 batches

UO2 Feed, Gd Feed, Once Burnt, Twice Burnt

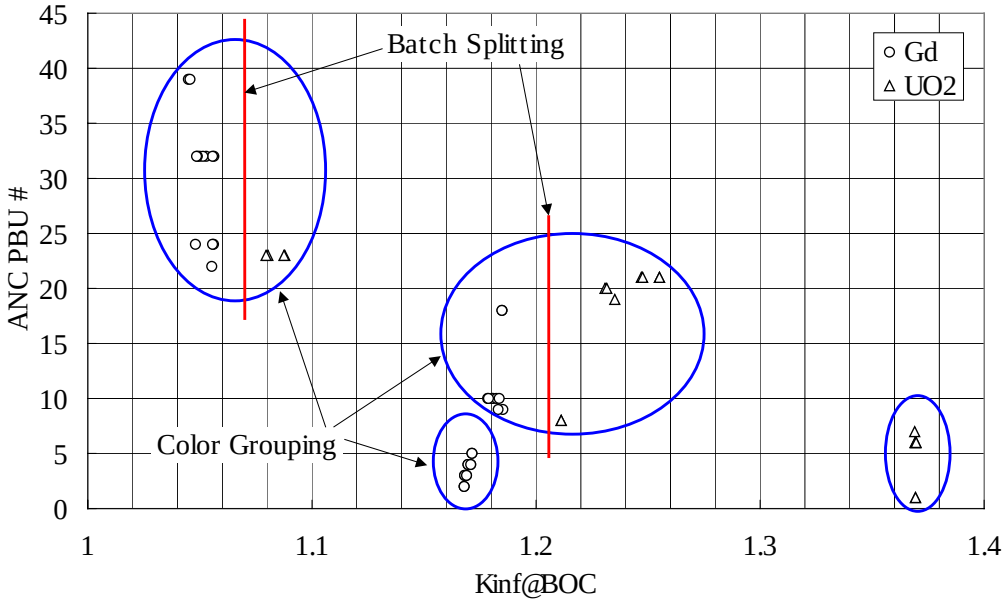

Example 2 for a 4-loop Core (continuing)
BPEC Enumeration for BLPs

- Position Constraints
  - Feed Locations Fixed
  - Gd Feeds (inboard) adjacent with Twice Burnt
  - No more than two Twice Burnt can be **inboard and adjacent**
- 404 BLPs

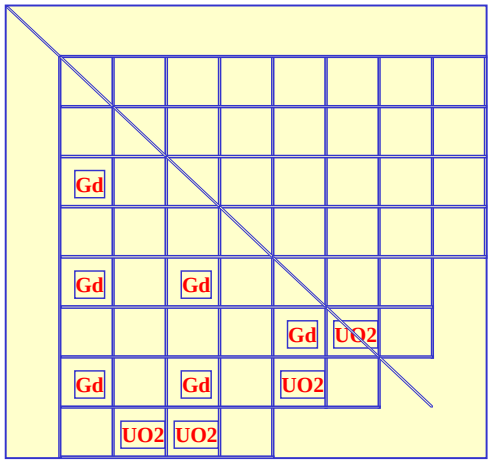

Example 2 for a 4-loop Core (continuing)
BOC Screening

FDH Limit=1.6 BLPs 404 → 160

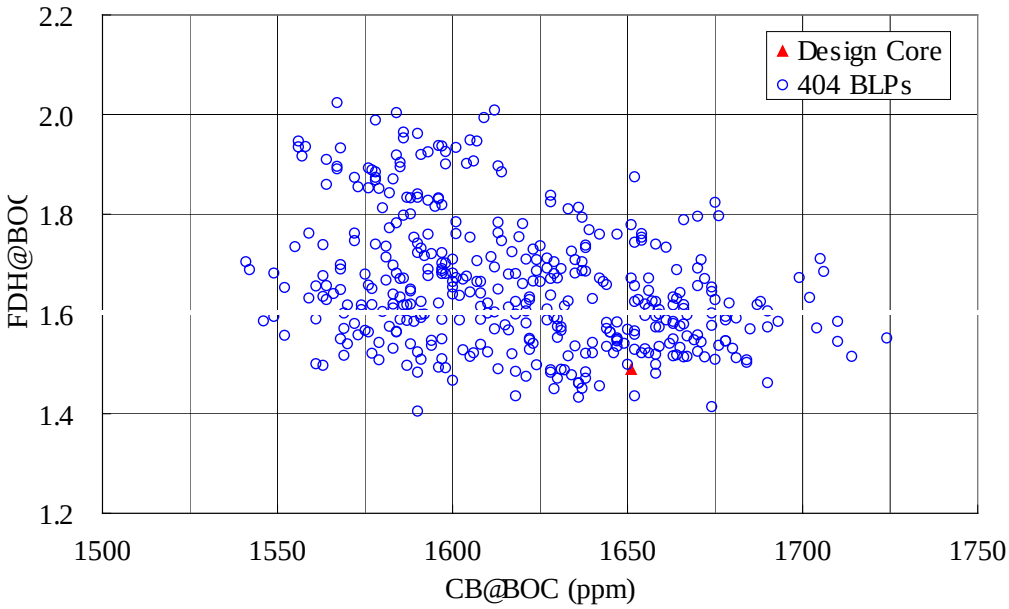

Example 2 for a 4-loop Core (continuing)
Split Batch 4 → 6 Minimize Power

FDH Limit is 1.5 BLPs 160 → 143

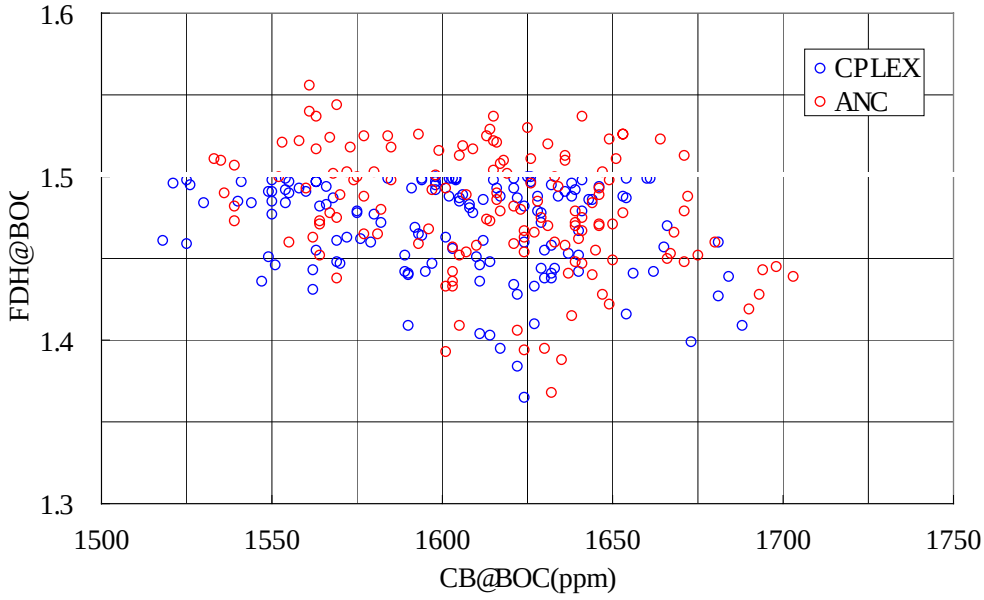

Example 2 for a 4-loop Core (continuing)

Split to Distinct Assemblies Maximize EOC ppm

FDH Limit is 1.42 BLPs 143 → 48 LPs

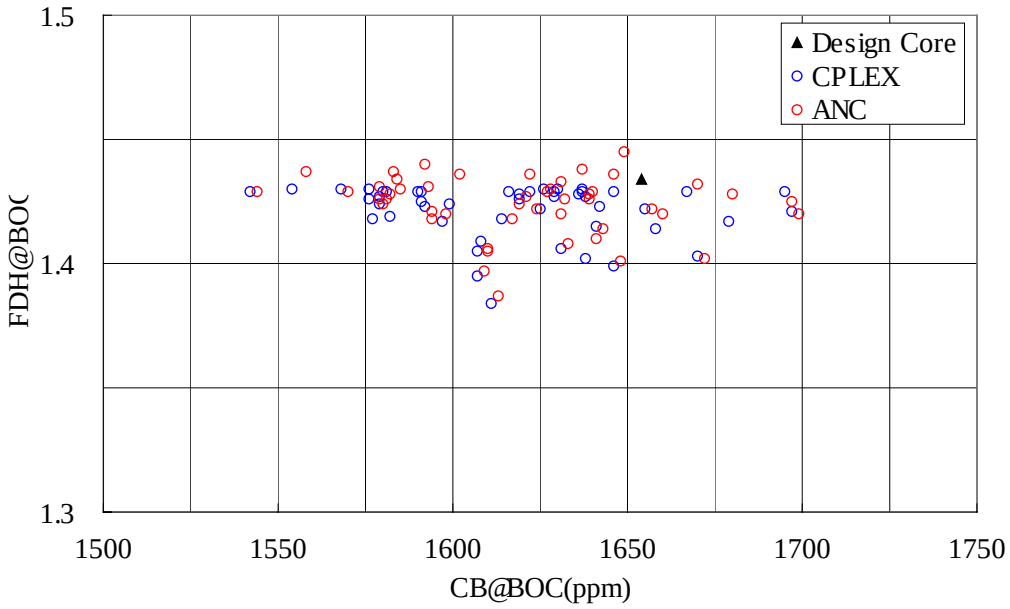

Example 2 for a 4-loop Core (continuing)

Split to Distinct Assemblies Maximize EOC ppm

FDH Limit is 1.42 BLPs 143 → 48 LPs

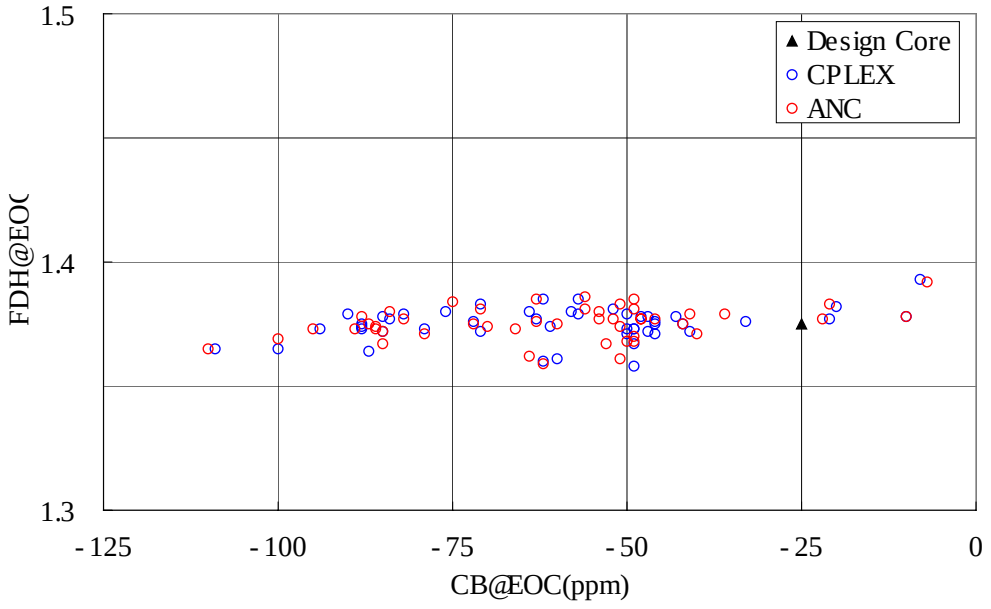

Conclusion

- A deterministic and comprehensive LP search method, B3PEC, is developed.
- The method consists of constrained enumeration, S-matrix and B&B.
- The method is implemented in the LP-fun code.
- LP-fun uses the ANC design code directly.
- Test applications showed very good results.
- LP-fun has transitioned to product development.

New LP-fun Team

- Software Programmers
  - Frank Popa (LP-fun Team Lead)
  - Tim Greenier (Java)
  - Dave Little (PERL)
- Core designers
  - Ho Lam (power user & trainer)
  - Mike Hone (tester)
  - Jack Penkrot (tester)
- Method consultant
  - Y. A. Chao (theory)

Supporting the SVEA-96 Optima designs with reliable methods

Juan J. Casal & Maria Petersson
Fuel Engineering
+46 21 347108
juan.casal@se.westinghouse.com/maria.petersson@se.westinghouse.com

Agenda

- Introduction
- Validation effort
  - Predictions at individual fuel rods level
  - Predictions at individual fuel bundles level
- Experience from core follow
- Summary

Introduction

The introduction of the SVEA-96 Optima generation of fuel designs implies a further increment in complexity and heterogeneity that needs to be dealt with.

The necessary transition, with mixed cores, represents an increased heterogeneity from the very beginning.

The introduction of a new nuclear data library, based on **END-F/B VI**, and the latest generation of our core simulator, **POLCA-7**, were aimed to tackle this kind of challenges.

The modeling of cores loaded with the new fuel designs rises some natural questions, concerning the performance of the standard analysis tools:

- Which has been the impact on modeling accuracy?
- Is there any need to review the methods/methodology to deal with the new fuel designs?
- Are transition cycles harder to evaluate with the latest fuel designs available?

Validation effort

Predictions at individual fuel rods level

- Accuracy at this level has an impact on Cell Data accuracy
- **LWR-PROTEUS** experiments (at PSI, Switzerland):
  - Unique experimental set-up for validation of 2D codes
  - LWR-PROTEUS Phase 1 project: EGL, PSI, W
  - Test-zone: 3x3 full-scale SVEA-96 bundles
  - Measurements at different conditions

Predictions at individual fuel rods level

Assembled LWR-PROTEUS Test Zone

Configurations evaluated:

- 1A/1B: Reference (**unperturbed**)
- 2A/2B/2C: Control blades in central position (**Hf/B_4C**)
- 3A/3B: Simulated void (polyethylene, **90%/25%**)
- 5A: **Control blades + simulated void**

Evaluations presented (from gamma-scanning at rod level)

- Total fission rate (= power distribution) ~ Thermal range
- Capture rate U238 ~ Epithermal range
- Pre- (nominal) & Post-calculations (actual dimensions)

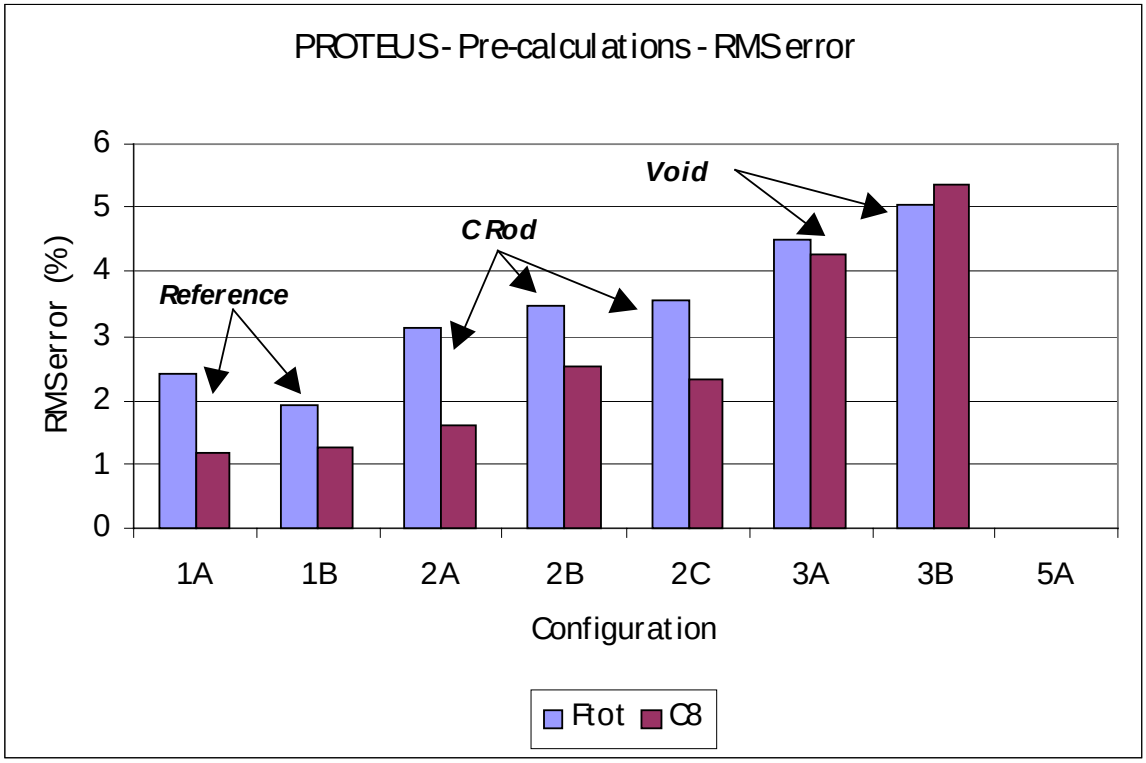
PROTEUS - Pre-calculations - RMS error
RMS error (%)
0
1
2
3
4
5
6
Reference
CRod
Void
1A
1B
2A
2B
2C
3A
3B
5A
Configuration
Ftot
C8

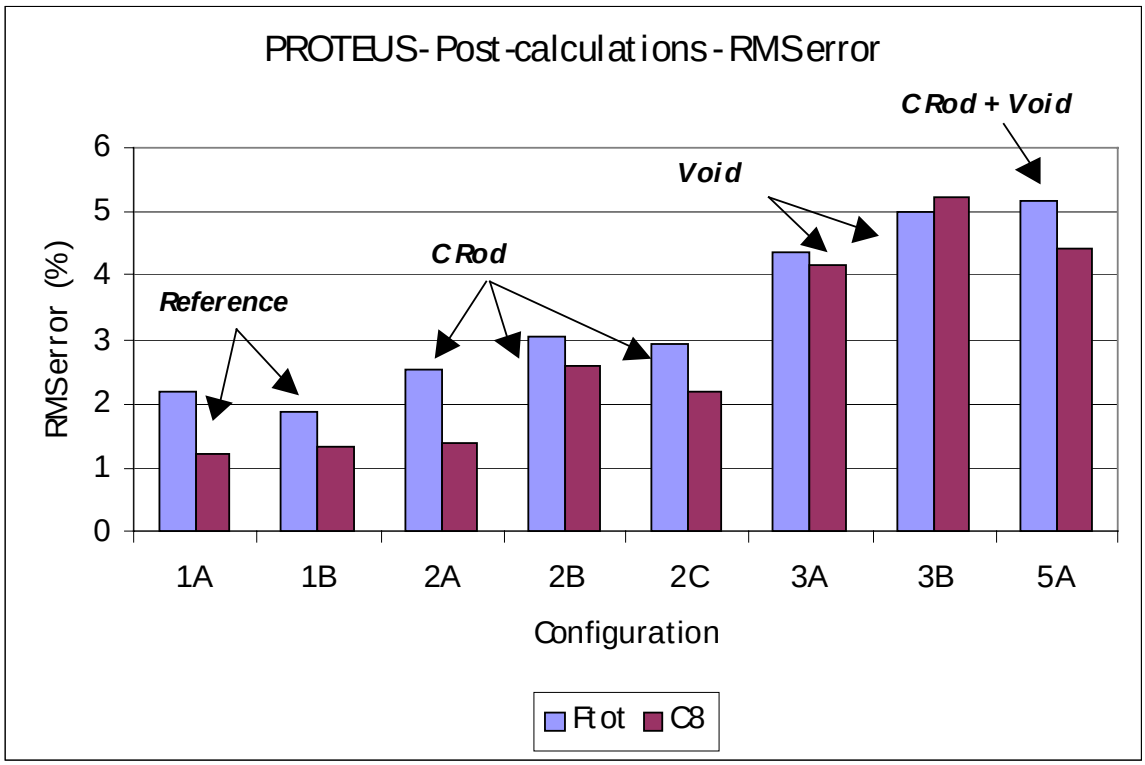
PROTEUS - Post-calculations - RMS error
RMS error (%)
0
1
2
3
4
5
6
Reference
CRod
Void
CRod + Void
1A
1B
2A
2B
2C
3A
3B
5A
Configuration
Ftot
C8

LWR-PROTEUS – Summary

- Controlled case
  - Excellent power tilt prediction, somewhat higher uncertainties (spectrum sensitive conditions)

- Voided case
  - Extreme scenario (heterogeneity not explicitly modeled) causes somewhat higher uncertainty

- All cases:
  - Systematic underestimation of reaction rates in BA-rods (generic problem of transport codes); it could explain observed within-cycle reactivity variations

- Similar accuracy in Pre- & post-calculations ⇒ assuming nominal dimensions is OK (!)

Validation effort

Predictions at individual fuel bundles level

- Power predictions accuracy, at nodal and bundle level, is best estimated from comparisons against gamma-scanning

  - Measurement at fuel bundle level of Lanthanum-140 gamma-radiation (from F. P. Barium-140 decay)

  - Representative of the last 7–8 weeks of operation

  - Enable estimation of uncertainties in bundle power sharing predictions beyond TIP-based comparisons

Predictions at individual fuel bundles level

Latest two gamma-scan campaigns particularly interesting

- Leibstadt NPP (KKL-c15): Homogenous core – 12m-cycles
  - 43 SVEA-96 (10x10 fuel – 10–48 MWd/KgU)

- Cofrentes NPP (CNC-c13): Mixed core – 18m-cycles
  - 22 SVEA-96 (10x10 fuel – 15–35 MWd/KgU)
  - 20 Fuel-A (9x9 w/PLR – 36–48 MWd/KgU)
  - 10 Fuel-B (10x10 w/PLR – 15–17 MWd/KgU)

Evaluation conditions *(challenges)*

- Each “fuel type” requires a specific set of Barium-to-signal (inter-calibration) factors that take into account:
  - The influence of different geometries on the gamma radiation reaching the detector
  - The influence of a given internal Barium distribution on the gamma radiation reaching the detector

- Partial length rods add “fuel types” to the comparison!

- Calculations
  - Standard PHOENIX4/POLCA-7 calculations
  - Ba-140 at bundle and fuel rod level tracked explicitly
  - Inter-calibration factors calculated with tomographic simulation code (Monte Carlo technique)

- Comparisons
  - Measurements & calculations normalized to same value
  - Nodes affected by structural materials excluded

Summary

- Excellent agreement with measurements, specially at bundle level
- Bundle & nodal accuracy fully in agreement with TIP comparisons
- No accuracy degradation observed due to the presence of either different bundle types or bundles with PLR
- Minor underestimation of Fuel-B most likely due to inaccuracy in its inter-calibration factor

Experience from core follow

Evaluation of two reactors (Leibstadt & Oskarshamn-3 NPPs) in their transition to SVEA-96 Optima/Optima-2

Code Package: PHOENIX-4 / POLCA-7

Parameters evaluated:
- (Hot) Keff at TIP (cycle averages)
- Local and global cold criticals (cycle averages & individual)
- TIP comparisons at nodal & bundle level (cycle averages)

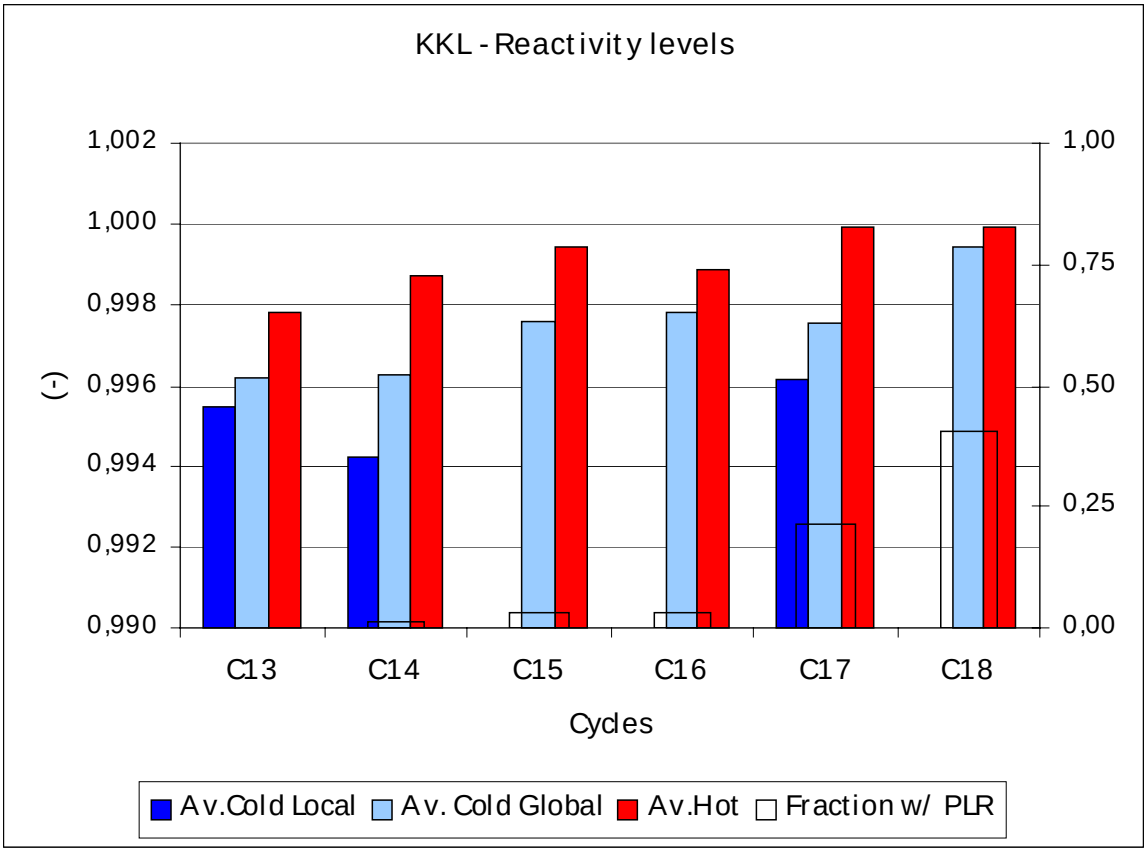
KKL - Reactivity levels
1,002
1,000
0,998
0,996
0,994
0,992
0,990
(-)
1,00
0,75
0,50
0,25
0,00
C13
C14
C15
C16
C17
C18
Cycles
Av.Cold Local
Av. Cold Global
Av.Hot
Fraction w/ PLR

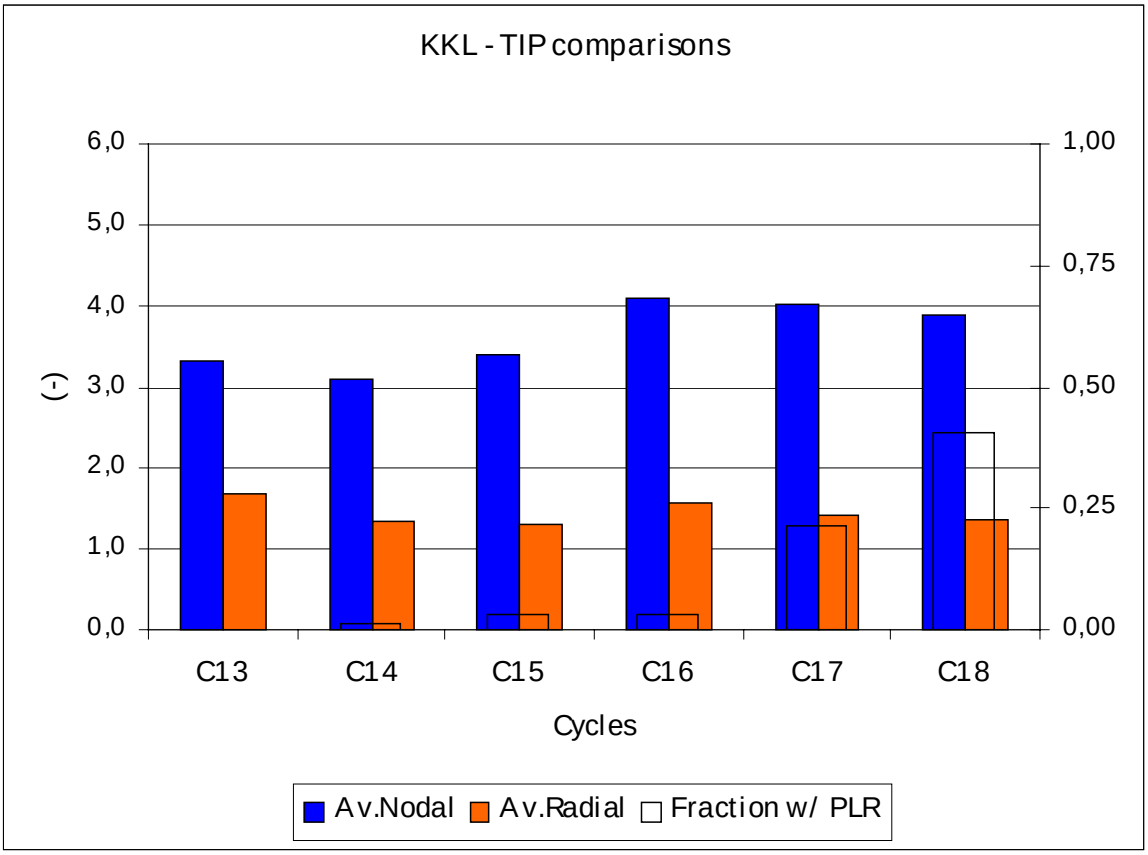
KKL - TIP comparisons
6,0
5,0
4,0
3,0
2,0
1,0
0,0
(-)
1,00
0,75
0,50
0,25
0,00
C13
C14
C15
C16
C17
C18
Cycles
Av.Nodal
Av.Radial
Fraction w/ PLR

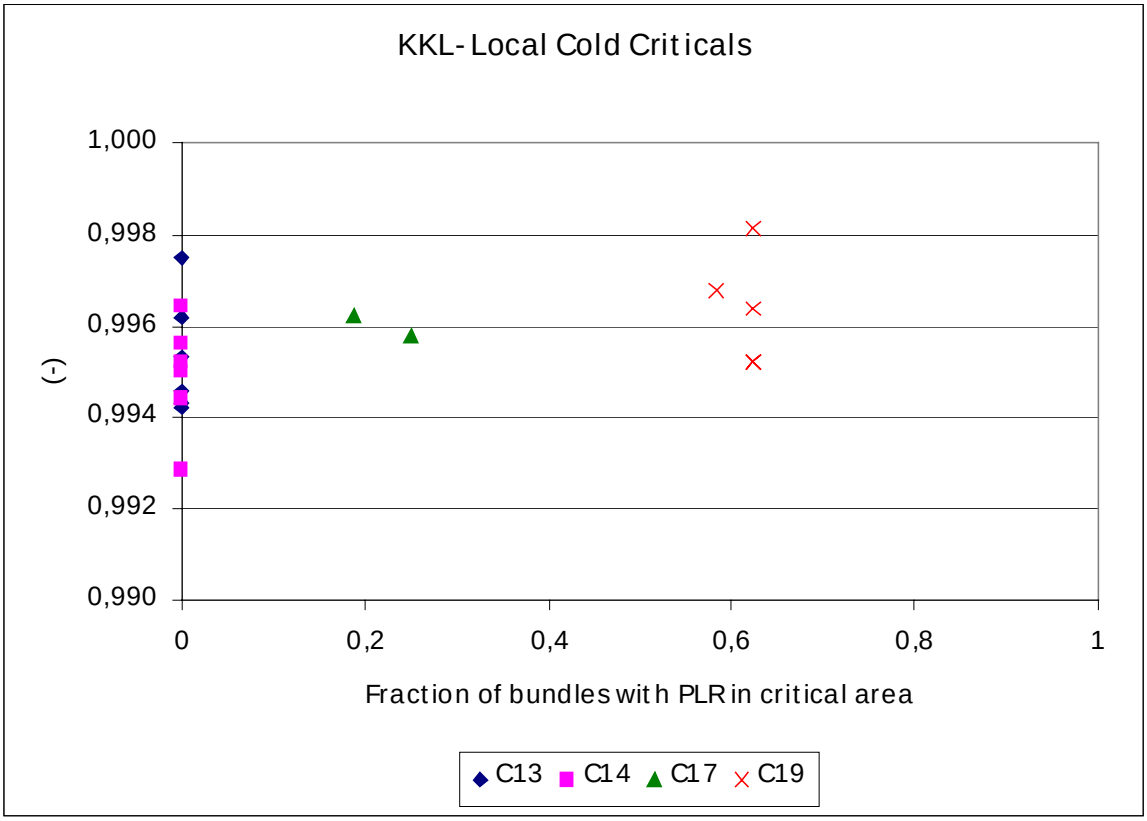
KKL- Local Cold Criticals
1,000
0,998
0,996
0,994
0,992
0,990
(-)
0
0,2
0,4
0,6
0,8
1
Fraction of bundles with PLR in critical area
C13
C14
C17
C19

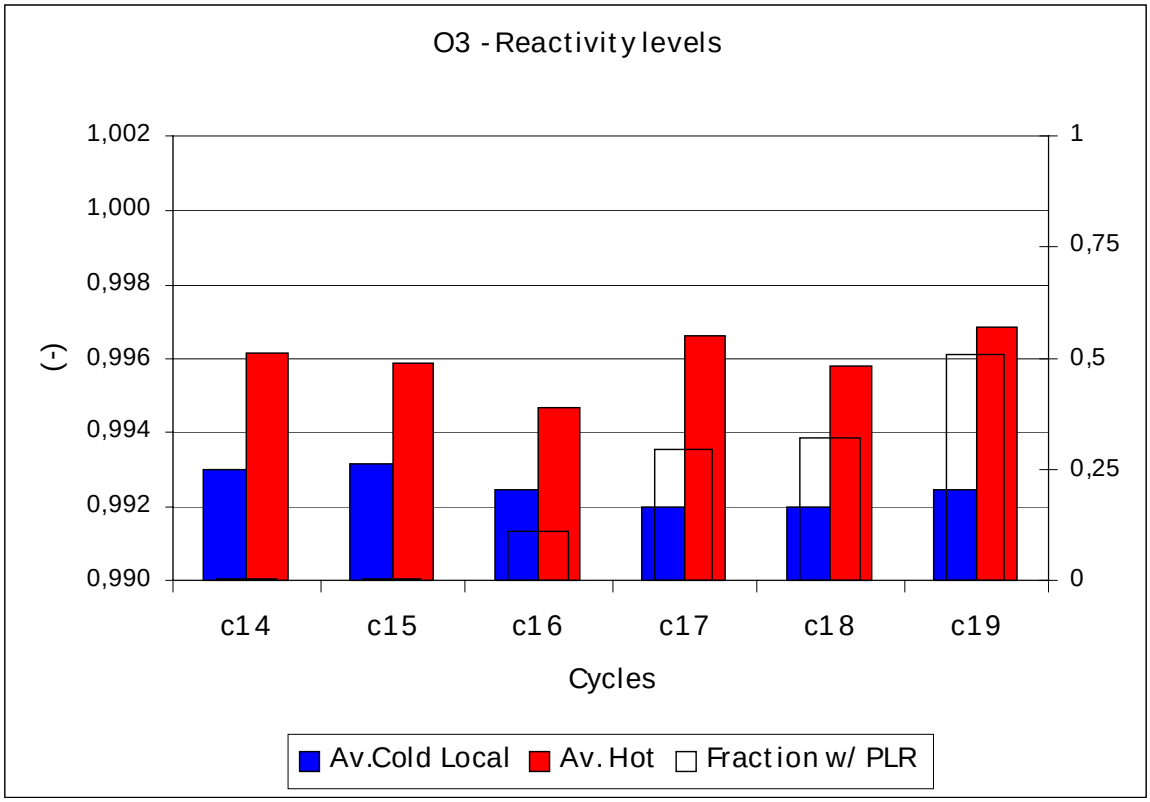
O3 - Reactivity levels
1,002
1,000
0,998
0,996
0,994
0,992
0,990
(-)
1
0,75
0,5
0,25
0
c14
c15
c16
c17
c18
c19
Cycles
Av.Cold Local
Av. Hot
Fraction w/ PLR

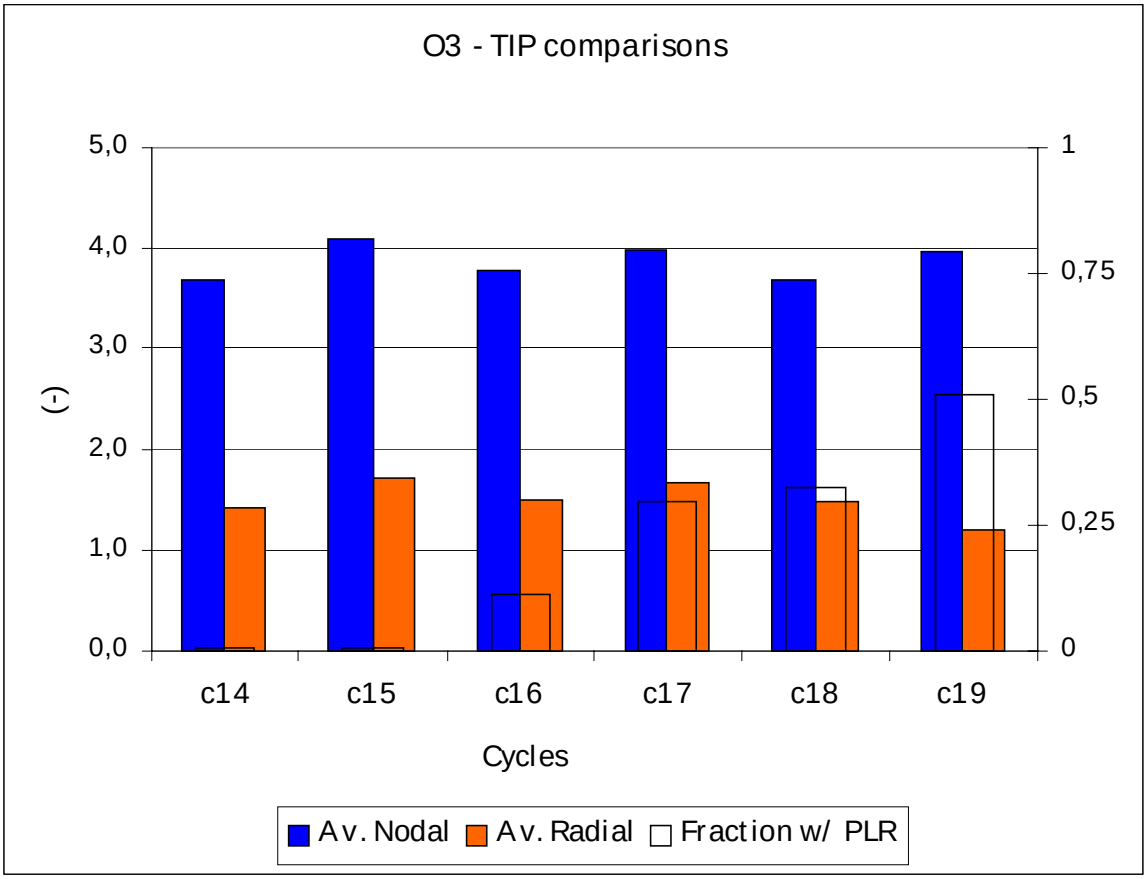
O3 - TIP comparisons
5,0
4,0
3,0
2,0
1,0
0,0
(-)
1
0,75
0,5
0,25
0
c14
c15
c16
c17
c18
c19
Cycles
Av. Nodal
Av. Radial
Fraction w/ PLR

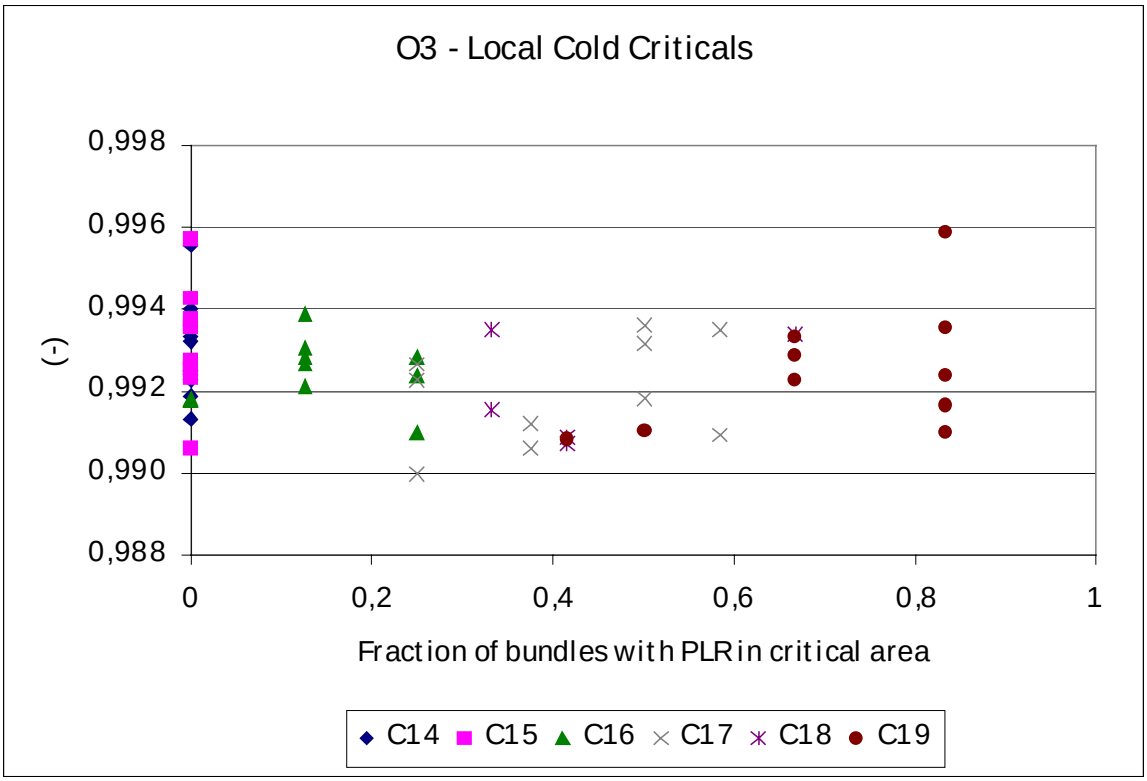
O3 - Local Cold Criticals
0,998
0,996
0,994
0,992
0,990
0,988
(-)
0
0,2
0,4
0,6
0,8
1
Fraction of bundles with PLR in critical area
C14
C15
C16
C17
C18
C19

Summary

- Reference level: no or weak correlation observed with no. of bundles with PLR
- Cold criticals: no or weak correlation observed with no. of bundles with PLR in critical area *(note different measurements techniques)*
- TIP comparisons: in general, no correlation observed.
- At individual TIP positions disregarding the PLR-plenum induces an accuracy degradation
- The methods have performed as expected during the transition to the SVEA-96 Optima fuel designs.

Supporting the SVEA-96 Optima designs with reliable methods

Overall summary

- PROTEUS benchmark
  - demonstrates the reliability of PHOENIX-4
  - Gamma-scanning campaigns at KKL and CNC
  - prove satisfactory performance of POLCA7 under different conditions
- Overall core follow experience
  - demonstrates the reliability of PHOENIX4/POLCA7 over a wide range of reactors and conditions.

Conclusions

- The Westinghouse methods fully support the transition to the new BWR fuel designs
- SVEA-96 Optima fuel designs deliver what is promised

BWR fuel development at Framatome

Dieter Bender & Peter Urban

- Incentives for fuel development so far
- New challenges
- ATRIUM 10 Fuel (today and tomorrow)

Low fuel cycle costs are a key parameter for power generation economics

Typical example for the distribution of power generation costs of a nuclear power plant:

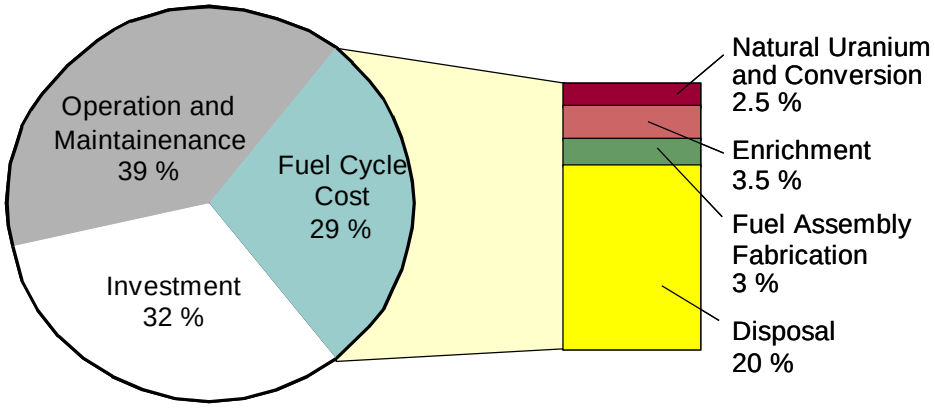

Optimum operation is plant specific and might be subject to change

- The optimum burnup depends on the backend cost model
  - Backend costs specific to fissile weight favor high burnup; medium burnup might be the optimum for burnup specific costs

- The optimum coast down length as well as the need for load following capability depends on the availability and price of alternative electrical power
  - Abundant hydropower favors long coast down operation
  - Expensive alternative base load power favors short coast down operation in spite of higher fuel cycle costs

- Good overall economics favor investments in power uprate

- The most limiting fuel parameter (MCPR, TMOL, MAPLHGR, core stability) is plant specific

BWR Fuel has to serve a broad spectrum of requirements

Discharge burnup:	40–65 MWd/kgU
Cycle length:	12–24 months
Coast down operation:	0–6 months
Short term cycle changes:	± 5 months
Power density:	45–60 kW/l
Load follow capability:	no constraints
Fuel failure rate:	zero failures
MCPR, TMOL, MAPLHGR, core stability, ...:	margins as high as possible
Manufacturing costs	low enough to allow competitiveness

Enrichment increase was the focus of the last decades

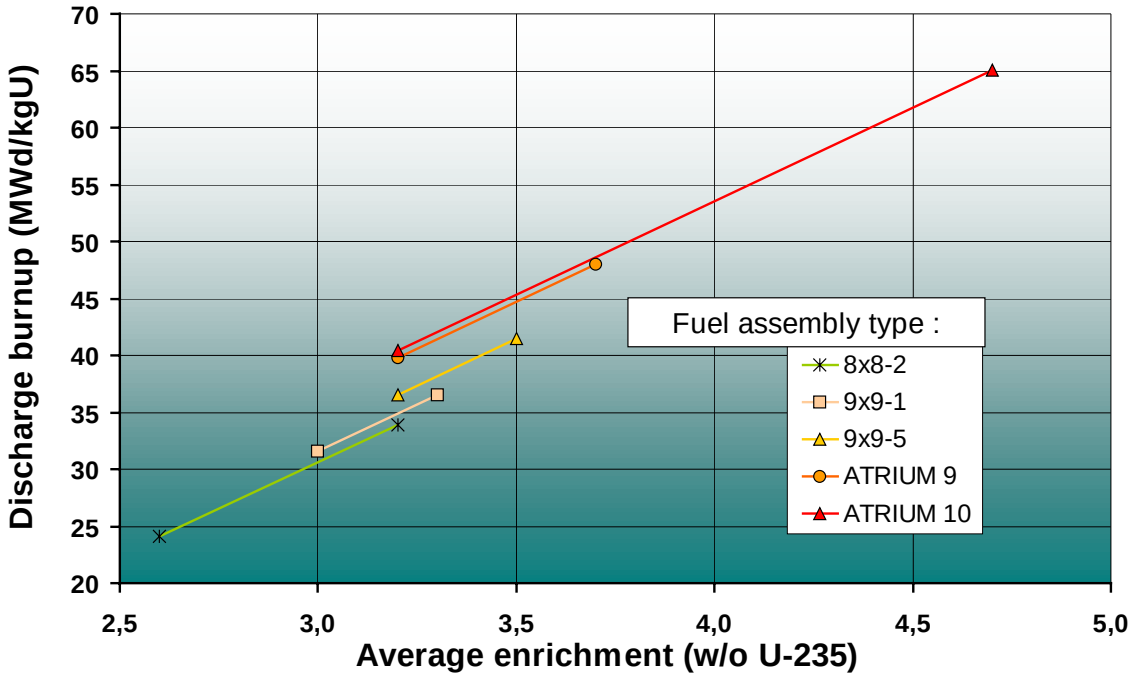

Fuel design played a 2-fold role

- As a „door opener“ to create the operating margins necessary for burnup increase
  - Migration from 8 x 8 to 10 x 10;
    High performance spacers;
    Partlength fuel rods

- As a measure to improve fuel utilization
  - Adjustment of water-to-fuel ratio;
    Large internal water structures

> ATRIUM™10 Fuel

New challenges

- Power uprates (60 kW/l and beyond)

- High energy cycles (18–24 months)

- Combination of both items with high burnup

Further optimization has to concentrate on margins to operating limits

- The optimum discharge burnup is already achieved or is limited by the 5% enrichment limit

- With ATRIUM 10 fuel as a basis, no „low hanging fruits“ wait to be picked

- Fine tuning to plant specific will gain importance

Design flexibility is needed to meet the requirements

ATRIUM™ 10: Design flexibility by high margins to limits

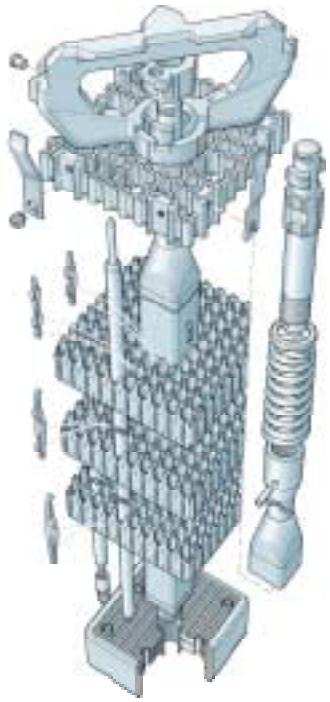

Main Features

- Internal water channel for optimum moderation and with load bearing function
- Easily removable upper tie plate
- ULTRAFLOW™ spacer with superior dryout performance
- Uniform fuel rod design (no tie rods)
- Part length fuel rods for optimum axial fuel distribution and favorable stability performance
- Option FUELGUARD™ as debris filter

The central ATRIUM™ structure provides very efficient moderation

Distributions of the thermal neutron flux

Hot, voided:

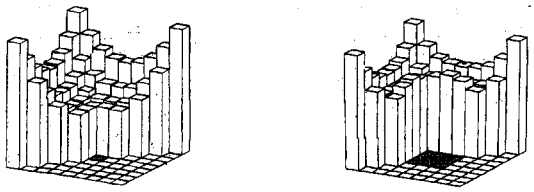

Cold:

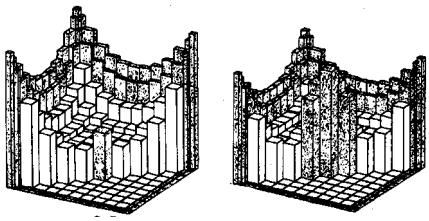

9-1 ATRIUM™ 9

- The more efficient moderation in the hot operating state saves about 0.2–0.3 w/o U-235
- In the cold state the central water structure acts as a neutron trap, thus increasing the hot-to-cold reactivity window
- The void feedback is reduced in a favourable manner, improving tnermalhydraulic/nuclear stability and pressure tansient performance

Design flexibility:
short term rescheduling of cycles

- ATRIUM 10 offers an excellent hot-to-cold reactivity swing
- Further improvement can be achieved by „2-stream“ Gadolinia loading strategies
- Detailed cycle studies demonstrated a flexibility of about 6 months

Design flexibility beyond nuclear design:
ATRIUM™ 10P for low pressure drop

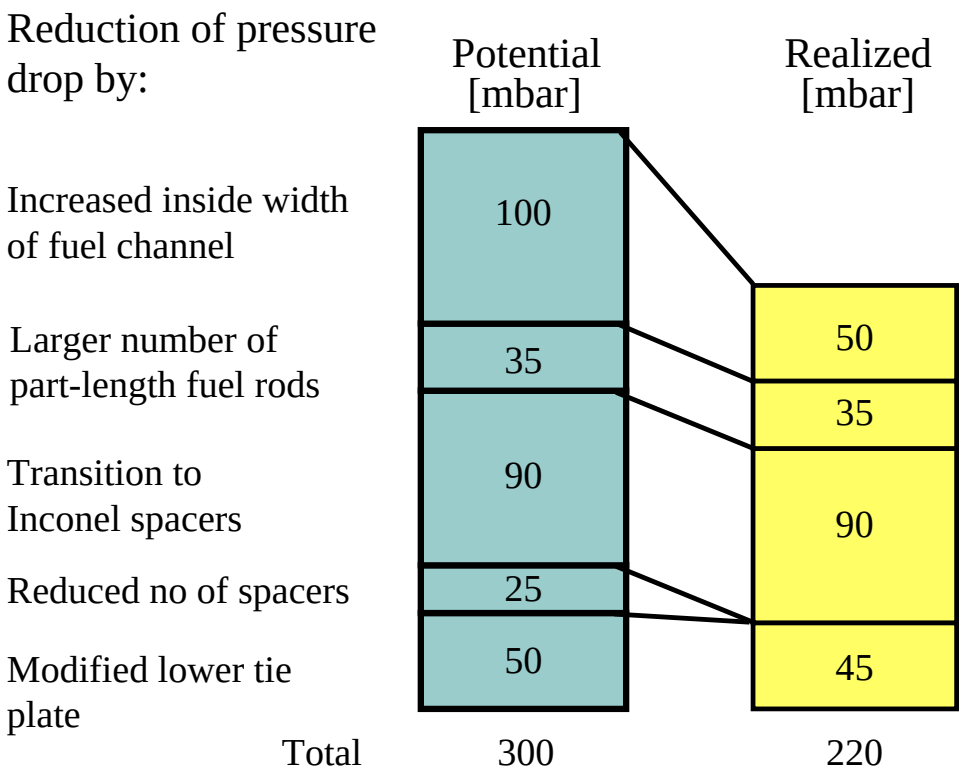

Design flexibility: ATRIUM™ 10XP for better stability and higher fuel weight

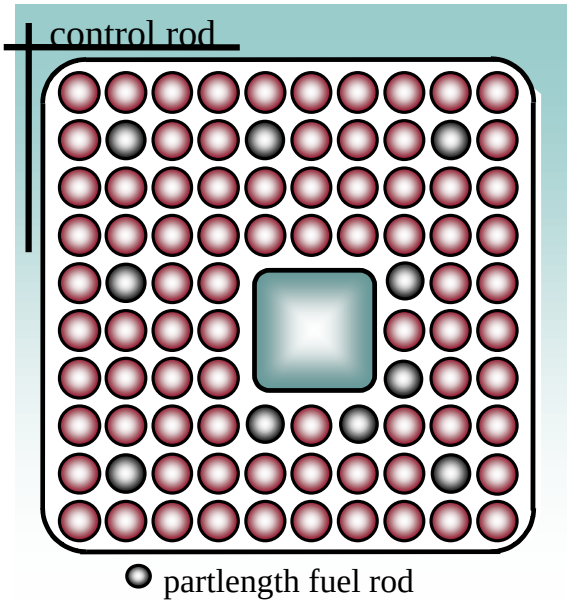

Main Features:

- Increased rod diameter
- Optimized Inconel spacers of „ULTRAFLOW“ type
- 10 partlength rods
- Better stability
- Higher fuel weight

Status of introduction:

Insertion of LTA’s in 2002
(designed for about 60 MWd/kgU)

Further LTA’s in 2004

Part reloads in 2003 and 2004

Full reloads from 2005 on

ATRIUM™10XP

Stability improvement up to 0.2 Decay Ratio

Example: German plant with high power density and burnup

	AT 10B (8 PLFR)		AT 10XP (10 PLFR)	
	DR[1] glob	DR[1] reg	DR[1] glob	DR[1] reg
8 Zry spacers	0.41	0.70		
8 Inconel spacers, 3 „high performance“ spacers; equal Δp			0.33	0.51
8 Inconel AH, 3 „high performance“ spacers; Δp = equal + 50mbar			0.30	0.47

1) Minimum pump speed, highest power flow line, same nuclear parameters

ATRIUM™10XP

Manufacturing of first LTAs

FA top

FA bottom

Conclusions

- Up to now burnup increase was a major driving force for BWR fuel development
- Reaching the 5 w/o U-235 limit and regarding the new challenges from power uprates and longer cycles fine tuning to specific customer needs will become more and more important
- Framatome‘s ATRIUM 10 family with ATRIUM 10A/B, ATRIUM 10P, and ATRIUM 10XP form an excellent basis for this ongoing process

Direct heating in a BWR assembly – investigations with the HELIOS lattice code

Waldemar Lipiec
Fuel Engineering
+46 21 347493
waldemar.lipiec@se.westinghouse.com

What is direct heating?

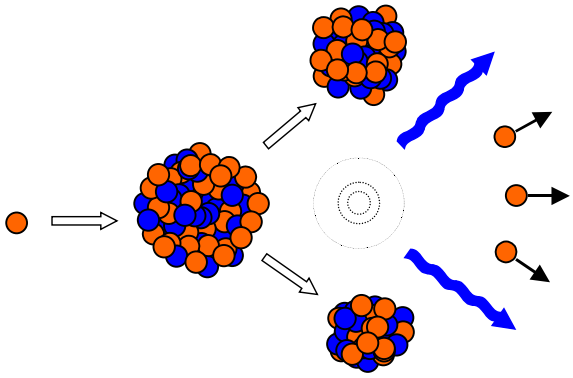

Direct heating: prompt transfer of fission energy to non-fuel regions.

Two physical processes involved:

- gamma radiation and absorption:
  - fission gamma
  - neutron absorption gamma
- neutron scattering and slowing down

Thermo-hydraulic and dynamic aspect

- No time delay in the heat transfer from fuel to non-fuel regions (active coolant, bypass, canning, box)
- Instant response to changes in the fission rate

⇩

Fission rate dependent heat source is also present in non-fuel regions and the corresponding term must be included in the thermo-hydraulic models of a reactor.

How direct heating is modeled?

Typically, it is represented in models as a fraction of the total fission power on per region basis:

$\gamma_{coolant}$, γ_{gap}, $\gamma_{int\ channel}$, γ_{can}, γ_{box}.

In general: direct heating fractions (DHF) are functions of many state parameters:

$\gamma = \gamma(\rho_{coolant}, \rho_{gap}, \rho_{int\ channel}$, burnup, CR, bor)

In practice (now): DHF's are functions of coolant density:

$\gamma = \gamma(\rho_{coolant})$

Is this good enough?

… and what are the values?

Generally: fuel type dependent

Practically: generic values and some prescribed rules are used for coefficients in DHF formulas as the ones in the current POLCA7/POLCA-T model:

$$\gamma^i = \gamma_0^i + \gamma_1^i(\rho_{cool} - 1), \quad i = cool, bypass, int\ channel$$

Sometimes even constant values are used.

Is this justified?

To answer the questions

State of the art simulations of a BWR fuel assembly (SVEA-96) using pure physics:

- energy deposition by neutron scattering
- gamma heating (scattering and absorption)

Done with the lattice code HELIOS v1.7 and the latest cross section library (45-neutron, 18-gamma energy groups)

Assumptions

Assembly

Type: SVEA-96
Enrichment: 3.97% U-235
Burnable absorber:
12 rods with 4% Gd_2O_3

Parameter range

Burnup:
0–80000 MWd/tU
Coolant density factor:
1.0–0.2 (one is water)
No bor, no CR

The results

Total heating from neutrons

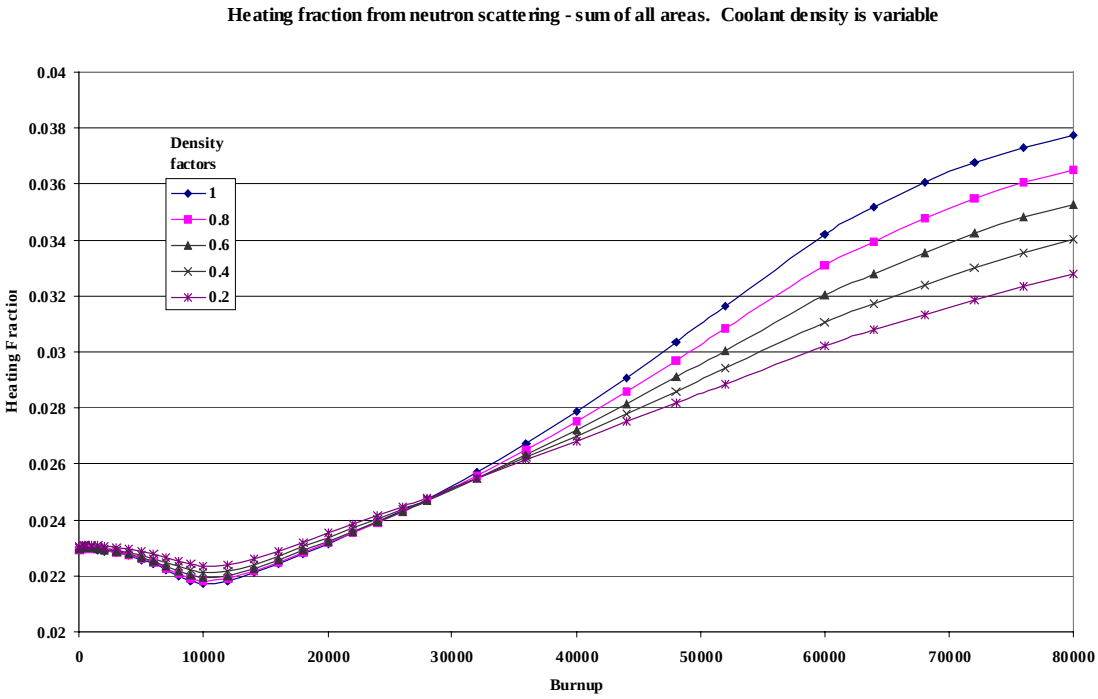

Total heating from gamma

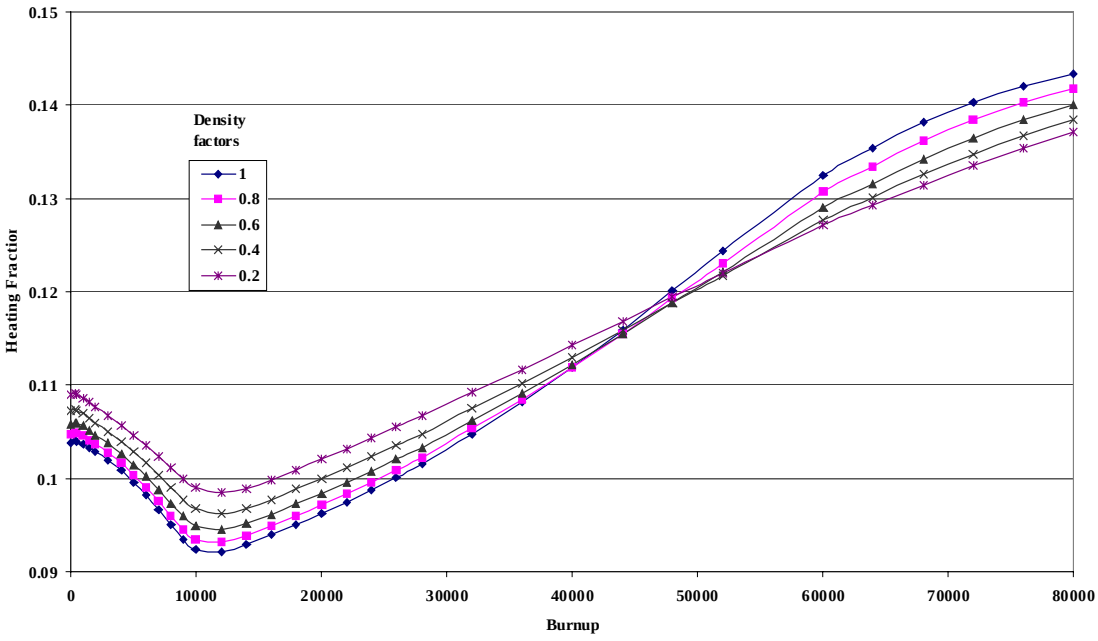

DHF for water cross

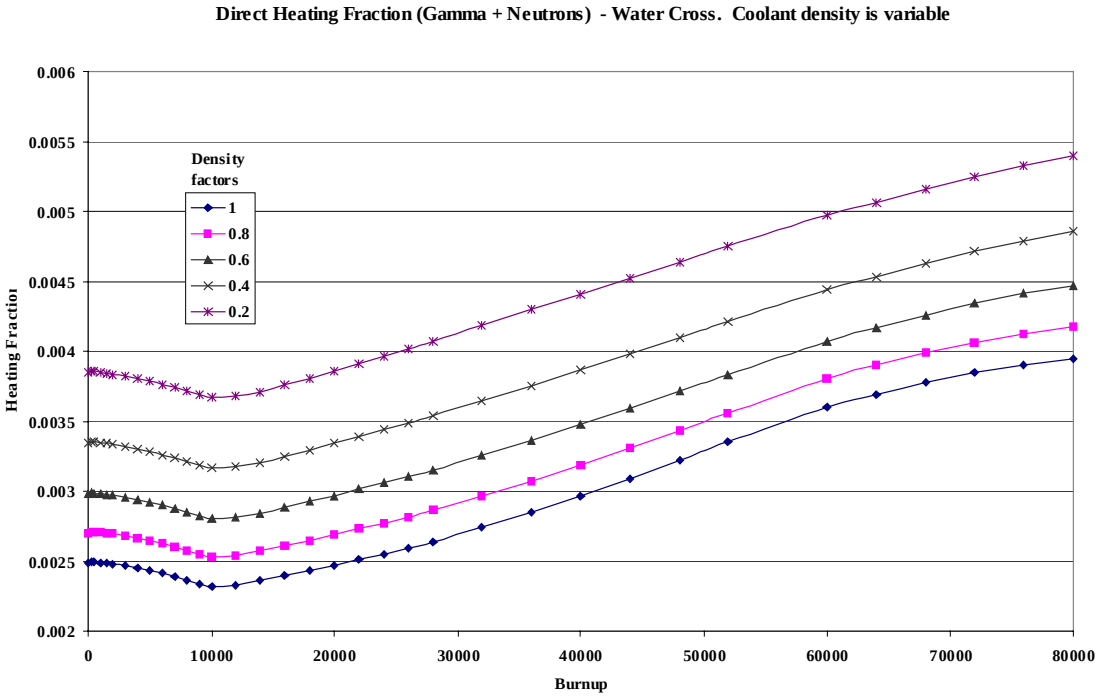

DHF for coolant

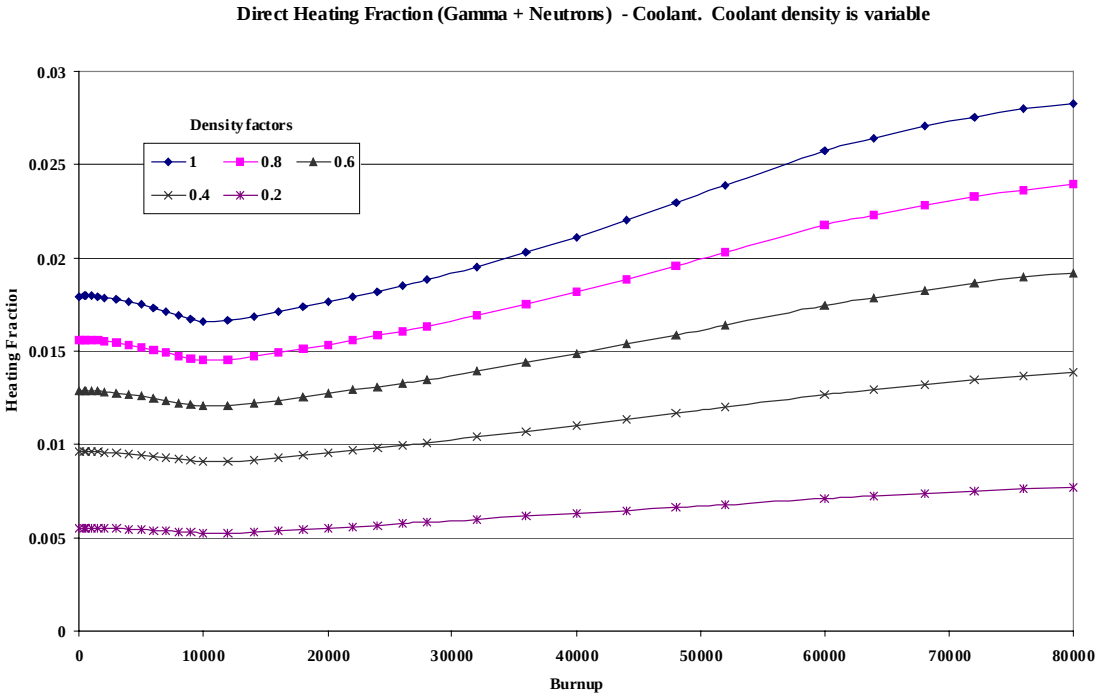

DHF for gap

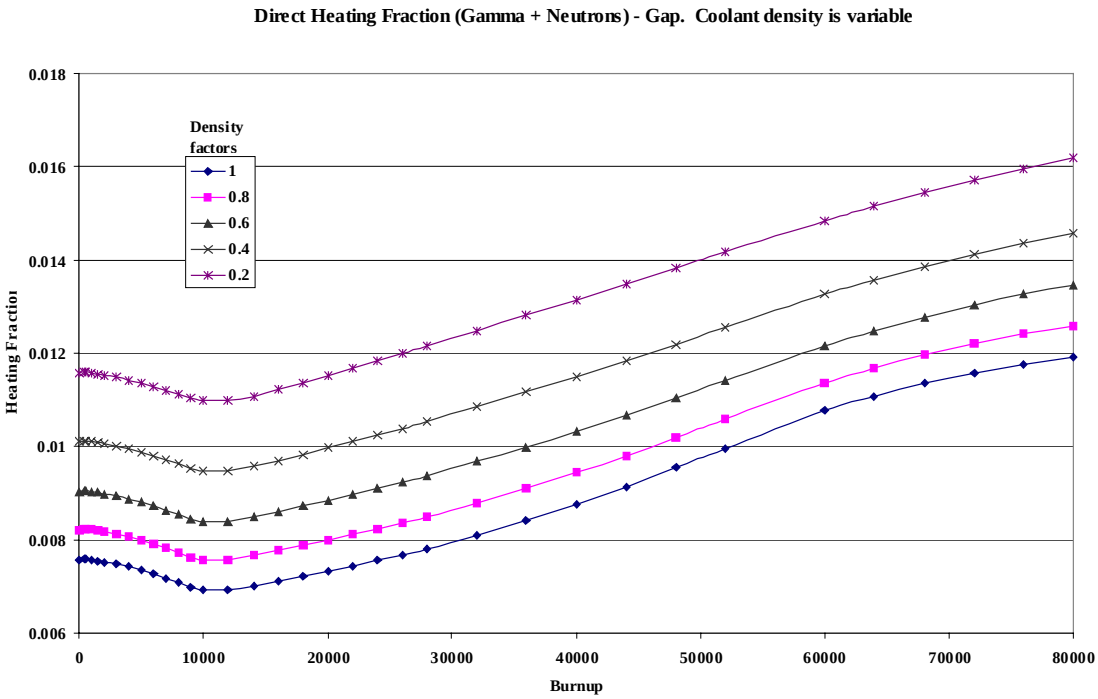

DHF for box

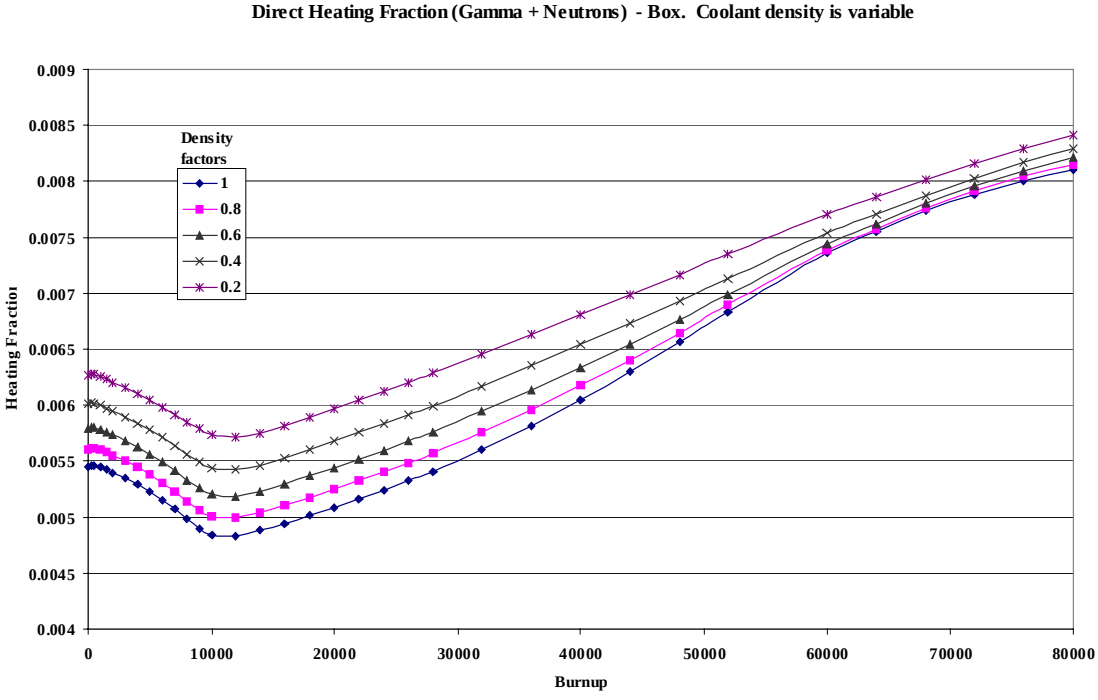

Some observations

Changes of DHF with coolant density fraction (1.0 to 0.2):

- for coolant: decrease more than 3.5 times
- for water cross and gap: increase by about 55%

Changes of DHF with burnup (0 to 80000 MWd/tU):

- for coolant:
  - increase by almost 60% (no void)
  - increase by about 35% (high void)
- for water cross and gap: increase by about 40% (almost coolant void independent)

… and some conclusions

- Coolant void is by far the predominant factor for DHF in the coolant region (rather obvious)
- For the coolant region, burnup influence is about 4 time lower than void, but it is still important
- Both coolant void and burnup are equally important factors influencing DHF of non-active coolant regions

The results

Coolant DHF as a density function

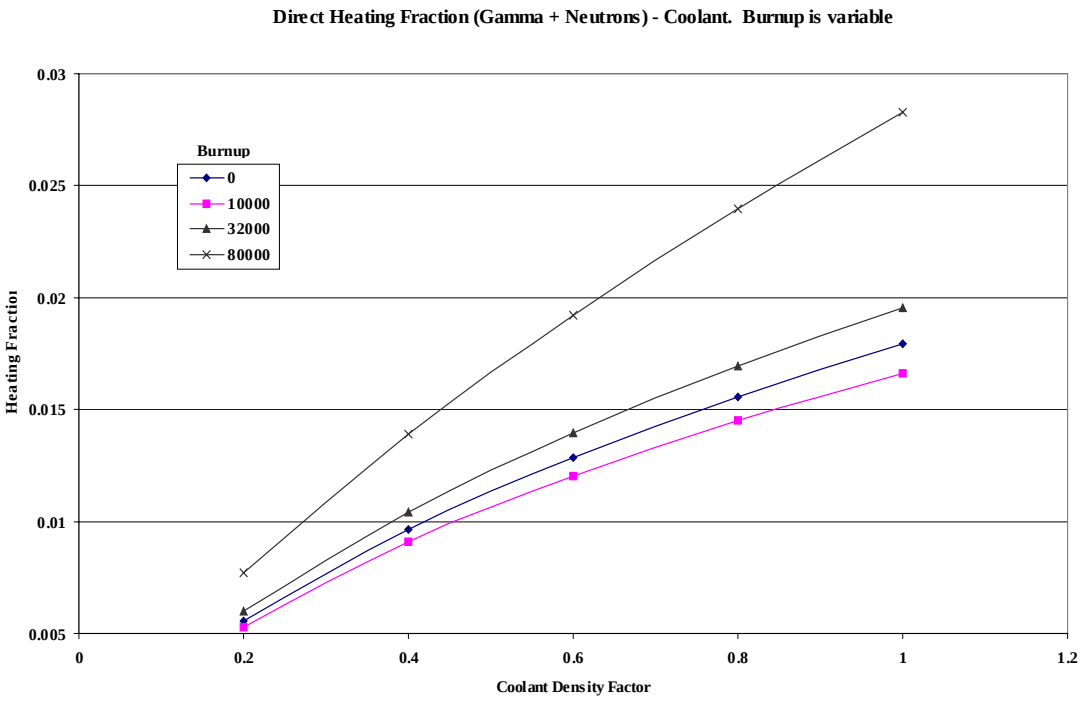

POLCA7 model vs HELIOS data

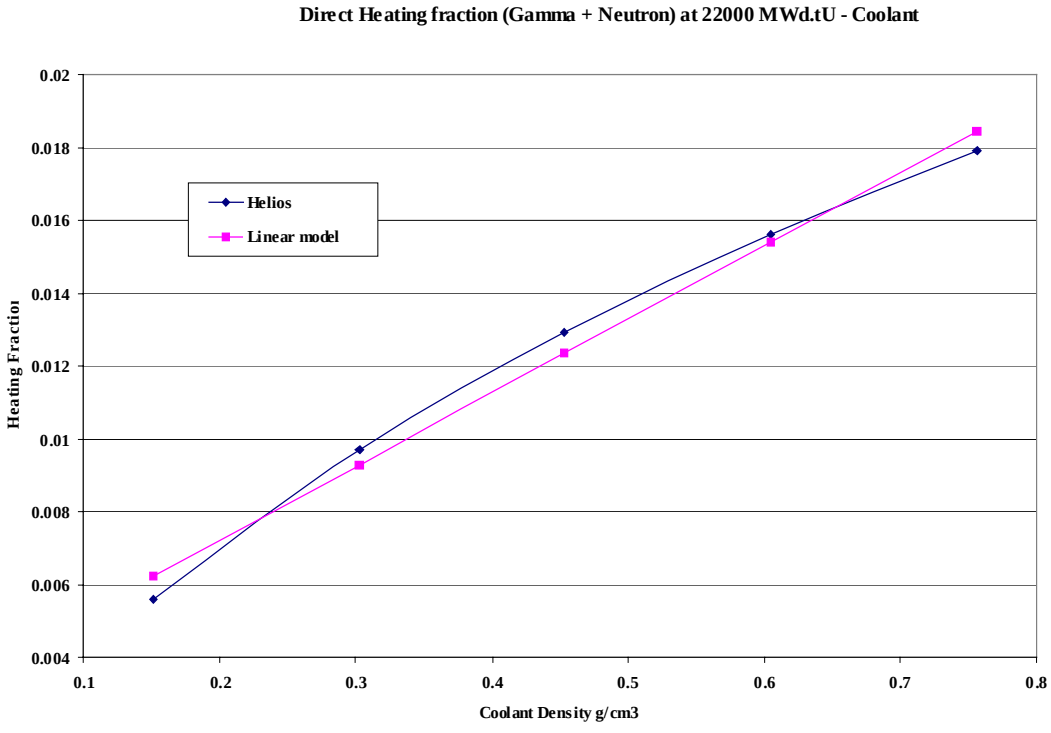

Can we do better?

Yes.

… but that’s another story
that is not quite finished yet.

Gamma scanning evaluation with PHOENIX4/POLCA7 on fuel rods in Barsebäck 1

Per-Olov Andersson, Westinghouse
Phone +46 21 347 343
E-mail per-olov.x.andersson@se.westinghouse.com

Gamma scanning campaign

- Measurements performed at the Barsebäck 1 (B1) NPP in January/February 2000
- Unique conditions: Only few weeks after a 2,5 months operating cycle
- Two SVEA-96S fuel assemblies were measured: #23177 and #23199

Gamma scanning equipment

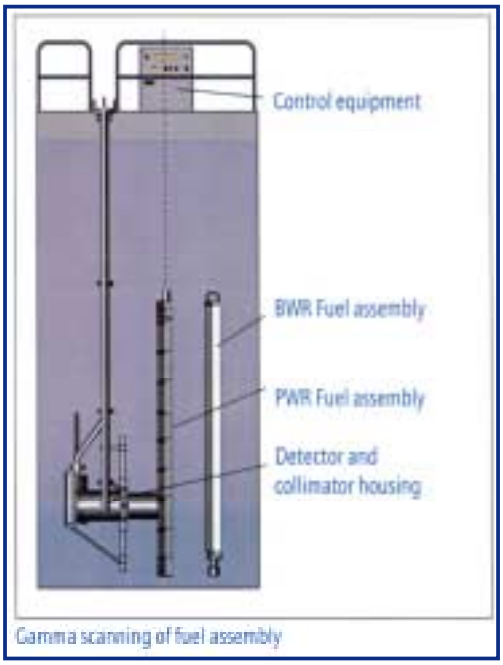

Gamma scanning of fuel assembly

- Ge-detector
- Measurements over 25 equally sized axial nodes
- For power measurements: Use of the gamma radiation 1596 keV peak in ^{140}La
- Decay of ^{140}La controlled by mother nuclide ^{140}Ba

Assembly characteristics – SVEA-96S

	23177	23199
Avg burnup:	9,7 MWd/ kgU	1,9 MWd/ kgU
Avg enrichment:	2,96%	2,96%
BA-rods:	9 x 3,00% Gd_2O_3	9 x 3,00% Gd_2O_3
Pins scanned:	25 (6 BA-rods)	30 (7 BA-rods)

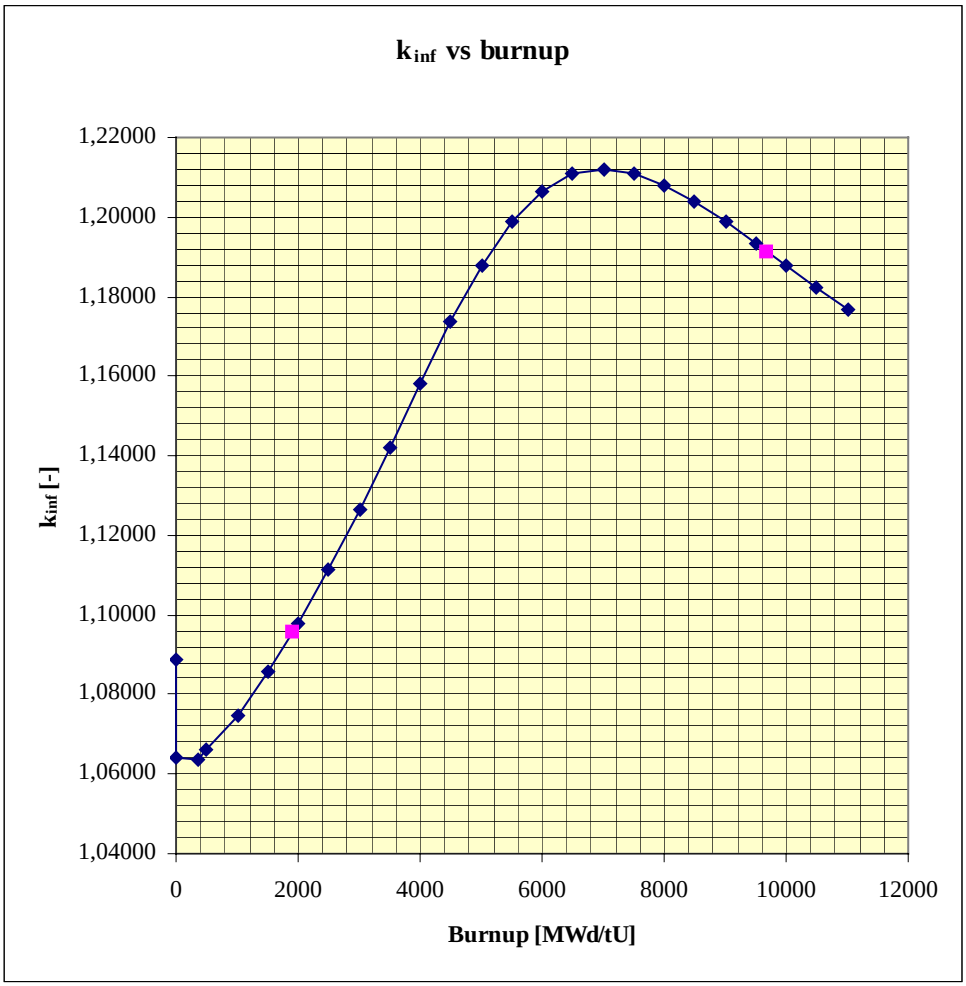

Core location of assemblies

1801	1455	1807	1793	1797	1461	1813				
1889	1885	1903	1891	21701	1823	1771	1811			
22809	23133	1847	23153	1871	23121	1841	1775	1751		
23139	21669	23131	21695	24025	22853	23137	21661	1915	1895	
21675	23185	96003	24027	22849	23187	22791	23173	1873	1837	1747
24029	1827	23165	1851	24033	1853	23197	22815	23149	1845	1753
22835	24037	1829	22845	22801	23147	21673	24089	22865	96001	1831
22859	1907	23189	22811	22863	21705	24039	1881	23179	21671	1791
1893	23183	1899	23181	21691	24043	21681	24045	22793	22847	1769
24047	1909	23135	21677	24049	21685	24051	22855	23145	1905	1805
22851	23167	1759	22867	22805	23123	22807	1883	22861	1739	1839
22799	1887	24055	22843	22813	21703	24057	21665	23155	21687	1745
1821	23169	1765	23171	1819	24059	1913	24061	22837	21689	1767
24063	1859	23157	21693	24065	1917	24067	1849	23163	22857	1777
22839	23151	1861	22821	22871	24073	22841	21699	22827	1901	1713
22833	1855	24069	22829	22795	22819	23195	1863	23122	1843	1757
1869	24071	1761	23175	21663	24075	22797	24091	23143	1865	1539
24035	22803	23201	1825	24079	21667	23125	21679	1877	1867	1809
1879	23199	22823	23161	22831	24083	23141	22817	1911	1817	
23177	21697	23159	1763	23124	22869	1897	1835	1743		
1755	1857	1875	21683	22825	1781	1799	1815			
1737	1749	1741	1773	1789	1459	1803				

Calculations and normalizations

- PHOENIX4/POLCA7 with the Core Master 2 system
- Nodal pin-wise ^{140}Ba distributions explicitly computed
- Standard production modeling
- Measured and calculated distributions normalized to unity
- Two different normalizations
- Over all pin segments in an assembly

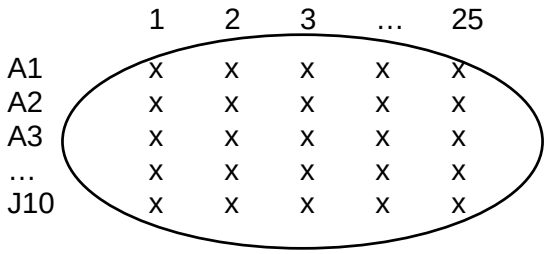

Results of concern:

Differences (calc-meas), $RMS_{overall}$, RMS_{rad}

”Total error”

- Locally, over pin segments in a given axial level

	1	2	3	…	25	(i)
A1	x	x	x	x	x	
A2	x	x	x	x	x	
A3	x	x	x	x	x	
…	x	x	x	x	x	
J10	x	x	x	x	x	

Results of concern:

Differences (calc-meas), $RMS(i)_{nodal}$, $Avg\text{-}RMS_{nodal}$

”Pin reconstruction error”

Overall normalization, results

Pin average errors:

23177

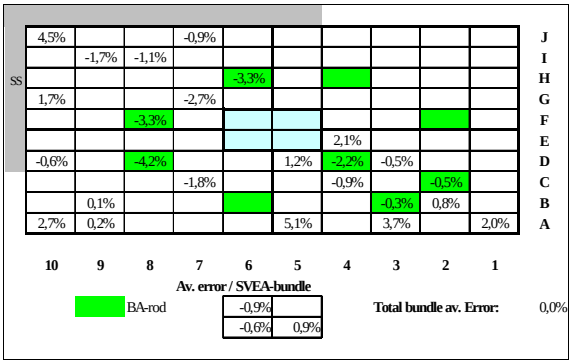

23199

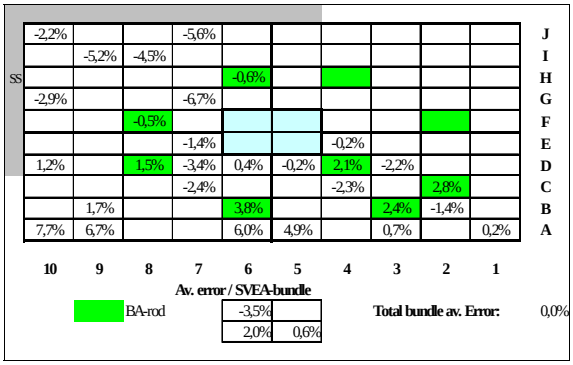

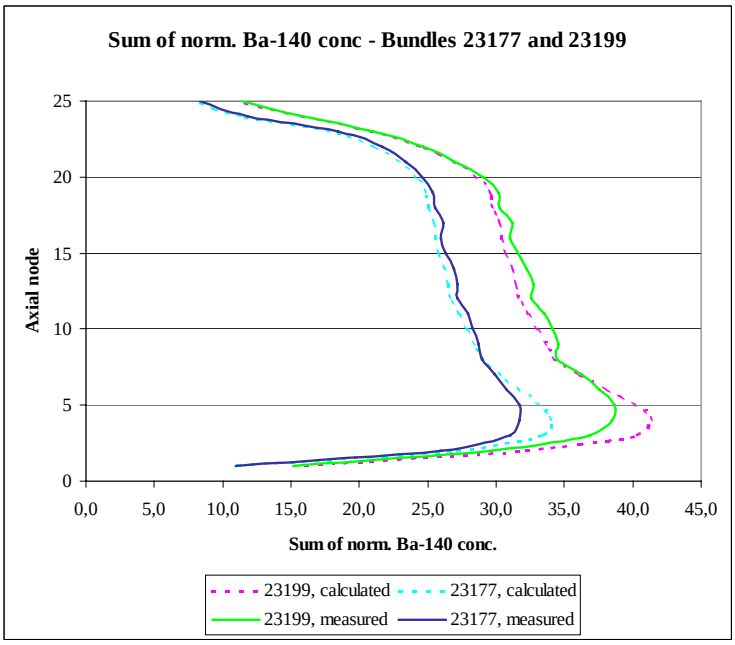

Nodal average errors vs axial level

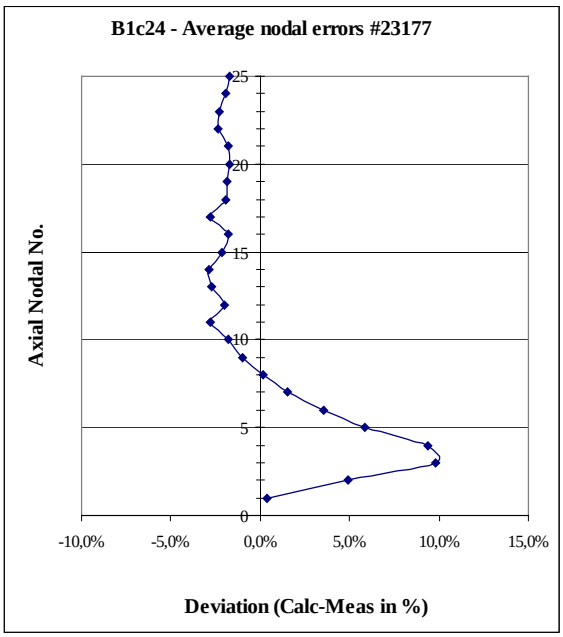

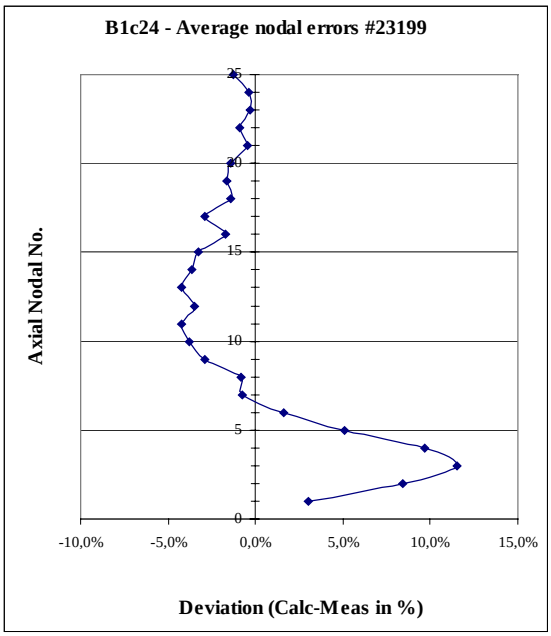

	23177	23199
$RMSe_{overall}$:	4,7%	6,0%
$RMSe_{radial}$:	2,4%	3,5%

- $RMSe_{overall}$ = an estimation of the accuracy in the calculation of fuel segment power
- $RMSe_{radial}$ = an estimation of the accuracy in the calculation of fuel rod power

Local normalization, results

Pin average errors:

Demonstrates each assembly's radial power error (axial error eliminated)

23177

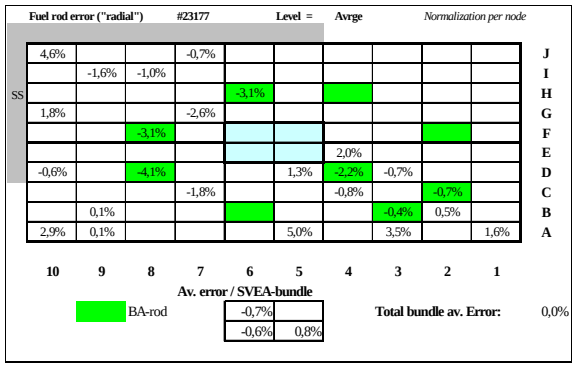

23199

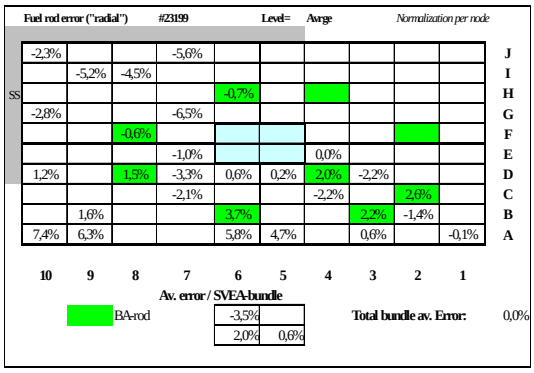

	23177	23199
Avg-RMSe$_{nodal}$:	2,9%	4,0%

(indicates uncertainty in pin power reconstruction model)

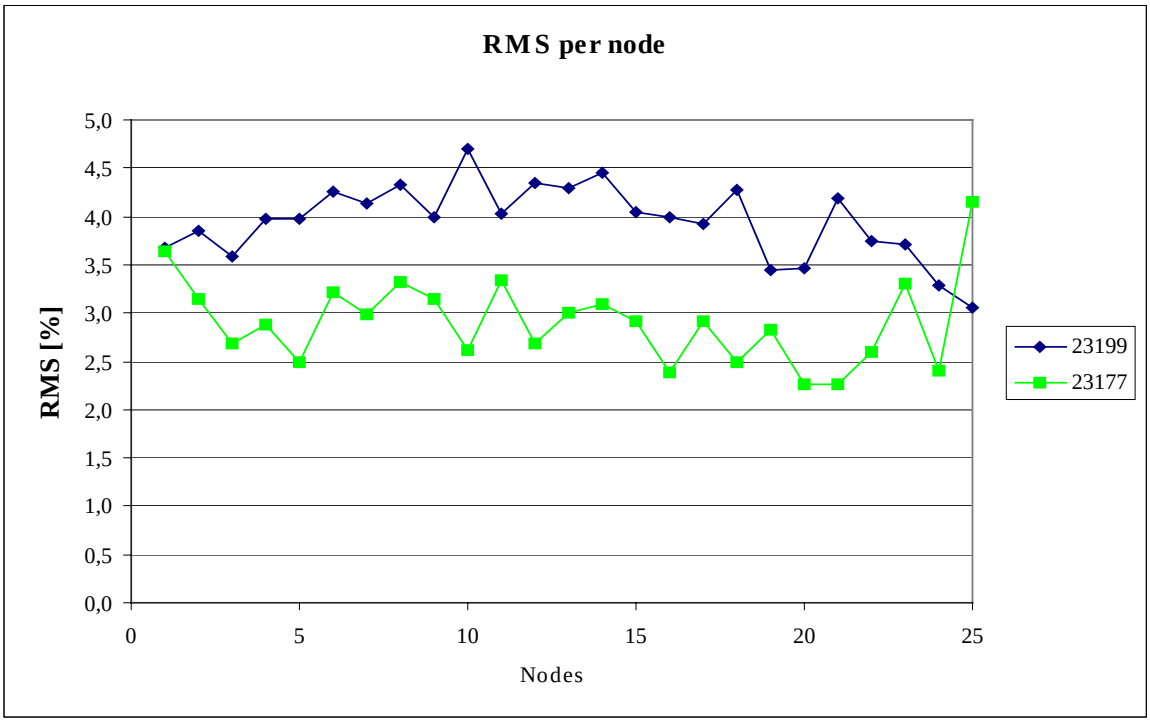

Conclusions

- PHOENIX4/POLCA7 predicts the internal pin power (^{140}Ba) distribution accurately
- Measurement errors/inaccuracies not accounted for
- Axial errors due to nodal solution (in agreement with TIP comparisons)
- Possible systematic error in Gd burnup rate
- Differences in results between both assemblies
  - Gd depletion at different stages
  - Different “environments” in core
  - True dimensions not considered

Simulation of reactor scram experiments in the Loviisa and Mochovce VVER reactors

Pertti Siltanen
Fortum Nuclear Services Ltd
Vantaa, Finland

Elja Kaloinen & Frej Wasastjerna
VTT Processes, Nuclear Energy
Espoo, Finland

Abstract

The paper summarises the experience and understanding gained in 3-D simulation of rod drop experiments, including the dynamic behaviour of the core, the signal of an ex-core ionization chamber, and the performance of a reactivity meter. The predicted output of the reactivity meter is compared with the output observed during the experiment. Simulation results are presented for reactor scram experiments performed on the VVER-440 reactors Loviisa-1&2 in Finland and on Mochovce-1 in Slovakia. The results show that a prediction accuracy of 5 % for reactor scram with or without a stuck control rod can be achieved. This demonstrates the overall good performance of the applied code system consisting of fuel data generated by CASMO-4, control rod data and detector response data generated by MCNP4B, and of the 3-D core dynamics code HEXTRAN. In particular, there are no significant errors in the modelling of VVER-440 control rods.

1. Introduction

In VVER reactors, rod drop experiments are typically performed for full reactor scram and/or for reactor scram with a stuck control rod. These experiments are typically performed at beginning of cycle in hot critical conditions. The drop time of the VVER-440 flux-trap type control rods is of the order of 10 seconds. Negative reactivity up to -10 % or -15 dollars can be involved. Most notably, the control rods introduce strong distortions into the neutron flux distribution.

Typically, the reading of a reactivity meter connected to an ex-core ionization chamber does not correspond to the calculated change in the static reactivity of the core, based on calculated k_{eff} values and a calculated β_{eff} for the core. Differences up to 30 % relatively are observed. This situation sets special requirements on the correct interpretation of these measurements. The measurements have good repeatability and hence they carry fairly precise information on the dynamic characteristics of the core.

Earlier attempts to explain the situation by simplified models, such as a 2-D prompt jump approximation for the core, were not entirely successful. In the late 1990's it was decided to model the experiment by full 3-D dynamic simulation of the experiment, including the core, the response of the ex-core ionization chambers, and finally the performance of a point kinetic reactivity meter. This approach proved to be successful. The entire simulation can be considered as an exercise in code system validation.

This paper summarises the experience and understanding gained in simulation of rod drop experiments. Final simulation results are presented for reactor scram experiments performed on the VVER-440 reactors Loviisa-1&2 in Finland (initial criticality 1977 & 1980) and on Mochovce-1 in Slovakia (initial criticality 1998). Both initial and burned cores as well as full and reduced cores are involved. The results have been reported previously at other meetings, particularly symposia of AER [1, 2, 3, 4].

2. The point kinetic reactivity meter

A reactivity meter solves the reactor kinetics equations of a point reactor for the reactivity in dollars (ρ/β), given the time-dependent neutron flux φ(t) or a proportional detector signal. Based on standard kinetics equations, the inverse point kinetics equations can be written in the useful form [1]

$$\frac{\rho}{\beta} = 1 + \frac{\Lambda}{\beta}\frac{d\varphi/dt}{\varphi} - \frac{1}{\varphi}\left[\sum_i \frac{\beta_i}{\beta} C_i' + \frac{\Lambda \nu}{\beta} Q\right]$$
$$\frac{dC_i'}{dt} = \lambda_i(\varphi - C_i') \;;\; i = 1,\ldots,6 \;. \qquad (1a, 1b)$$

Here the quantities C'_i are no longer the original concentrations of delayed neutrons C_i, but have been transformed by constant coefficients according to

$$C_i' = \frac{\lambda_i \Lambda \nu}{\beta_i} C_i \;. \qquad (2)$$

These quantities have the dimension of the neutron flux φ, as is evident from equations (1b). They are in effect filtered values of the neutron flux, obtained by simple filtering of the measured time-dependent neutron flux using different time constants λ_i according to equations (1b).

If we set the external source Q = 0 and let the neutron generation time $\Lambda \to 0$, then equation (1a) can further be simplified into the form

$$\frac{\rho}{\beta} = 1 - \frac{\varphi_d}{\varphi} \text{ , where } \varphi_d = \sum_i \frac{\beta_i}{\beta} C_i' \;. \qquad (3)$$

The quantity φ_d is a delayed neutron flux value obtained as the weighted average value of the filtered neutron flux values. The reactivity in dollars at any particular time is determined by the ratio of the delayed and instantaneous neutron flux values. A more physical interpretation is that the reactivity at any time is determined by the ratio of the magnitude of the delayed neutron source and the actual neutron flux level that is maintained by this source. This prompt jump approximation is helpful in understanding how the reactivity meter essentially works.

Particularly for large negative reactivity insertions, a reactivity meter is unable to distinguish between different causes of jumps (or changes) in the neutron flux. Aside from a real reactivity change, all effects that influence the proportionality between a detector signal and the rate of fission neutron production in the core will distort the reactivity reading of the meter. A typical distortion is caused by a change in the spatial neutron flux distribution, such as that due to the drop of control rods. Also, the kinetic parameters of the meter can differ from the true ones governing core behaviour.

In Appendix A, results of numerical tests are given for a simplified model of the core, local detector, and reactivity meter. Even with perfect kinetic data, the recovery of the reactivity meter reading towards the correct reactivity value is extremely slow, when the reactivity insertion exceeds one dollar of negative reactivity.

3. Simulation of rod drop experiments

Reactivity measurements during rod drop experiments are used extensively on VVER reactors. Particularly for reactor scram with or without stuck control rods, it is now well understood that the reading of a reactivity meter connected to a particular ex-core ionization chamber does not represent the desired static reactivity worth of the dropped rods. One approach to utilising the measurements for code validation is to simulate the entire dynamic experiment and to predict the reading of the meter. This prediction can then be compared directly to the measurement.

3.1 Simulation steps

The complete simulation of a rod drop experiment such as reactor scram involves three major steps. These are briefly described below.

The first step involves the simulation of the time-dependent behaviour of the neutron flux and production of fission neutrons in the core using a 3-dimensional core kinetics model. The simulation extends over the useful time interval of the experiment, typically no more than 100 seconds. The nodal code HEXTRAN at VTT Processes was used for this purpose [5]. The code requires both static 2-group data and neutron kinetics data for all nodes in the core. These have been generated with the assembly code CASMO-4/hex using a data library based mostly on ENDF/B-IV. Neutron kinetics data are based on ENDF/B-V.

The second step involves the simulation of neutron transport from the core nodes to the different locations of ionization chambers outside the core. This problem can be solved for a particular core configuration by precalculating the detector response to a fission neutron source in each node of the core. Relative values of the thermal neutron flux at the detector locations are sufficient to simulate a proportional detector signal. These calculations have been performed with the Monte Carlo code MCNP4B using adjoint calculations for the appropriate core geometry and chamber location [2]. The resulting precalculated detector response kernels are applied in HEXTRAN by folding them with the fission neutron source distribution to generate simulated detector signals.

The final step is the simulation of the reactivity meter used in the experiment in order to obtain a prediction of the actual measurement. This implies the use of inverse point kinetics with the particular set of kinetics parameters that have been used in the meter during the experiment. In terms of required calculations this is the simplest part of the whole simulation. It is performed separately after the HEXTRAN calculation.

3.2 Detector response kernels

Figure 1 illustrates the overall transverse geometry of the core and surrounding structures up to the serpentinite concrete shield containing the channels for ionization chambers. Azimuthally, there are altogether 24 channels 15° apart. Due to the geometric symmetry of the core periphery, there are only three geometrically differing channel locations that are shown on Figure 1. Axially, the ionization chambers are located at core mid-elevation and have a sensitive length of ca. 30 cm. This geometry is applied to determine detector response kernels; with or without 36 shield assemblies (dummies) made of stainless steel in the core periphery.

Figure 2 illustrates the spatial behaviour of the detector response kernel in one case for a full core, averaged axially over the fuel assemblies. The influence of the fission neutron source on the detector is reduced by approximately one order of magnitude for each layer of fuel assemblies into the core. However, azimuthally the response is relatively wider. This is evidently due to the streaming of neutrons in the air gap outside the reactor pressure vessel.

Prompt fission neutrons give the main contribution to the detector signal. The relative importance of delayed neutrons is only ca. 0.03 due to their lesser migration. In a full scram (typically k_{eff} = 0.9) up to 10 % of all source neutrons are delayed. Nevertheless, their contribution to the signal is only 0.3 % and is ignored in HEXTRAN.

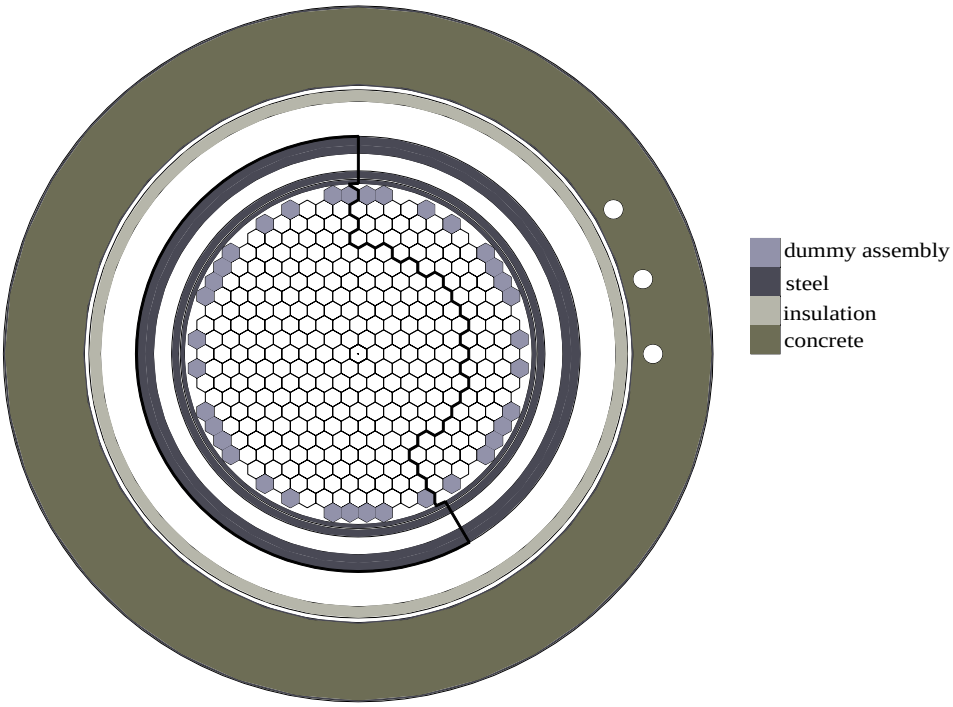

Fig. 1. Overall transverse geometry. The thick line is the boundary of the excluded part of the reactor in MCNP4B calculations of detector response.

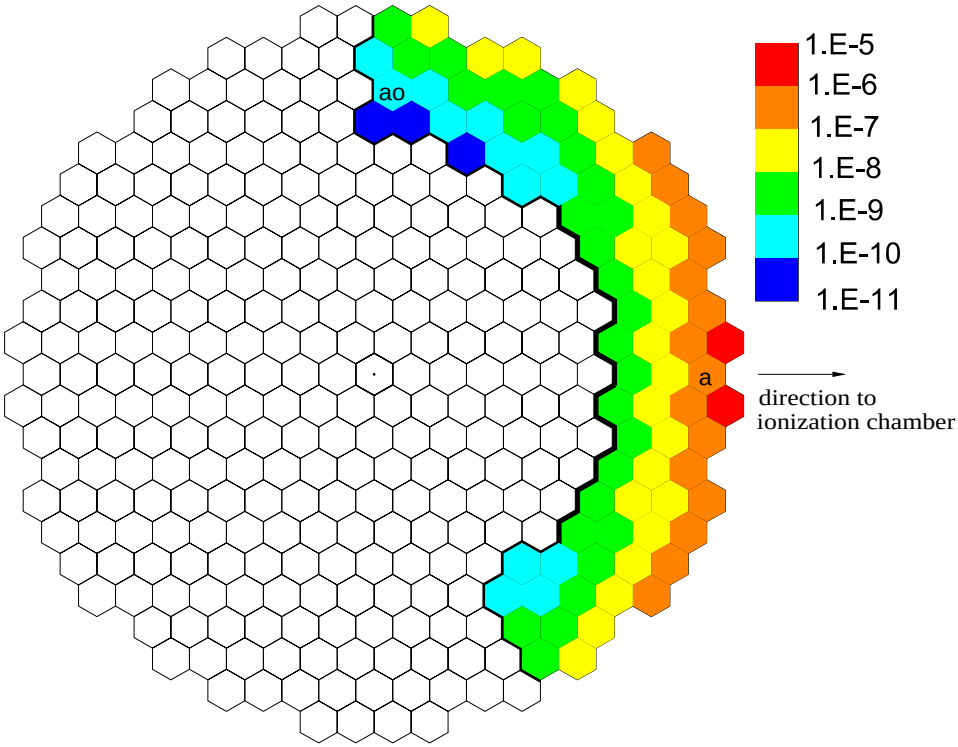

Fig. 2. Approximate spatial dependence of a detector response kernel averaged over fuel assemblies.

3.3 Improvements and weaknesses in HEXTRAN and data

Several improvements have recently been introduced into the HEXTRAN code and/or to the given input data [4]. These are briefly reviewed here.

The description of VVER-440 control rods by albedos in HEXTRAN has been extended to include a full response matrix consisting of partial albedos from face-group to face-group. Each partial albedo gives the probability of neutrons entering the control rod through a given face in a given energy group (incoming current) to leave the control rod through another given face and energy group (outgoing current). This model is capable of describing the net transport of neutrons through the control rod in steep flux gradients across the control rod. The code MCNP4B was used to calculate the two-group partial albedos for the boron steel zone of the control rod. In test calculations for the initial core of Loviisa NPP the new albedos were found to influence the static reactivity worth of all control rods relatively by +4.5 %. The partial influence of applying partial albedos instead of total albedos was +2.5 %.

In a two-group model of the core no explicit distinction is made between prompt fission neutrons and delayed neutrons. Both types of source neutrons are born in the fast group, even though they have different energy spectra. Their mutual importance to the chain reaction must be weighed separately and an effective fraction (β_{eff}) must be determined for the delayed neutrons born in each node. The formally correct importance weighting for neutrons of different energy is given by the spectrum of the adjoint flux in each node. However, this spectrum is not precisely known in advance. In CASMO-4, the adjoint spectrum is determined by assuming zero buckling, i.e. no leakage. This is an approximation for large cores; a basis has been demonstrated by K. Smith [6]. In HEXTRAN the delayed neutron fractions are determined separately for each node, but the time constants of the delayed neutron groups are common to the whole core and are estimated on the basis of core average burnup.

After reactor scram from the hot critical state the reactor becomes deeply subcritical (typically k_{eff} = 0.90). The buckling of the neutron flux in the fuel assemblies increases accordingly and becomes greater than the material buckling. This has an influence on the neutron flux spectrum and hence on the two-group cross section for the fuel, particularly in the fast group. It was found that the migration area (M^2) of neutrons in the fuel increases typically by 2.5 % in a full scram. This enhances neutron leakage into the control rods and the radial reflector, thereby enhancing the reactivity worth of the control rods by ca. +3 % relatively. This effect from non-critical buckling (or system k_{eff}) is not described in HEXTRAN and is a cause for some underestimation by the code.

3.4 Interpretation of results

The predicted output of the reactivity meter can be directly compared with the measurement. In this approach, no specific meaning is attached to the absolute value of the meter reading. Essentially, the reactivity meter can be viewed as an instrument of observation that performs a

useful mathematical transformation of the rapidly changing local neutron flux (detector current) to a much more constant function of time after the drop of the of control rods is over. This is more convenient than comparing rapidly decaying neutron detector current predictions and readings.

The prime purpose of the rod drop tests is to "measure" the reactivity worth of control rods. However, in such strong changes to the core, simple interpretations fail for reactivity meter readings based on ex-core detectors. The experiment becomes an integral test for the ability of the calculation system to predict a large neutronic transient. Both static and kinetic models and data are put to a severe test. Thereby the simulation of the experiment is an exercise in code system validation.

If there is a discrepancy between prediction and experiment, this cannot be simply interpreted as an error of control rod modelling. All models and data need to be examined carefully. In the end, when other sources of error have been exhausted, the control rod model can be adjusted to achieve a better agreement with experimental data. The best static reactivity worth of the control rods is then the one calculated by the validated model for the core.

For small residual deviations between experimental and predicted readings of a reactivity meter, a straightforward approach to obtain a semi-empirical static reactivity worth is the following. The calculated static reactivity worth (ρ) of the control rods is corrected by the ratio of the experimental and predicted readings of the reactivity meter (R) in the dynamic experiment:

$$\rho_{stat}^{\exp} = \frac{R_{dyn}^{\exp}}{R_{dyn}^{calc}} \cdot \rho_{stat}^{calc} \,. \tag{4}$$

Nevertheless, one should always keep in mind the possibility of other sources of error than just the modelling of the control rods. Note for example, that the absolute values of β_{eff} do not influence the reactivity meter, but they do influence the behaviour of the core in the dynamic calculation.

4. Comparisons with measurements

Simulations of actual rod drop experiments were performed with the HEXTRAN code for a representative set of different cores of the Loviisa reactors and for the initial core of Mochovce-1. The set of simulated experiments includes both full scrams and partial scrams with one or two stuck control rods. Both full cores and reduced cores are included. Measurements of reactor scram with a reactivity meter are made during start-up physics test performed in the hot critical state. Signals of one or two ionization chambers located around the reactor are typically available for such reactivity measurements.

In the simulations, the initial state of the core was described as well as possible, including the burnup state of the core, the initial position of the control rods in the regulating group 6, and the

boron concentration in the coolant. Also, the delayed neutron data applied in the reactivity meters of the different experiments was taken into account case by case. Different reactivity meters have been used at different plants and at different times.

In the following, calculated predictions of reactivity meter readings in a given experiment are compared to the actual measured readings. Predictions may also be given for sensor locations without an actual measurement. Although the predictions and the measurements are in fact negative reactivity values, they are reported as positive values of "control rod efficiency".

4.1 Initial cores of Loviisa-1 and Loviisa-2

The initial cores of Loviisa-1&2 are identical full cores. Also, the measurement results for full scram are practically identical. Results for full scram are given in Table 1 and for partial scram in Table 2. Both measured and calculated readings of the reactivity meter are taken about 60 seconds after scram initiation. All relative deviations between calculated and measured values are in a surprisingly tight band -6.9 to -7.6 % for six different measurements. There is a systematic under-prediction, but it is not too big. The absolute static reactivity worth of full scram is calculated to be 11.54 %.

4.2 Burned cores of Loviisa-1

Three different reduced cores of Loviisa-1 with different loading patterns were chosen to represent burned cores up to the present. These cores are:

- Cycle 7 having a traditional out-in-in loading pattern.
- Cycle 19 having a fully low-leakage loading pattern (in-in-out).
- Cycle 24 having a partly low leakage loading pattern for 1500 MW_{th} operation.

The results for full scram are given in Table 3. Results are presented for two different times about 15 and 50 seconds after scram initiation. The latter results are perhaps more representative and comparable to the results for the initial cores. Both the measured and calculated readings show a drift with time in the same direction, but not always at equal rates. There is also a tendency for the under-prediction to get smaller over the cycles. The inaccuracy of recording and then interpreting a representative reading for the reactivity meter is estimated to be no more than 0.5 $ or 2.5 % relatively. The absolute static reactivity worth of full scram is calculated to be 10.26 % for BOC 7, 10.20 % for BOC 19, and 10.08 % for BOC 24 in the experimental conditions.

Table 1. Comparison of calculated and measured values of reactivity meter readings for full scram in Loviisa-1, BOC 1. Initial height of group 6 is 204 cm.

Ionization chamber	Measured value ($)	Calculated value ($) and its relative deviation (in brackets)
IC 3 (0 deg)	19.7	18.29 (-7.2 %)
IC 12 (15 deg)	17.7	16.36 (-7.6 %)
IC 5 (30 deg)	-	15.08

Table 2. Comparison of calculated and measured values of reactivity meter readings for partial scram with one stuck control rod in Loviisa-2, BOC 1. Initial height of group 6 is 183 cm.

Ionization chamber	Measured value ($)		Calculated value ($) and its relative deviation (in brackets)	
	Group 3 rod stuck	Group 4 rod stuck	Group 3 rod stuck	Group 4 rod stuck
IC 3	19.6	19.6	18.16 (-7.3 %)	18.16 (-7.3 %)
IC 12	12.6	10.1	11.68 (-7.3 %)	9.40 (-6.9 %)

Table 3. Comparison of calculated and measured values of reactivity meter readings for full scram in Loviisa-1 burned cores at beginning of cycle.

Ionization chamber	Type of value and time	Reactivity value ($) and its relative deviation (in brackets)		
		BOC 7	BOC 19	BOC 24
IC 12	Meas. 15 s 50 s	20.3 19.6	22.8 22.3	22.5 21.0
IC 12	Calc. 15 s 50 s	18.68 (-8.0 %) 18.47 (-5.8 %)	22.01 (-3.5 %) 21.26 (-4.7 %)	21.84 (-2.9 %) 21.08 (0.4 %)
IC 3	Calc. 15 s 50 s	18.85 18.64	22.17 21.40	22.08 21.31
IC 5	Calc. 15 s 50 s	18.89 18.68	22.60 21.83	22.02 21.25

4.3 Initial core of Mochovce-1

The initial core of Mochovce-1 differs from those for Loviisa, although the three enrichments of fresh fuel are the same. Experiments have been performed with one and two stuck control rods followed by dropping these stuck rods to get a full scram. Results for the stuck rod cases are given in Table 4 and for the final full scram states in Table 5. All three ionization chambers used in the experiments (IC 2, 8, 10) are located in equivalent symmetric directions relative to the core (15 deg). This explains why the experiments produce practically equal reactivity readings after all control rods are inserted and full symmetry is restored in the core.

The calculations under-predict the reactivity meter readings only slightly. All relative deviations are in a fairly tight band -4.6 to -2.2 % for ten different measurements. The absolute static reactivity worth of full scram is calculated to be 11.19 %.

Table 4. Comparison of calculated and measured values of reactivity meter readings for partial scram with one or two stuck control rods in Mochovce-1, BOC 1. The initial height of group 6 is 200 cm.

Number of stuck rods	Ionization chamber	Measured value ($)	Calculated value ($) Its relative deviation (in brackets)
1	IC 8	8.81	8.62 (-2.2 %)
1	IC 2	15.14	14.77 (-2.4 %)
1	IC 10	11.25	10.83 (-3.7 %)
2	IC 8	6.33	6.11 (-3.5 %)
2	IC 2	15.25	14.80 (-3.0 %)
2	IC 10	6.44	6.17 (-4.2 %)

Table 5. Comparison of calculated and measured values of reactivity meter readings after drop of all control rods in Mochovce-1, BOC 1. The initial height of group 6 is 200 cm.

Number of temporary stuck rods	Ionization chamber	Measured value ($)	Calculated value ($) Its relative deviation (in brackets)
1	IC 8	15.43	14.72 (-4.6 %)
1	IC 2	15.14	14.77 (-2.4 %)
1	IC 10	-	14.76
2	IC 8	15.34	14.75 (-3.8 %)
2	IC 2	15.25	14.79 (-3.0 %)
2	IC 10	-	14.88

5. Conclusions

In large inhomogeneous changes in the core, such as in a reactor scram, the reading of a reactivity meter connected to a particular ex-core ionization chamber does not directly represent the static or dynamic reactivity of the core. In order to use the measured information for code validation, it is necessary to simulate the experiment, including the performance of a reactivity meter, and to compare calculated predictions with actual measured values. Such simulations have been performed for a number of different cores of Loviisa NPP and for the initial core of Mochovce-1 using the code HEXTRAN for 3-dimensional kinetics calculations in the core.

Predictions of reactivity meter readings are in reasonably good agreement with actual measurements. Relative deviations for Loviisa are in the range -7 to 0 % and for Mochovce they are in the range -4 to -2 %. This points towards a slight underprediction in the efficiency of reactor scram.

The agreement can be further improved by some +3 % by describing better the influence of buckling changes on two-group cross sections. Thereby, a prediction accuracy of ±5 % is obtained for reactor scram with or without a stuck control rod. This is sufficiently accurate and demonstrates that there are no significant errors in the modelling of VVER-440 control rods in HEXTRAN. Any remaining deviations between predictions and measurements are not necessarily due to inaccuracy in modelling the control rods. Inaccuracy in other parts of the models and data, such as in neutron kinetics data can also cause deviations. There is also some inaccuracy in the performance of a reactivity meter and in recording its output.

References

1. P. Siltanen: *The reactivity meter and core reactivity*. Proc. of the ninth Symposium of AER, Demänovska Dolina, Slovakia, 4–8 Oct. 1999, pp. 413–428.

2. F. Wasastjerna, P. Siltanen: *Response kernels for ex-core ionization chambers*. Proc. of International Topical Meeting PHYSOR 2000, Pittsburgh, Pennsylvania, USA, 7–12 May 2000, paper 261.

3. E. Kaloinen, R. Kyrki-Rajamäki, F. Wasastjerna: *Simulation of rod drop experi-ments in the initial cores of Loviisa and Mochovce*. Proc. of the ninth Symposium of AER, Demänovska Dolina, Slovakia, 4–8 Oct. 1999, pp. 367–379.

4. P. Siltanen, E. Kaloinen, A. Tanskanen, R. Mattila: *Further experience in simu-lation of rod drop experiments in the Loviisa and Mochovce reactors*. Proc. of the eleventh Symposium of AER, Csopak, Hungary, 24–28 Sept. 2001, pp. 387–394.

5. R. Kyrki-Rajamäki: *Three-dimensional reactor dynamics code for VVER type nuclear reactors*. VTT Publications 246, Technical Research Centre of Finland, Espoo, 1995 (Thesis for Dr. Tech.).

6. K. Smith: *Beta-effective calculation in CASMO-4*. Studsvik Scandpower, Inc., proprietary report, March 2000.

Appendix A

In this appendix, the behaviour of a point kinetic reactivity meter is illustrated by simple numerical examples. The simulations were performed using in series a point kinetic core model, a simple local detector model, and a reactivity meter model based on standard inverse point kinetics.

The input to the core is a reactivity change in dollars (ρ/β). The output represents the average fission neutron source (power) in the core. A detector signal is then generated by modifying the core output by a local flux distortion factor K, changing in parallel with the reactivity change. This simulates spatial changes in the power distribution, occurring at the location of the detector. Another way of interpreting K is a change in the detector efficiency: $K = \varepsilon_1/\varepsilon_0$. This detector signal is the input to the reactivity meter. The output of the meter is again reactivity in dollars, as interpreted by the meter. The neutron kinetics parameters of the core and the meter can be identical or differences can be introduced.

The effect of spatial flux distortions is illustrated in Figures A1 to A4 for different values of negative reactivity insertion. The time for reactivity insertion is always 10 seconds. The point kinetics parameters in the core and in the reactivity meter are the same. This is why the simulated meter reproduces faithfully the input reactivity to the simulated core, when K = 1. Clearly, it is necessary to account for spatial distortions when interpreting experimental data in rod drop experiments.

Once a deviation is introduced into the meter reading, it persists for a long time for large negative reactivity. Even for reactivities smaller than 1 dollar the recovery of the meter towards the correct reactivity is slow from the practical point of view. The reason that the meter is unable to recover from the local spatial distortion is the following. A reactivity meter derives the reactivity essentially based on the prompt jump that is sees. After the reactivity change is over, the asymptotic behaviour of the core and the detector signal contains very little information on reactivity. The behaviour is practically the same for different values of negative reactivity in a wide band. Note also that in a real rod drop case the spatial distortion tends to increase somewhat with time.

Another test illustrating the influence of differences in neutron kinetics parameters is shown in Figure A5. In this simulation, the data in the meter is always that given by Keepin for the thermal fission of U-235. This is the data nominally used in the PIR meters employed during physical start-up tests of Loviisa-1&2. The data simulating the core is varied from Keepin data to data produced by the assembly code CASMO-4 for different fuel types in the initial core and by HEXTRAN for the core as a whole in its initial state. Both delayed neutron fractions and decay constants are different. The data is shown in Table A1. The reactivity insertion into the core was always –15 dollars. This eliminates the influence of differences in total β_{eff}. When the data in the core is entirely based on CASMO, the output of the “Keepin reactivity meter” at 60–100 s is –16.75 dollars or almost 12 % more in absolute value. This is a significant effect and needs to be taken into account when interpreting experimental data.

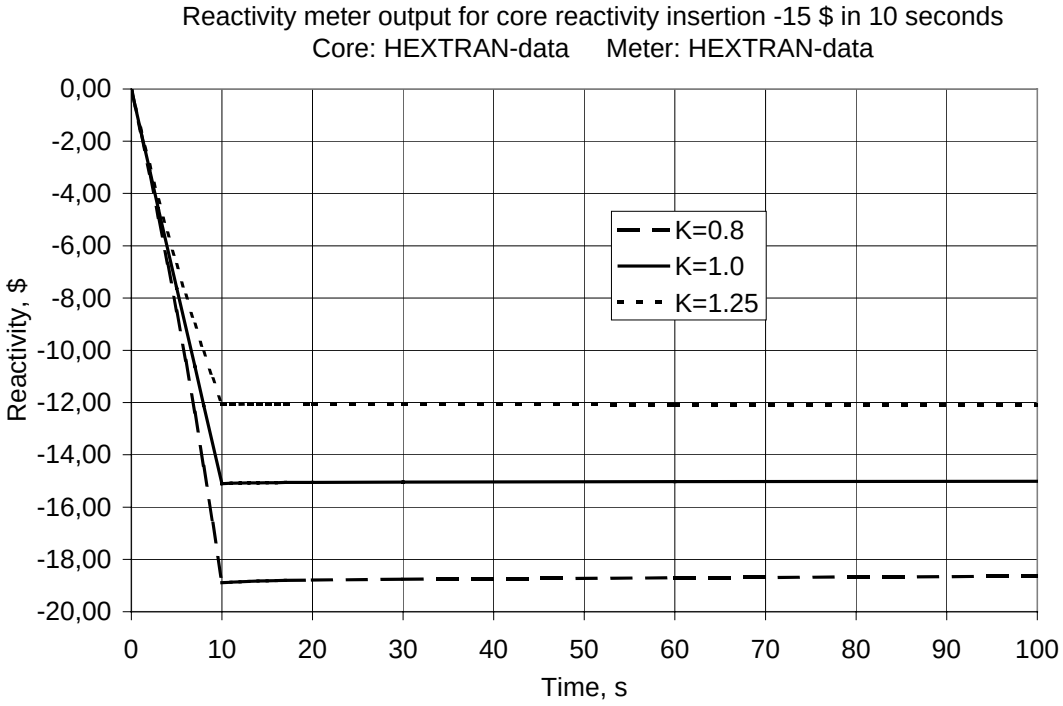

Fig. A1. Simulation of reactivity meter performance for different values of the local flux distortion factor K. Core reactivity insertion –15 dollars.

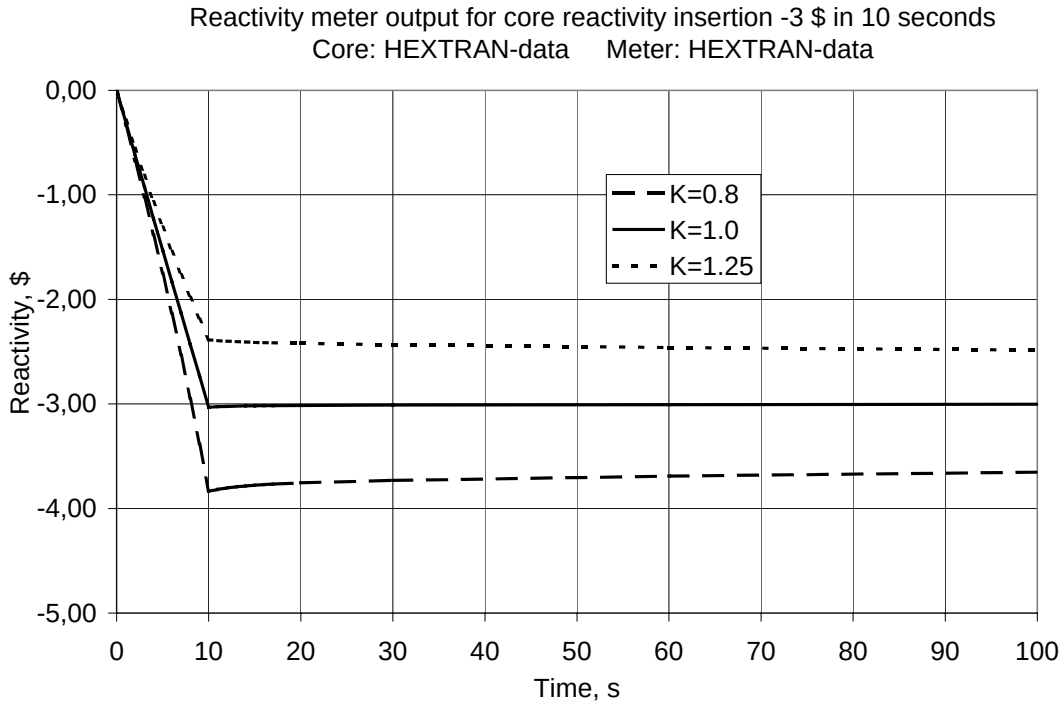

Fig. A2. Simulation of reactivity meter performance for different values of the local flux distortion factor K. Core reactivity insertion –3 dollars.

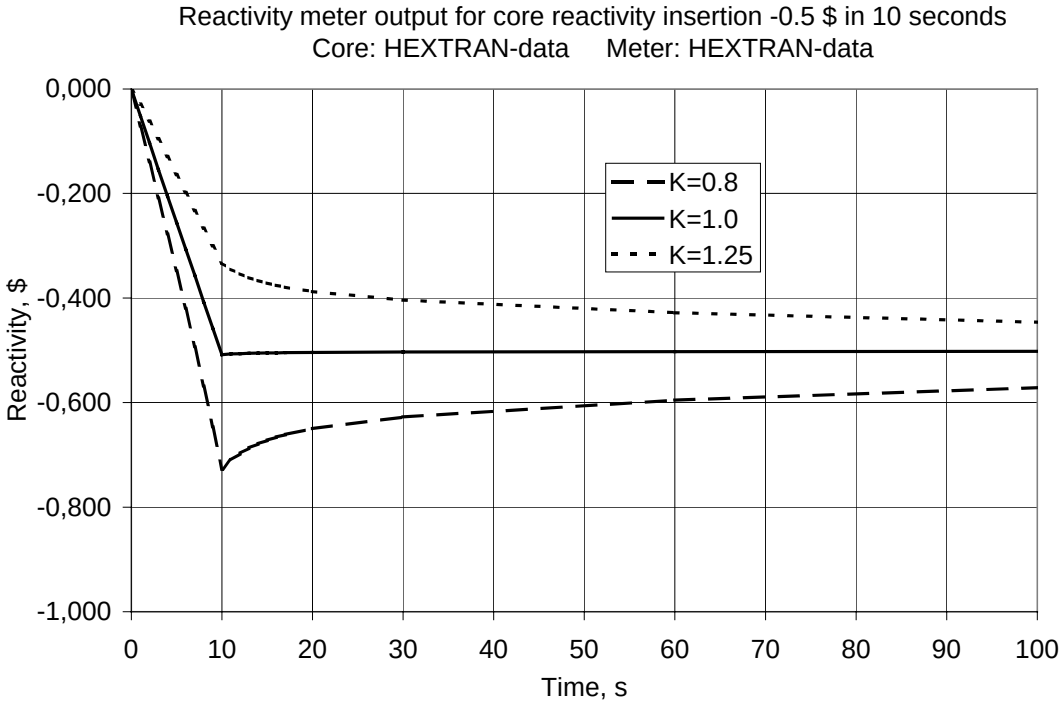

Fig. A3. Simulation of reactivity meter performance for different values of the local flux distortion factor K. Core reactivity insertion –0.5 dollars.

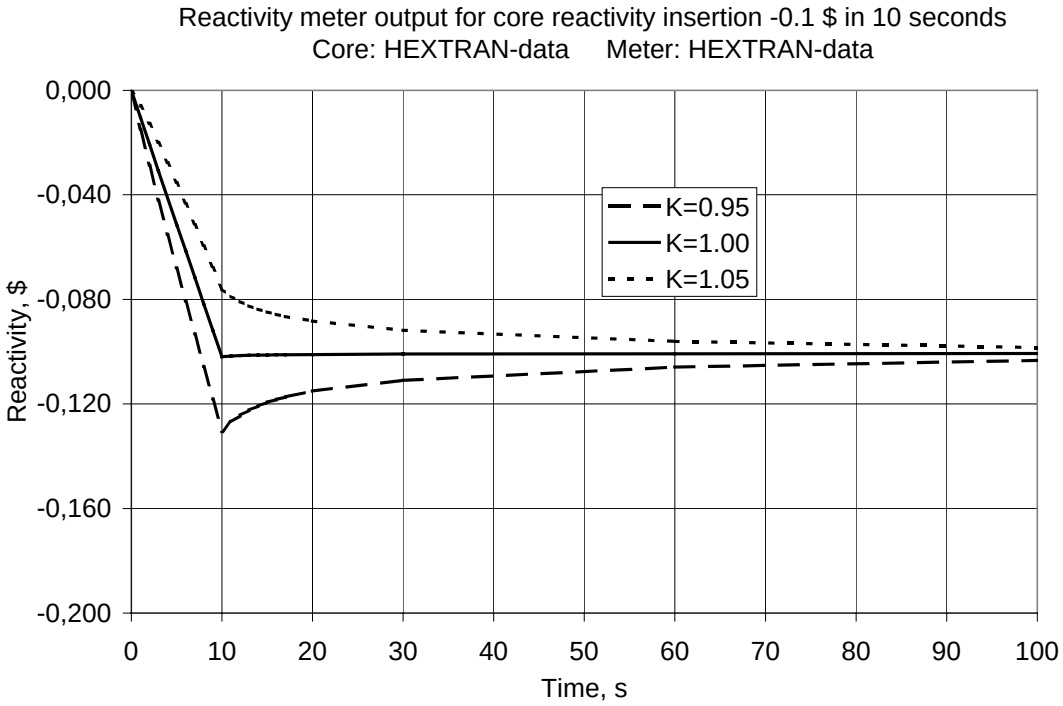

Fig. A4. Simulation of reactivity meter performance for different values of the local flux distortion factor K. Core reactivity insertion –0.1 dollars.

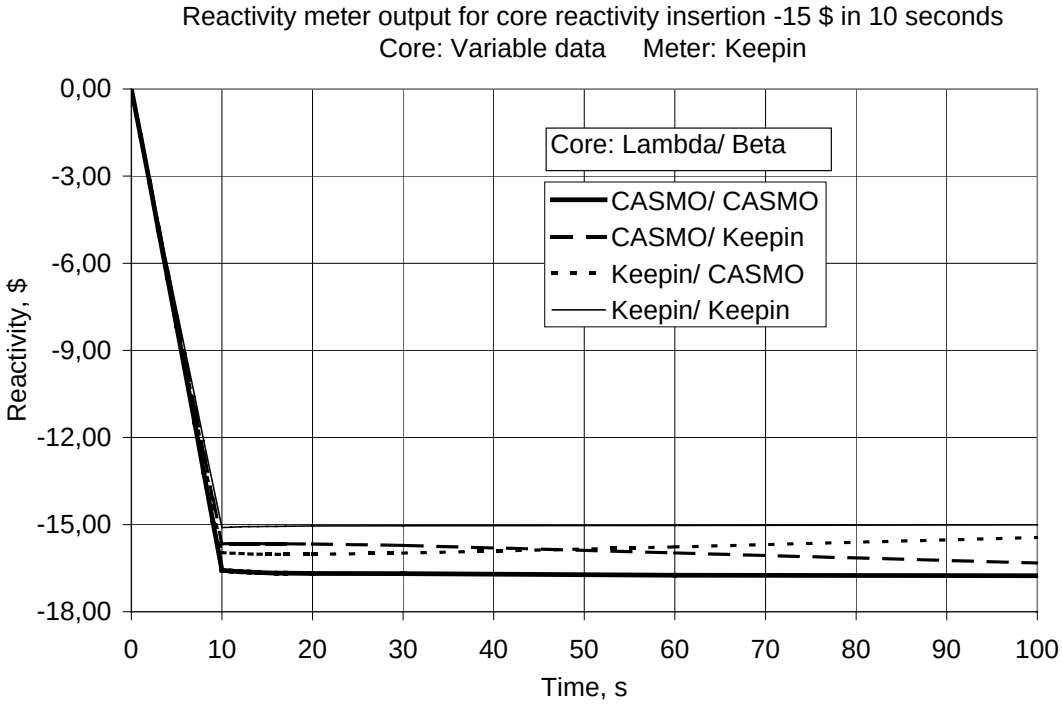

Fig. A5. Simulation of the "Keepin reactivity meter" performance for different sets of neutron kinetics parameters in the core. Core reactivity insertion –15 dollars.

Table A1. Neutron kinetics parameters applied in simulations of the core and the reactivity meter (See Fig. A5).

i	**KEEPIN** λ_i **(1/s)** β_i/β	**CASMO** λ_i **(1/s)** β_i/β
1	0.0124 0.033	0.0128 0.034
2	0.0305 0.219	0.0318 0.201
3	0.1110 0.196	0.1190 0.184
4	0.3010 0.395	0.3180 0.404
5	1.1400 0.115	1.4020 0.143
6	3.0100 0.042	3.9250 0.034
β	0.00650	0.00716
Λ (μs)	25	25

Validation of PHOENIX4 against critical measurements at the PROTEUS facility

Petri Forslund & Morgan Johansson
Models Development
+46 21 347277
petri.forslund@se.westinghouse.com

Introduction

The main objective of nuclear fuel development activities is to improve the LWR fuel economy with preserved safety

- More advanced LWR fuel assembly designs
- New challenge to the core analysis tools applied for predicting the neutronic behavior of the reactor core

Modeling of cores loaded with new fuel designs rises some questions about the performance of the core analysis tools

- What is the impact on computational accuracy?
- Are there needs for improvements in the modeling?

LWR-PROTEUS experiments

Overview

- Setup to provide experimental data for code validation
- Accurate measurements at individual pin level
- 3x3 array of full size SVEA-96+ fuel assemblies
- Measurements at different physical conditions
  - Non-voided conditions
  - (Simulated) voided conditions
  - Controlled conditions
  - Assembly bowing

Investigated core configurations

- 1A /1B Reference cores
- 2A/2B/2C Control blade (Hf/B_4C)
- 3A/3B Simulated void (polyethylene, 90%/25%)
- 5A Simulated Void + Control blade
- 7A Displaced assembly

Evaluations for

- Total fission rates (F_{tot})
- U-238 Capture rates (C_8)

Pre-calculations

- Nominal input-data used
- Estimation of uncertainties in routine production calculations

Post-calculations

- Measured input-data used
- Estimation of uncertainties in the lattice code

Numerical results

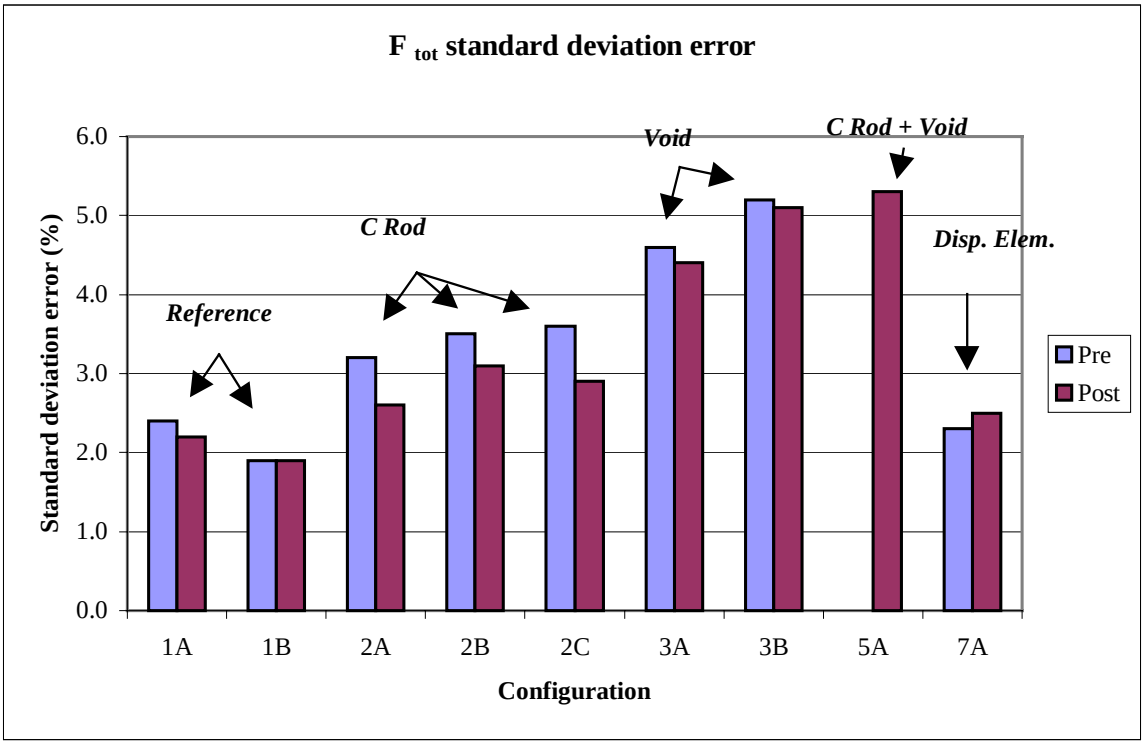

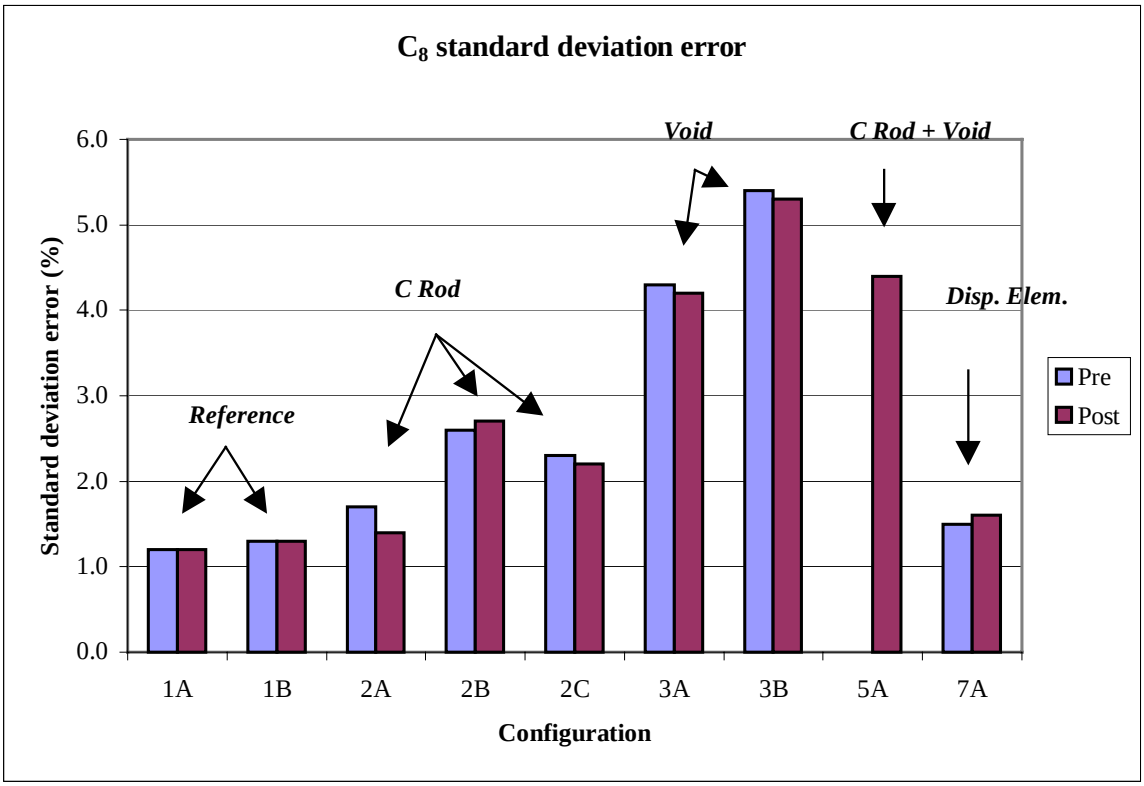

Overall performance

- The reaction rate errors increase with increased core complexity
  - Voided cores show largest errors
- Same accuracy in pre- and post-calculations
  - F_{tot} for controlled cores exception
  - Post-model of CR's more accurate
- C_8 errors < F_{tot} errors
  - Epithermal spectrum well predicted

Modeling improvements identified

- Shifted sub-assembly pin lattice
  - Pin distance between sub-assemblies preserved
  - F_{tot} error at WX and AC reduced with 2–3 %
  - F_{tot} st.dev. error improved with 1 %
  - C_8 error unaffected
- Reduced WX water pin radius (affects voided cores)
  - F_{tot} error at central WX channel reduced with 8–10 %
  - C_8 error at central WX channel reduced with 3 %
  - F_{tot} and C_8 st.dev. errors mainly unaffected

F_{tot} for Configuration 1A Post (Reference)

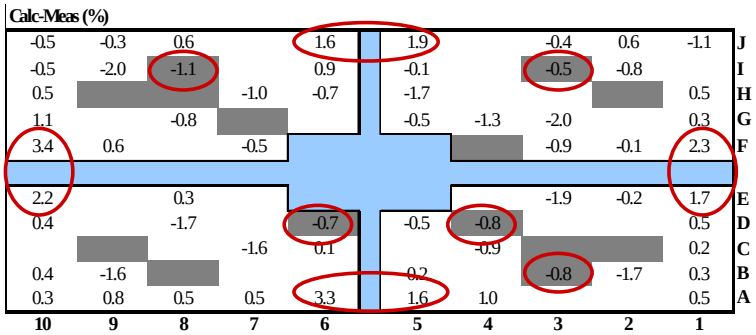

Nr. Rods:	61
Average:	0.0
St. Dev.:	1.2
Min.:	–2.0
Max:	3.4

Average Sub-bundles

0.1	–0.2
0.2	0.0

Reference cores (1A and 1B)

- F_{tot} and C_8 predicted rather well in all the pins
  - Standard deviation (%)

	1A	1B
F_{tot}	1.2	1.7
C_8	1.3	1.5

  - Max/min deviation (%)

	1A	1B
F_{tot}	3.4/-2.0	3.8/-3.3
C_8	2.4/-2.4	5.3/-2.8

Reference cores (1A and 1B)

- F_{tot} and C_8 trends
  - F_{tot} and C_8 overestimated at WX dimples
  - F_{tot} and C_8 underestimated in BA-pins and inner-pins
- Comparison of results between core 1A and 1B
  - The errors have the same magnitude for both cores
  - Similar behavior at the different assembly regions
  - No dependence on enrichment distribution

Voided cores (3A and 3B)

- Similar results for 3A and 3B, pre and post configurations
- F_{tot} & C_8 trends
  - Large F_{tot} and C_8 errors at AC and WX dimples
  - Small F_{tot} error and large positive C_8 error in BA-pins next to the central WX channel
  - F_{tot} and C_8 underestimated in remaining BA-pins and in inner-pins

F_{tot} for Configuration 2A Post (Controlled)

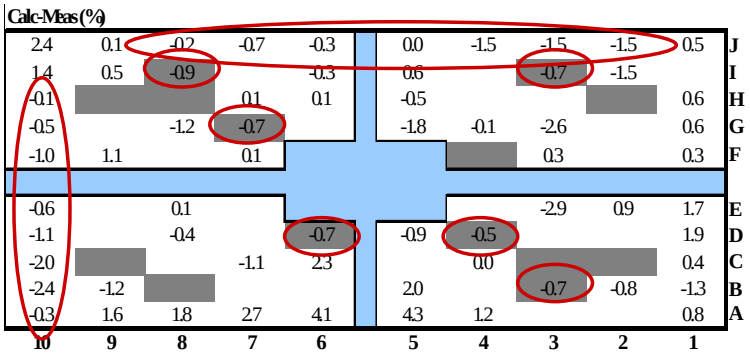

Nr. Rods:	64
Average:	0.0
St. Dev.:	1.4
Min.:	–2.9
Max:	4.3

Average Sub-bundles

0.0	–0.6
0.2	0.4

Controlled cores (2A, 2B, 2C and 5A)

- Results for core 2A representative for non-voided cores
  - Similar results for controlled cores as for ref. cores
    - F_{tot} and C_8 underpredicted in BA-pins
  - Similar results for pre and post configurations
    - Smaller errors in post-model at the CR tip
  - F_{tot} and C_8 underpredicted at the CR
- Similar results for controlled+voided core 5A as for core 3A
  - F_{tot} underpredicted at the CR
  - C_8 overpredicted at the CR

F_{tot} for Configuration 7A Post (Displaced assembly)

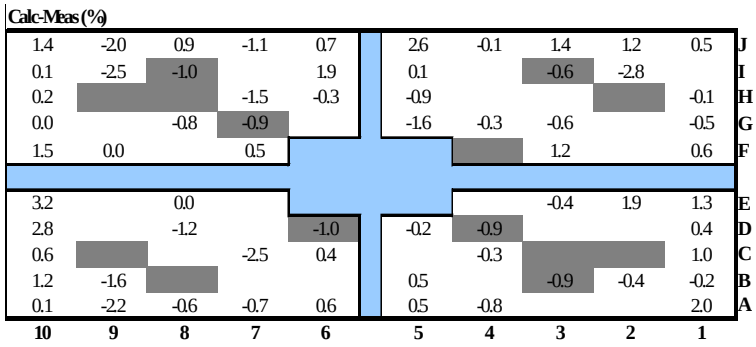

Nr. Rods:	64
Average:	0.0
St. Dev.:	1.3
Min.:	–2.8
Max:	3.2

Average Sub-bundles

–0.2	0.0
–0.1	0.2

Core with displaced assembly (7A)

- Quality of SZCF's especially important
- Mainly the same results as for core 1A
- Smaller errors compared to 1A at WX dimples of south and east assembly sides with smaller gaps

Conclusions

- The neutronic behavior of the SVEA-96+ fuel assembly is predicted very well by PHOENIX4
- Modeling of the mock-up heterogeneity in voided cores very difficult
- Refined modeling
  - Preserving the distance between sub-assemblies
  - Reducing the size of the water pins

Transmutation of nuclear waste in accelerator driven reactors

Janne Wallenius
Royal Institute of Technology, Sweden
Department of Nuclear & Reactor Physics

Radiotoxicity of spent LWR fuel

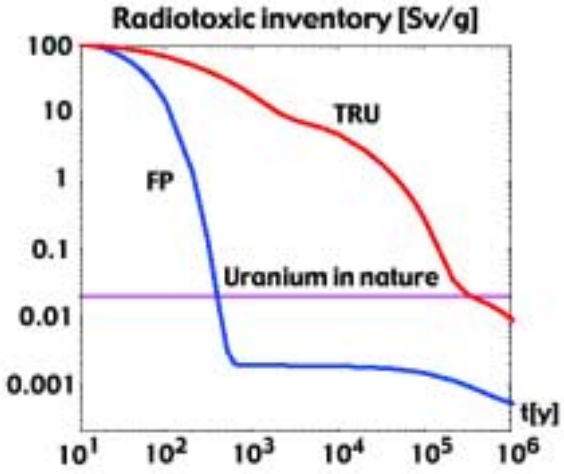

- Specific radiotoxic inventory of spent LWR fuel in the repository is dominated by transuranic elements (TRU).
- The fission product (FP) contribution to the radiotoxic inventory vanishes with the decay of Sr-90 and Cs-137.
- Equilibrium radiotoxic inventory of uranium in nature ~ 20 mSv/g.
- 300 000 years of storage required for spent fuel to return to "natural inventory".

Radiotoxicity of transuranium nuclides

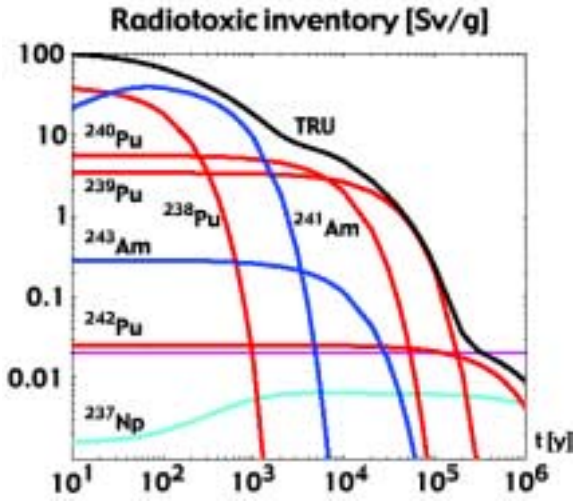

- Long term radiotoxic inventory dominated by
- Am-241 ~ 1 000 years
- Pu-240 ~10 000 years
- Pu-239 ~100 000 years
- Radiotoxic inventory due to presence of Np-237 is less than that of uranium in nature.

Why not recycle the waste in LWRs?

- In a thermal spectrum, Am is converted to Pu-238 & Cm-244, resulting in intense heat production and neutron emission.
- Multi-recycling of Pu in LWRs leads to poor Pu quality & positive void coefficient.

Multi-recycling of Pu & Am should be made in a fast neutron spectrum!

Recycling Am in fast reactors

- Addition of Am to fast reactor fuel suppresses Doppler feedback
- Combination of liquid metal coolant & americium presence in fuel yields large positive void coefficient

Multi-recycling of Am should be made in a sub-critical Accelerator Driven System!

Double strata fuel cycle

Double Strata Fuel cycle minimizes cost penalty for Partitioning and Transmutation

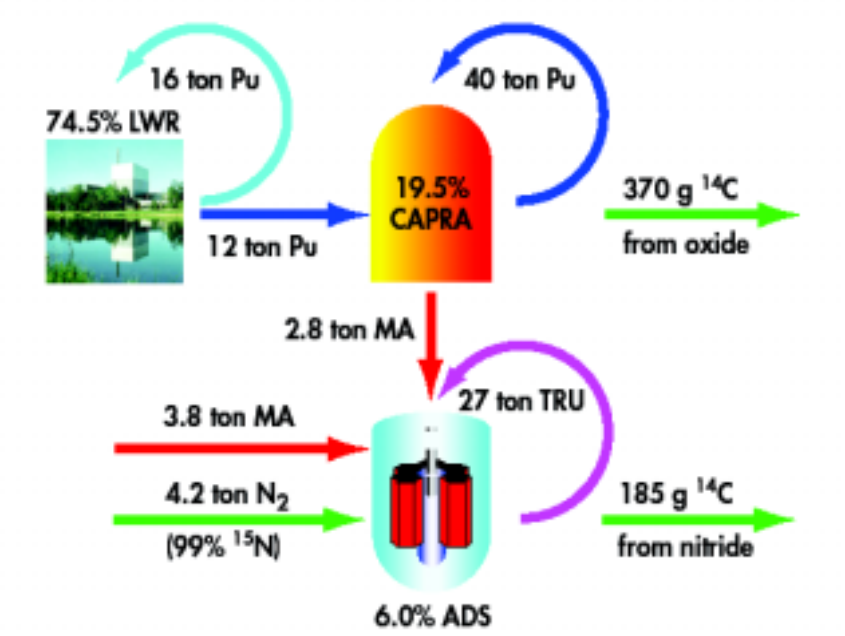

Secondary waste stream

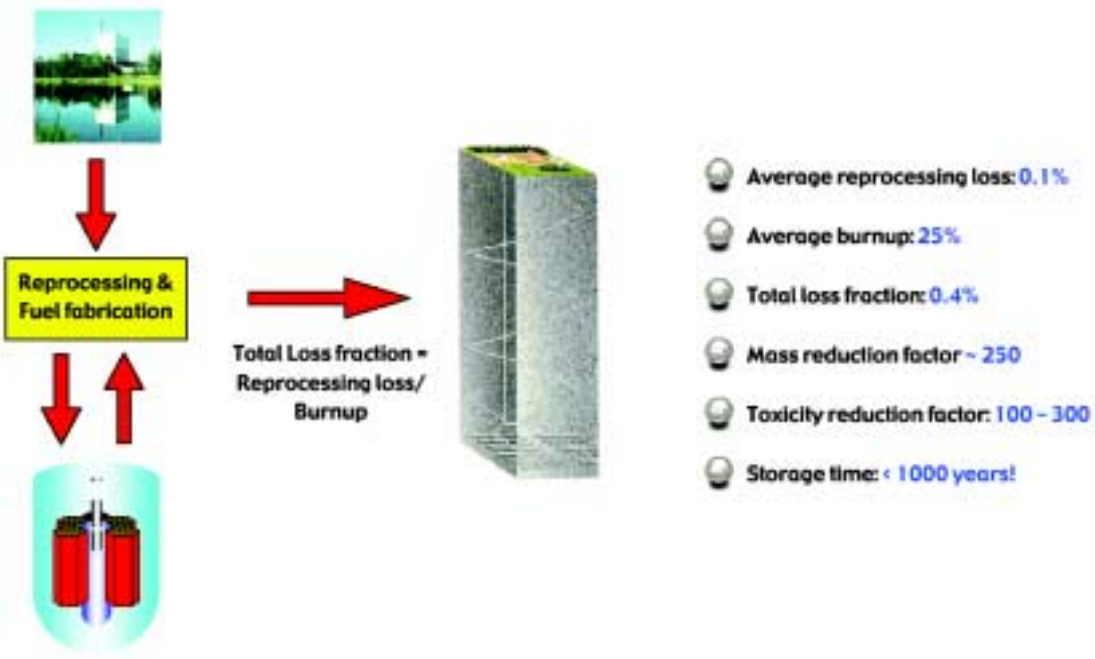

Accelerator Driven System

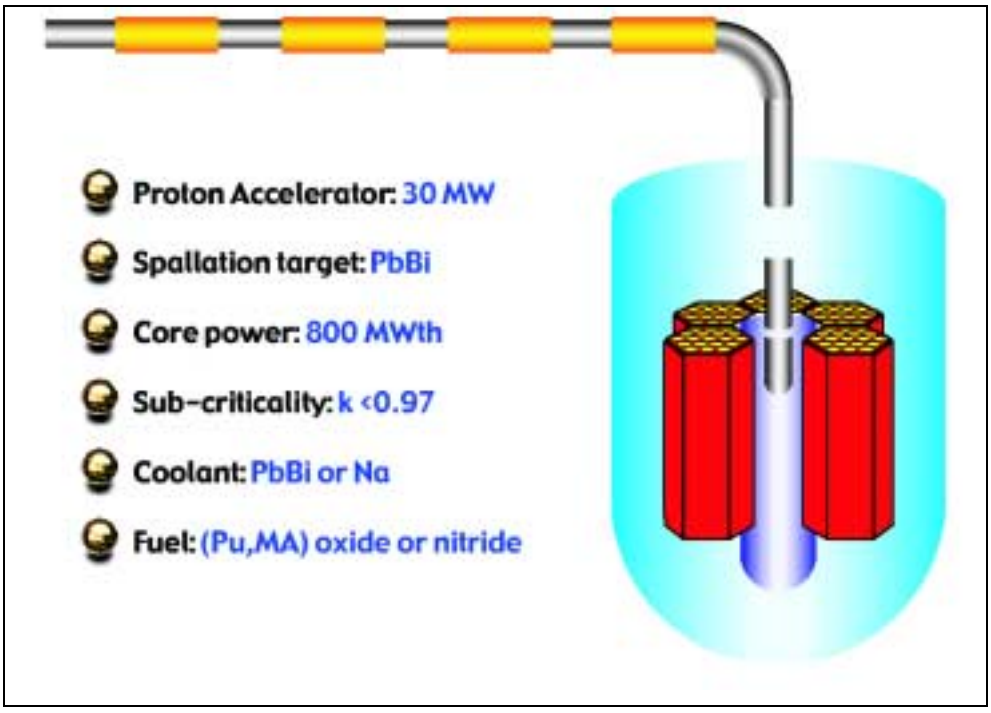

ADS characteristics

- Americium based fuel →
- Insignificant Doppler feedback
- Small or zero presence of Uranium →
- Small delayed neutron fraction
- Liquid metal coolant →
- Positive void coefficient
-
- Margins to prompt criticality must be sufficient not only during normal operation, but also under off-normal conditions!

Fuel composition (single zone cores)

Inert matrix fraction depends on absorption cross section, pin diameter and pin pitch

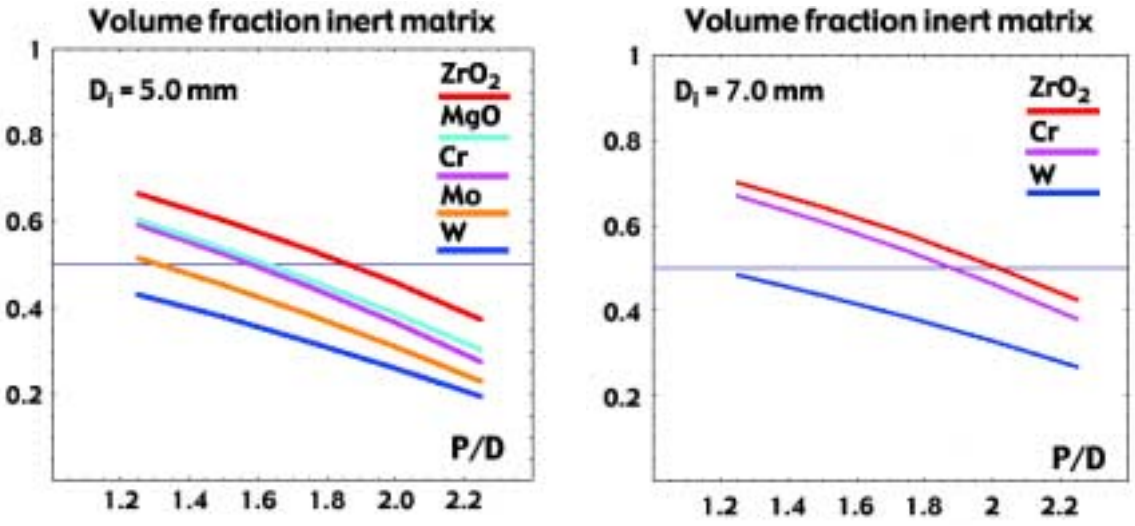

Fission probability

Fission probability of americium is sensitive to the spectrum of neutrons moderated by fuel and coolant

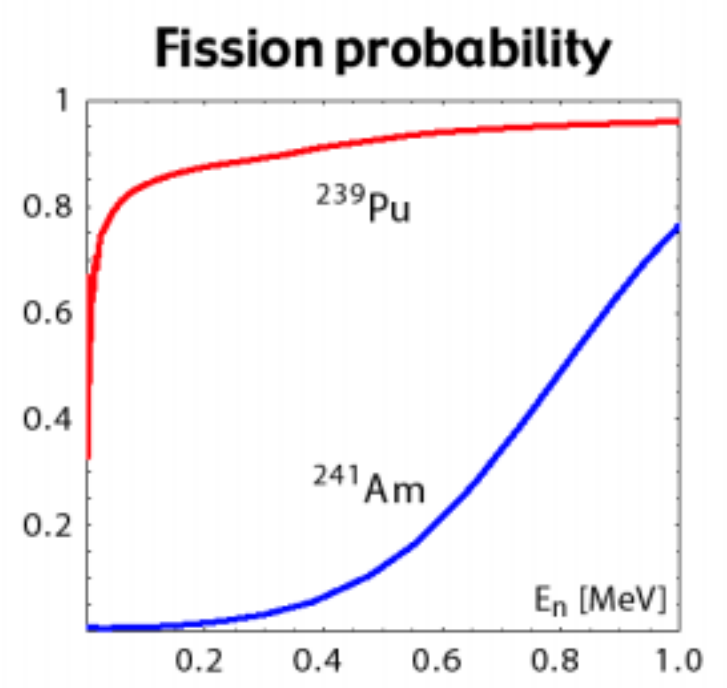

Void worth: Sodium versus PbBi

PbBi yields lower void worth if steel reflector is used!

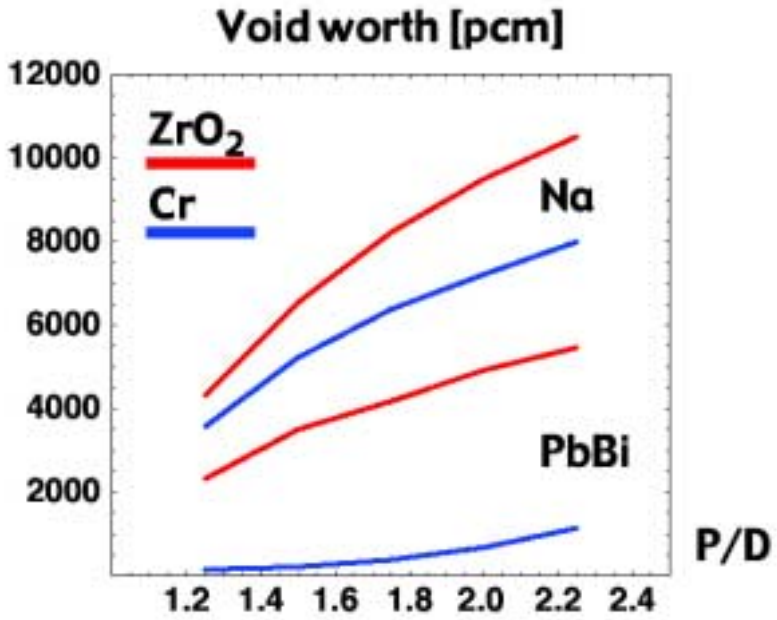

Void worth: Impact of pin diameter

Smaller pin diameter yields smaller void worth!

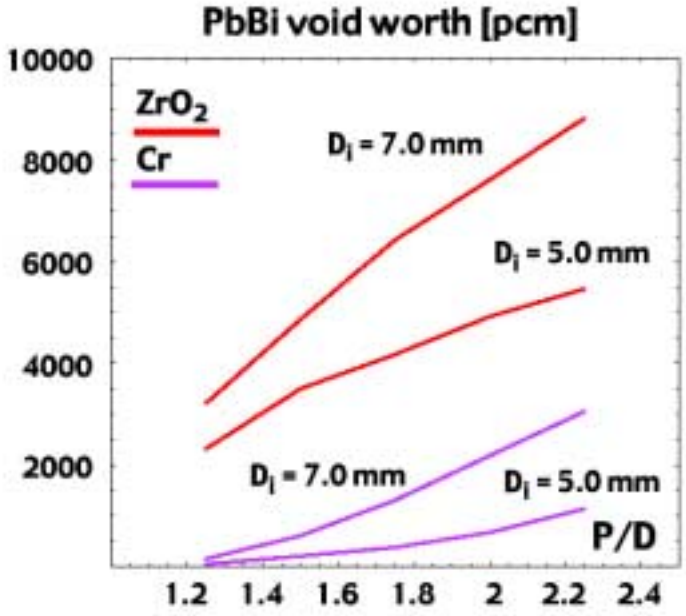

Void worth: Oxide versus nitride

Matrices with high thermal conductivity and full neutron shell provide the smallest void worths!

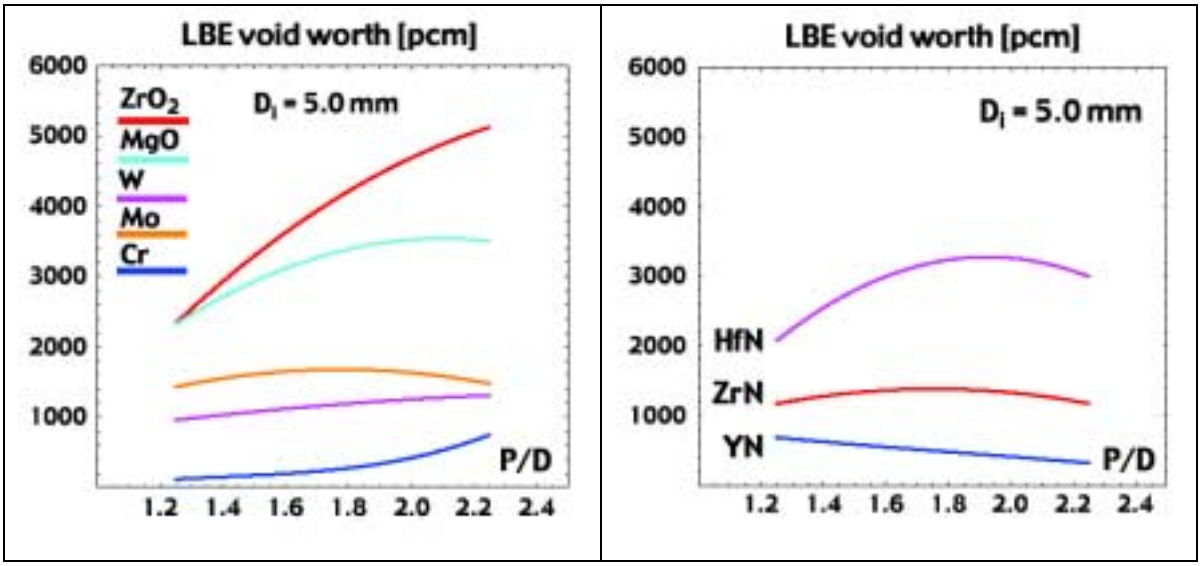

Coolant temperature coefficient

PbBi void coefficient ~ 0.5 pcm/K for CERMET fuels

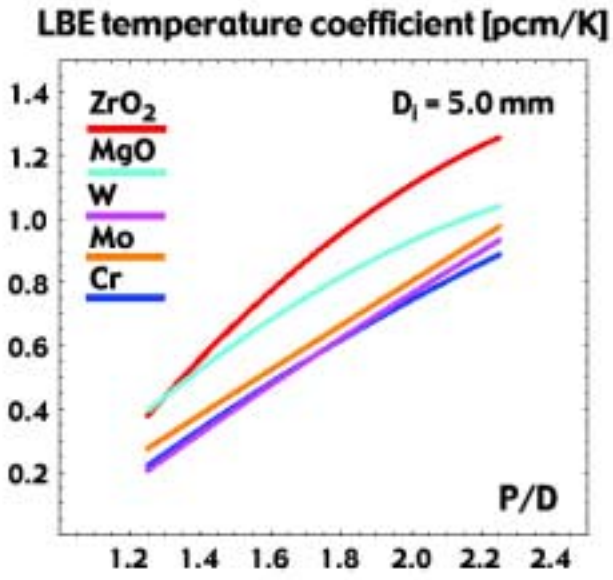

Safety coefficients for Cr matrix core

The low void coefficient pertaining to LBE may be compensated for by thermal expansion of the fuel!

Mechanism	Temperature coefficient
Coolant expansion (LBE)	+0.4 pcm/K
Coolant expansion (Na)	+1.5 pcm/K
Fuel axial expansion	-0.4 pcm/K
Radial grid expansion	-0.3 pcm/K
Doppler broadening	-0.05 pcm/K

Summary of safety issues in ADS

- Sub-criticality does not qualify use of arbitrary fuel composition!
- Sodium cooling is questionable for americium based fuels
- Smaller pin diameters yield lower void worths
- Oxide fuel with metallic matrix or nitride solid solution fuel provide good thermal conductivity, small void worths and large power to melt
- Microstability is achieved by thermal expansion of structural materials
- High temperature stability of Am compounds remains to be proven!

Calculation of energy deposition in the moderator tank of the Forsmark 1 BWR

C. F. Højerup & Erik Nonbøl
Risø National Laboratory
Roskilde, Denmark

Abstract

It is important to know the neutron doses received by reactor components in order to assess the degree of radiation damage they may have suffered. Also, it is important to know the neutron induced activities of the components for planning of their dismantling and subsequent storage.

Such calculations (both flux and activation) were previous done for the Forsmark 1 BWR.

The heat deposition mainly from absorption of gamma radiation in materials near the core is also of importance for evaluating material conditions. This report focus on calculation of heat deposition from gamma radiation in the moderator tank of the Forsmark 1 reactor by means of the Monte Carlo code MCNP.

1 Introduction

It is important to know the neutron doses received by reactor components in order to assess the degree of radiation damage they may have suffered. Also, it is important to know the neutron induced activities of the components for planning of their dismantling and subsequent storage. Such calculations (both flux and activation) were previous done for the Forsmark 1 BWR and reported in Ref. 1, 2, 3.

The heat deposition mainly from absorption of gamma radiation in materials near the core is also of importance for evaluating material conditions. This report focus on calculation of heat deposition from gamma radiation in the moderator tank of the Forsmark 1 reactor by means of the Monte Carlo code MCNP.

2 Radiation sources contributing to heat deposition

The following three radiation sources are responsible for the heat deposition in materials near the core:

1. Prompt γ from fission, 7 MeV/fission, account for 20 %
2. Prompt γ from neutron capture, 10 MeV/fission, account for 60 %
3. Delayed γ from fission products, 7 MeV/fission, account for 20 %

Furthermore a small amount comes from neutron slowing down, but it is only about 0.3 %, most of the slowing down power is dissipated in the water.

2.1 Prompt gamma calculation

Calculation of item 1+2, prompt gamma, comes from a MCNP calculation similar to the flux calculation, with focus on energy tally in each MCNP-cell instead of flux tally. A so-called n-p (neutron-photon or neutron-gamma) calculation is made with MCNP, taking both neutron and gamma processes into account. This calculation is identical to the previous reported MCNP-calculation, Ref. 6, with improved neutron source representation.

We have previous analysed the relative variation of the total neutron flux in the mode-rator tank wall, Figures 1 and 2, as function of the angle from the x-axis. Here we have found, that only the two outermost fuel assemblies are responsible for the neutron flux and thus also for the heat deposition. The moderator tank is positioned about 17 cm from the nearest fuel assembly. Therefore, the geometry shown in Figure 3 is applied.

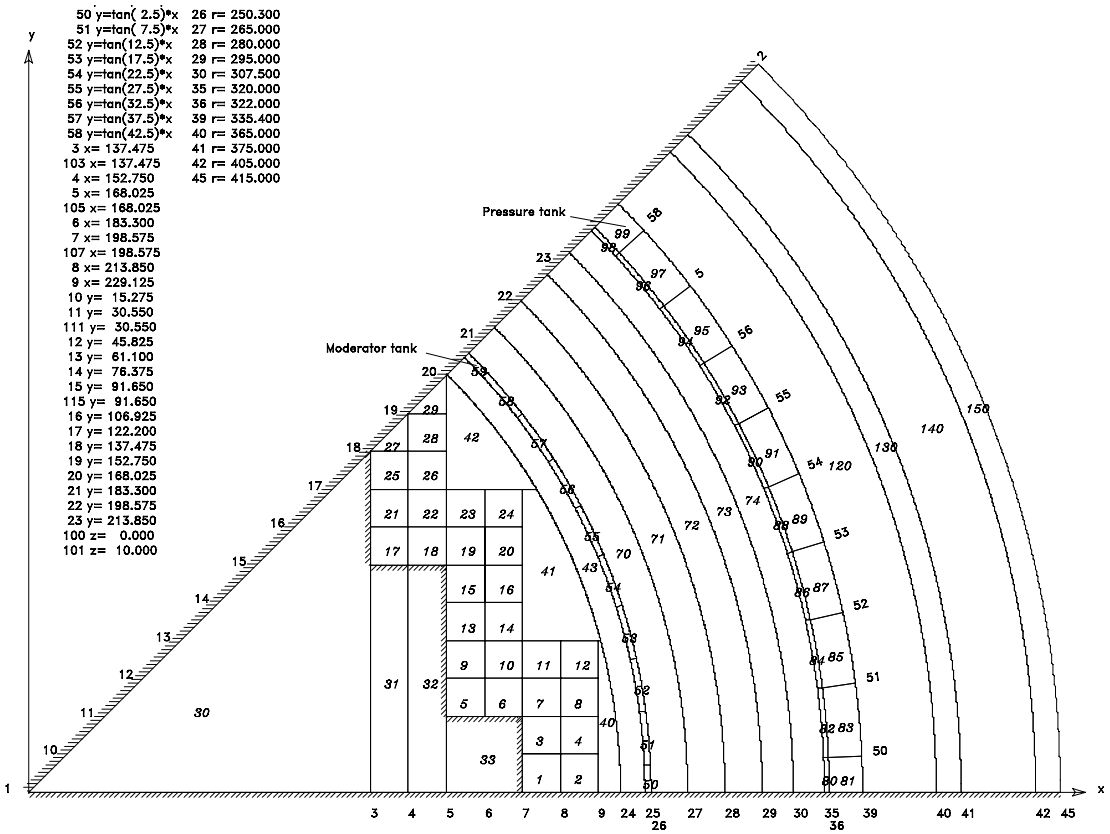

Figure 1. Forsmark 1 core geometry for xy-calculation.

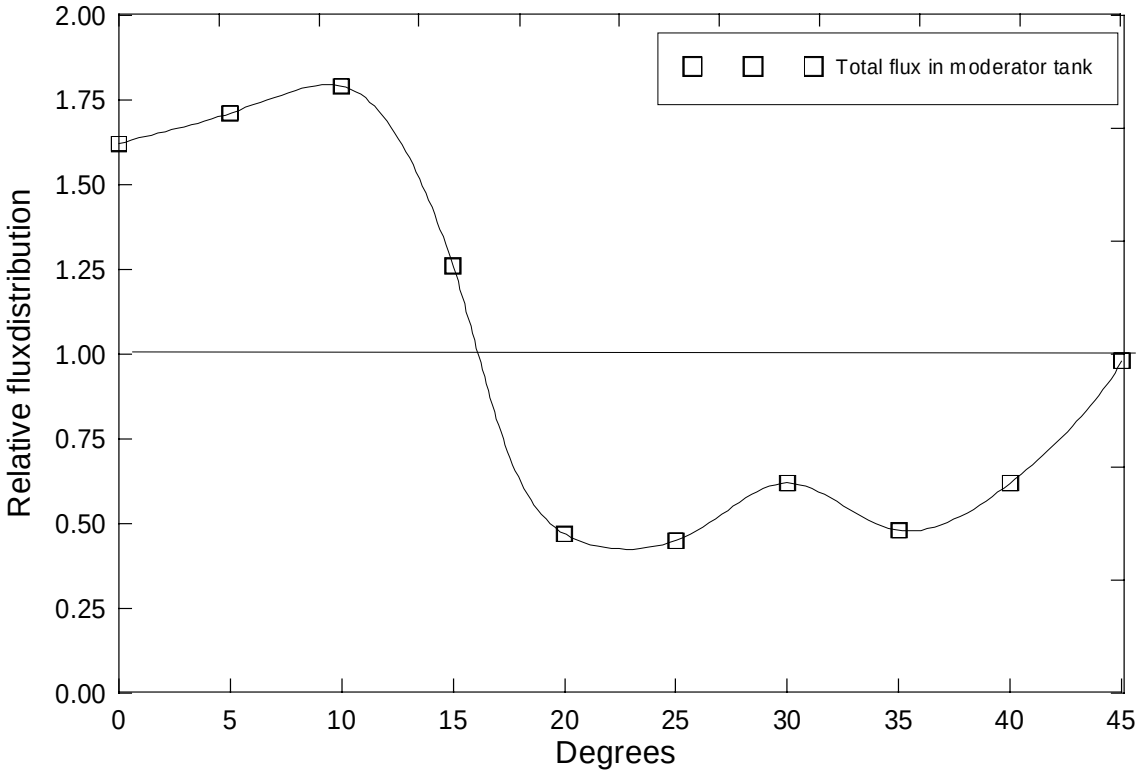

Figure 2. Fluxvariation along the periferies of the moderator tank. (Compare Figure 1 for the angle.)

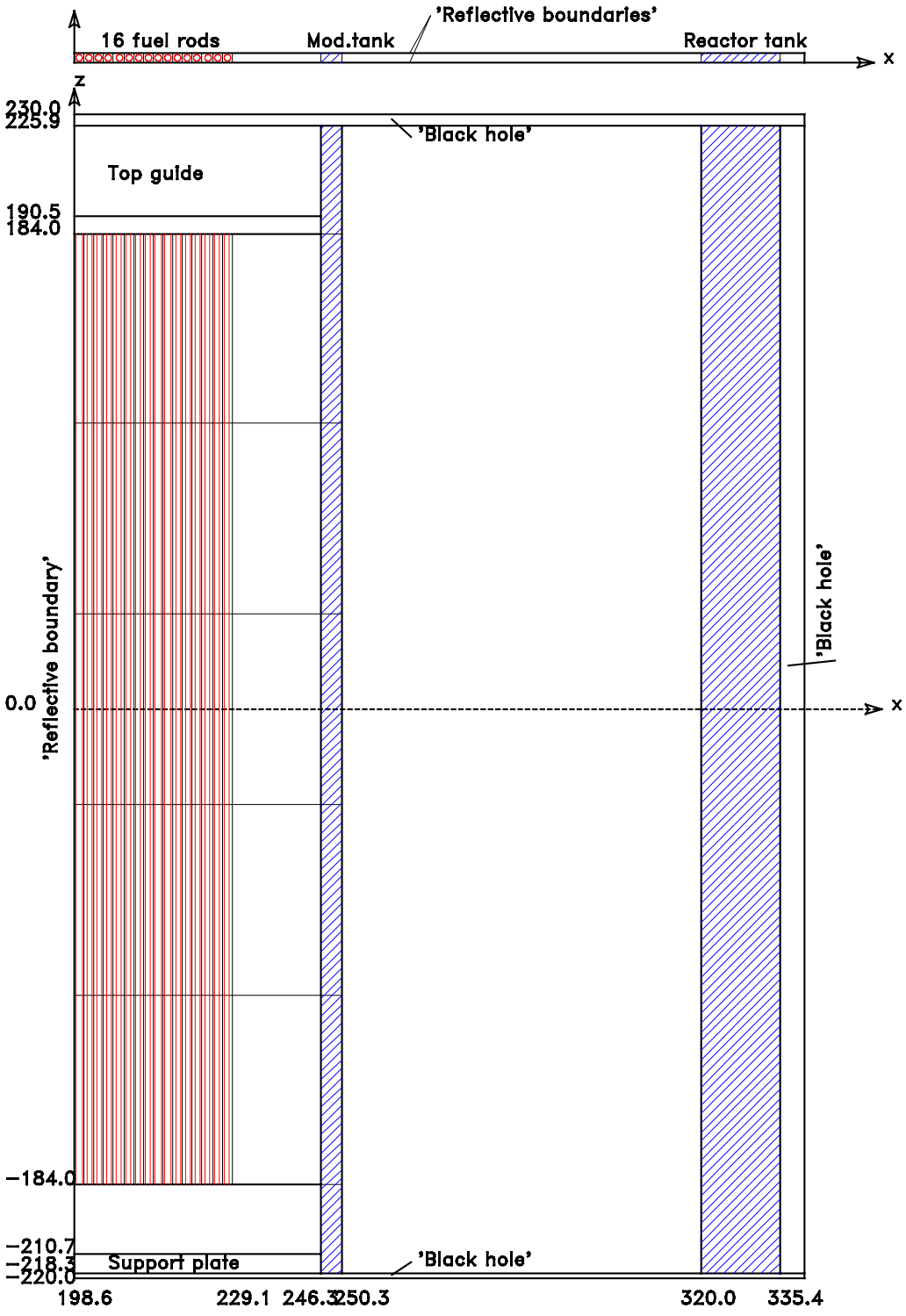

Figure 3. Geometrical layout of the (n-p) calculation, where 16 fuel pins are considered representing the assemblies closest to the moderator tank.

Here 16 fuel rods are considered representing the two outermost fuel assemblies taking power distribution and form factors into account, obtained from the given COREMASTER power distribution, simulating the power history. The boundaries in the y-direction are assumed to be reflective. The fuel pins and moderator tank are divided into 5 meshes in axial (z) direction The moderator tank is divided into 5 meshes in radial direction.

Delayed gamma calculation

Item 3 however, needs a separate MCNP p calculation where the source is photons (γ) coming from the fission product distribution. This distribution is assumed to be the same as the power distribution from the neutron calculation from which the number of fissions per sec can be calculated. The energy spectrum of the source photons is given as

$$N = 1.1 \cdot E_{FP,\gamma} \cdot e^{-1.1 \cdot E_{\gamma}}$$

and calculated in 30 energy groups from 0.1–10 MeV.

3 Results

Adding all three items gives at the hottest spot of the moderator tank wall, which is at the centre of the core, the radial heat deposition distribution shown in Table 1. The left column is closest to the core.

Table 1. Radial heat deposition in the moderator tank wall at the centre of the core. The left column is closest to the core.

1.32 w/cm^3	1.02 w/cm^3	0.82 w/cm^3	0.64 w/cm^3	0.52 w/cm^3
0–8 mm	8–16 mm	16–24 mm	24–32 mm	32–40 mm

4 Temperature calculation

With the heat deposition in the moderator tank wall known it is possible to calculate the temperature distribution in radial direction assuming a definite surface temperature on the inner and outer wall of the tank (boundary conditions).

In Figure 4 is shown a sketch of the temperature calculation in 5 radial zones in the moderator tank wall.

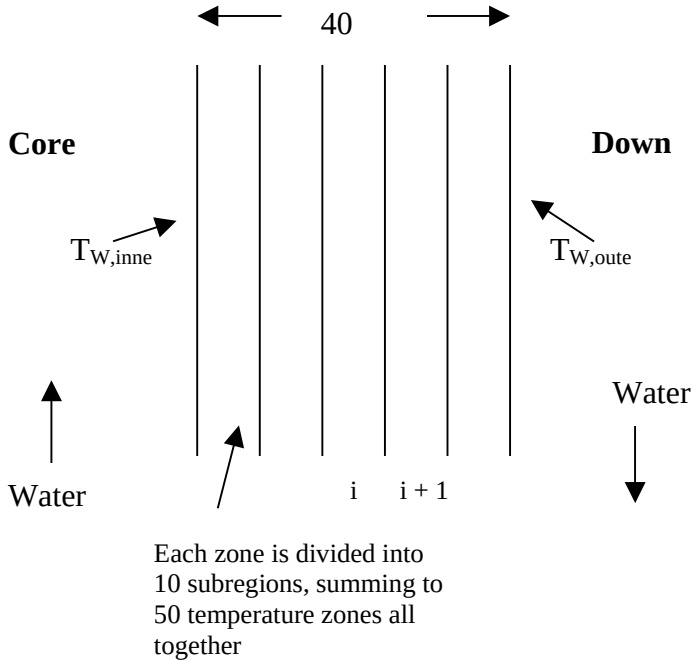

Figure 4. Sketch of the subdivision of the moderatortank wall.

The temperature distribution is obtained from dynamic iteration assuming $T_{start} = T_{W,inner} = 286$ °C with the heat balance expressed as $Q_i = \gamma_i + H_{i-1} - H_{i+1}$.

Here Q_i is the total heat in region i expressed as the gamma heat γ_i produced plus the heat conduction from preceding region H_{I-1} subtracted the heat conduction to the following region H_{i+1}

A mixing ratio, which can be varied, is also applied, accounting for the mixing in the down comer of feed water and recirculation flow.

In Figure 5 is shown the temperature distribution assuming a surface temperature of 286 °C (saturation temperature at 70 bar) at the inner wall and a temperature of 274 °C at the outer wall (down comer). The temperature 274 °C corresponds to the mixing water temperature in the down comer, assuming a feedwater temperature of 180 °C and a mixing ratio of eight.

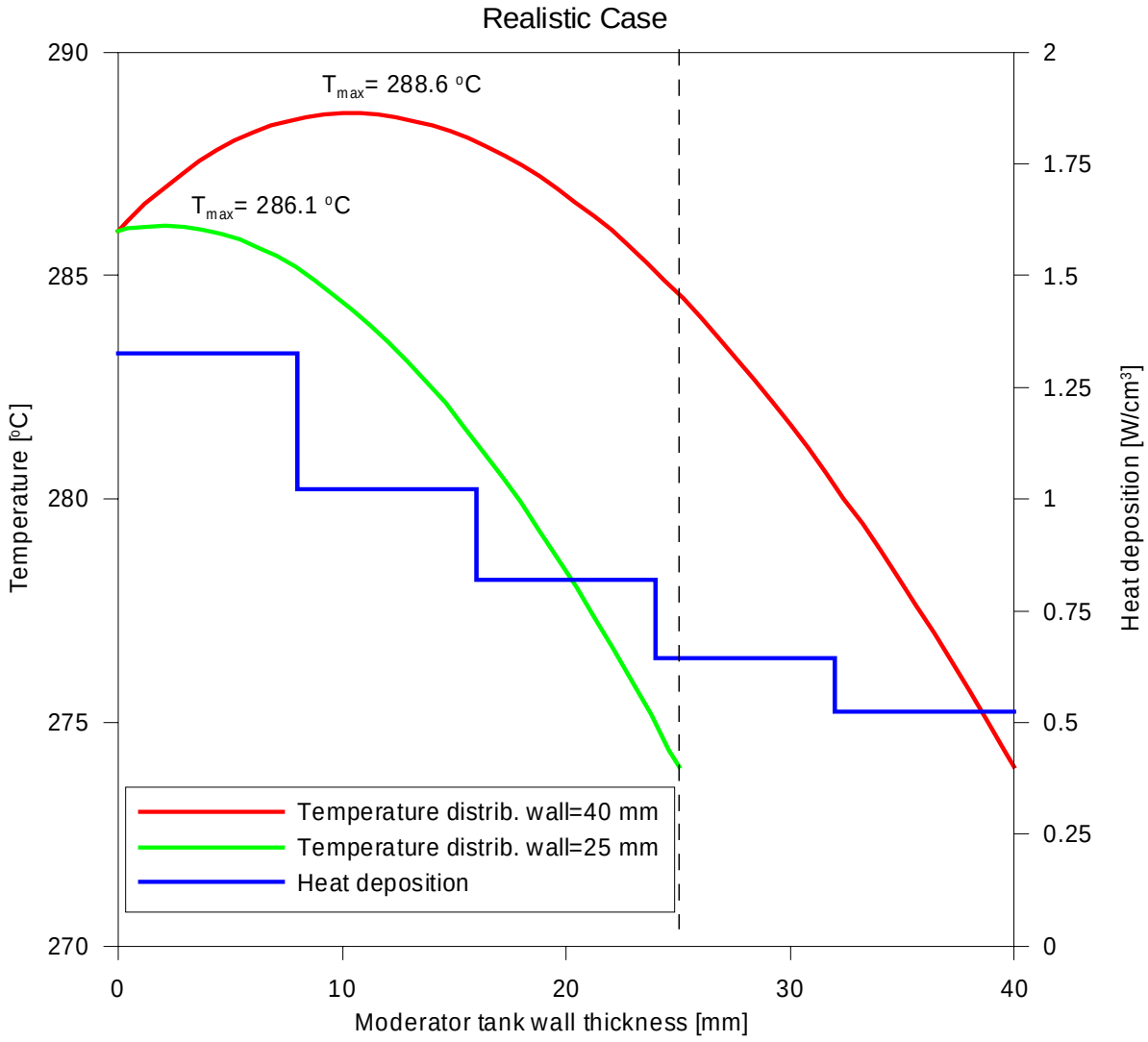

Figure 5. Temperature distribution in radial direction in the moderator tank at the core central plane level.

Assumptions: Inner surface = 286 °C, Outer surface=274 °C
Heat capacity = 0.51 J/gr/°C; Heat conductance = 0.25 J/cm/sec/°C.

The temperature distribution is also shown for the old 25 mm thick moderator tank.

Figure 6 shows the most conservative case, with no mixing, where the outer surface temperature is equal to the inner surface of 286 °C.

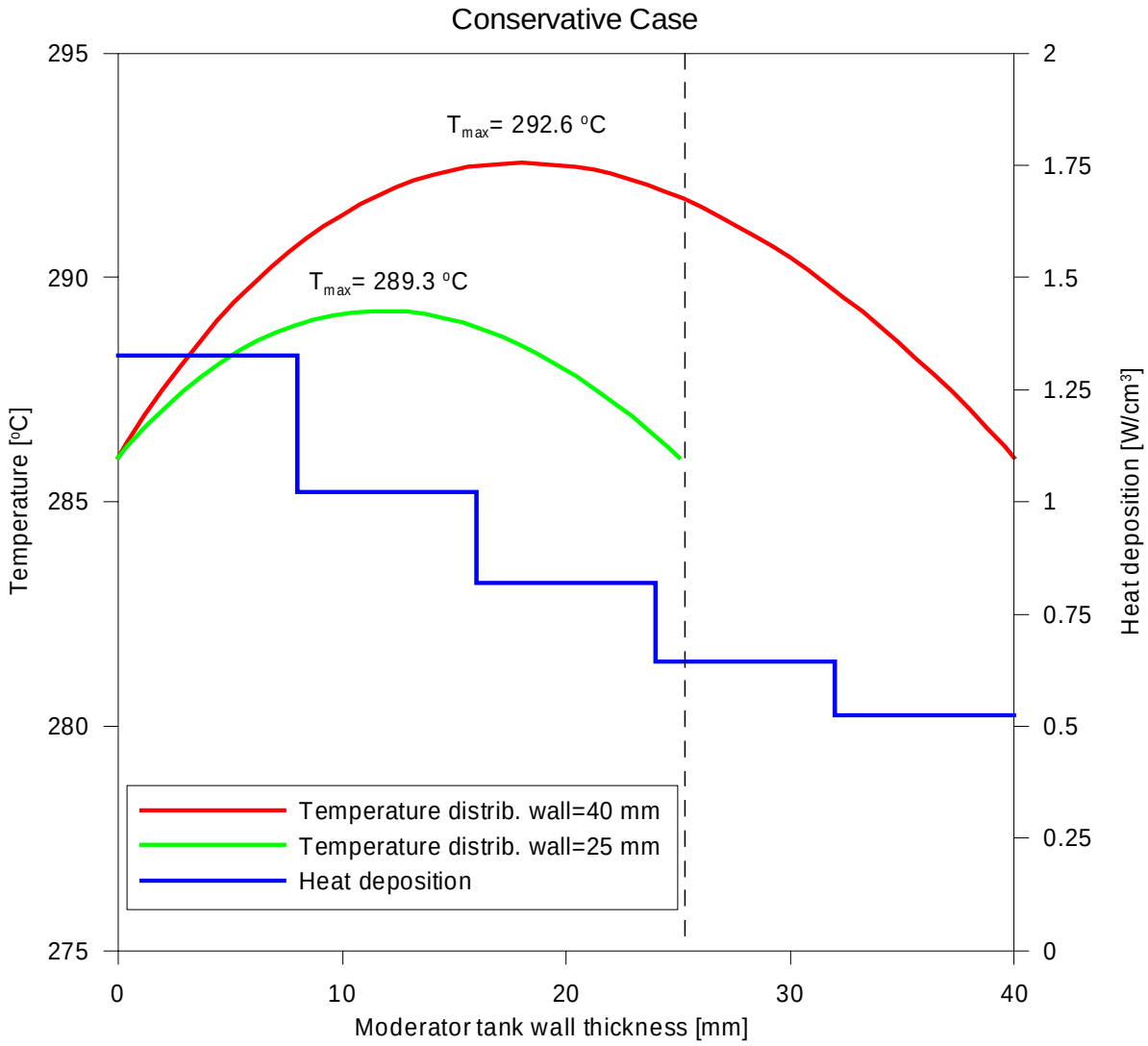

Figure 6. Temperature distribution in radial direction in the moderator tank at the core central plane level.

Assumptions: Inner surface = 286 °C, Outer surface = 286 °C
Heat capacity = 0.51 J/gr/°C; Heat conductance = 0.25 J/cm/sec/°C.

5 Conclusion

It has been shown by a combined Monte Carlo and heat transport calculation, the max temperature of the new moderator tank at Forsmark 1 (292.5 °C) is well below 300 °C even in the most conservative case. It is also clear, that the temperature of the old moderator tank was even more fare from 300 °C.

References

Ref. 1. *Calculation of Neutron Fluxes and Activations of Components of the Forsmark 1 BWR,* Højerup, C.F., Risø-I-1055, August 1996.

Ref. 2. *Monte Carlo Calculation of Neutron Doses to Components of the Forsmark 1 BWR,* Højerup, C.F., Nonbøl, E. Risø-I-1155, June 1997.

Ref. 3. *Monte Carlo Calculation of Neutron Doses to Components of the Forsmark 1 BWR (Extended version),* Højerup, C.F., Nonbøl, E. Risø-I-1286, June 1998.

Ref. 4. *MCNP – A General Monte Carlo N-Particle Transport Code, LA-13709-M, Ver. 4C., March 2000.*

Ref. 5. *Monte Carlo Calculation of Neutron Doses to and Activation of Components of the Forsmark 1 BWR with improved neutron source distribution.,* Højerup, C.F., Nonbøl, E. Risø-I-1815, Sep. 2001.

25 years of surveillance dosimetry for the Loviisa reactors – highlights and trends

Tom Serén
VTT Processes, P.O.B. 1608
FIN–02044 VTT

Abstract

The two VVER-440 units in Loviisa have been operating since 1977 (Lo 1) and 1980. Pressure vessel embrittlement is recognised as one of the major lifetime-limiting factors. Indeed, several measures have been taken to reduce the radiation-induced pressure vessel embrittlement. A large effort has been devoted to surveillance programmes involving irradiations, material testing and, as an important component, neutron dosimetry. The first fumbling steps in neutron dosimetry were taken in the late 70's. Since then the tools have been immensely refined and the accuracy decisively improved. In this process international co-operation has played an important role. The present situation is quite satisfactory with extremely good agreement between calculations and measurements. However, some special features of the VVER-440 reactors make it necessary to always include experimental dosimetry with the material irradiations. The recent increase in power output and the use of new types of fuel pose new challenges for the near future.

1. Introduction – principles and methods

Exposure to fast neutrons is an important cause of embrittlement of materials in various reactor structures. Pressure vessel embrittlement is, in fact, the main lifetime-limiting factor for PWR reactors. Thus there is a strong incentive to reduce the uncertainties in the fluence estimates for both surveillance specimens exposed to accelerated irradiation and the pressure vessel itself.

The methods for fluence measurements are somewhat limited in power reactors due to the hostile physical environment: pressure, temperature, vibrations etc. The number of possible measurement positions is also restricted and as a rule it possible to insert and extract dosimeters only during shutdown. Figure 1 shows a 60-degree sector of the reactor core and surroundings in the Loviisa VVER-440 reactors.

Due to these limitations activation methods are most commonly used, with metal foils or wires serving as detectors. Since the time span for the irradiations is usually at least one year it is desirable to use reactions with reasonably long-lived product nuclides. The response characteristics of some commonly used fast-neutron reactions are displayed in Table 1. Most fast-neutron reactions have a step-like cross section with a more or less sharp threshold. One serious shortcoming is the lack of response in the lower end of the fast-neutron region (near and below 1 MeV).

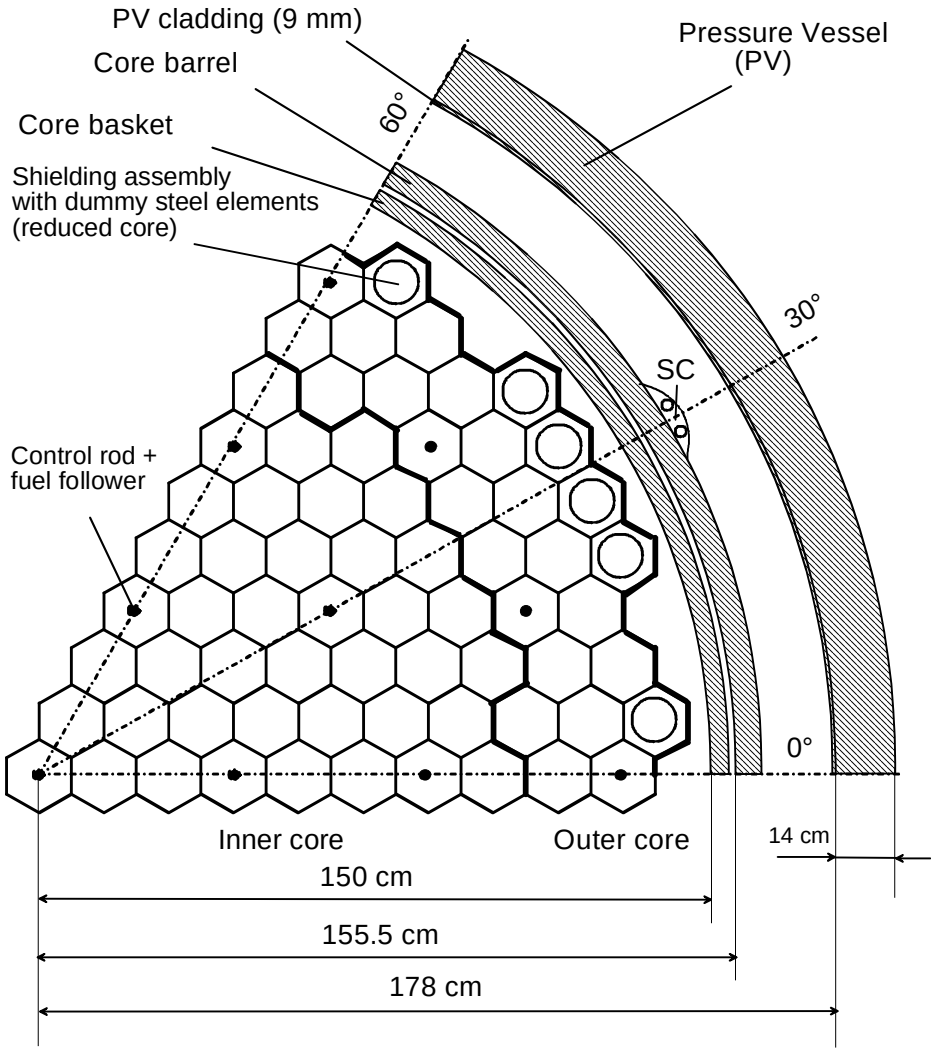

Figure 1. 60-degree sector of the Loviisa VVER-440 core and surrounding structures.

The neutron fluence is never determined by activation measurements alone. Since these carry only integral information over certain response regions, the results can be interpreted only if prior (calculated) information about the shape of the neutron spectrum is available. Comprehensive calculations are also needed to extrapolate dosimetry results to locations where no measurements are normally possible (e.g. inside the pressure vessel wall).

Before powerful computers and transport theory codes were available it was common practice to use simplified analytical models of the neutron spectrum in different energy regions and scale it to activation measurements (see e.g. Ref. [1]). In thermal reactors a much-used model was a fission spectrum in the fast-neutron energy region joined by a 1/E-shaped spectrum at intermediate energies and a Maxwell-type spectrum in the thermal energy region. Nowadays neutron dosimetry is always a synthesis of transport theory calculations and measurements.

Table 1. Basic characteristics of some common threshold detector elements and reactions.

Element	Reaction	Approx. resp. range (MeV)	Product half-life	Disturbing Impurities	Comments
Np	^{237}Np(n,f)F.P.	0.5–4.1	Several	^{239}Pu	
Nb	^{93}Nb(n,n')^{93m}Nb	0.6–5.6	16.1 y	^{181}Ta	No γ-rays
U	^{238}U(n,f)F.P.	1.3–6.7	Several	^{235}U	
Ni	^{58}Ni(n,p)^{58}Co	1.8–8.2	70.86 d		
Fe	^{54}Fe(n,p)^{54}Mn	2.1–8.3	312.3 d		
Ti	Ti(n,X)^{46}Sc$^{*)}$	3.9–11.0	83.79 d	^{45}Sc	
Cu	^{63}Cu(n,α)^{60}Co	5.0–12.1	1925.5 d	^{59}Co	

$^{*)}$ Composed mainly of the reactions ^{46}Ti(n,p) and ^{47}Ti(n,np).

A large number of standard test methods, guides and practices related to neutron dosimetry for surveillance purposes have been published by the American Society for Testing and Materials (ASTM) [2]. Although they do not always reflect the most up-to-date knowledge in the field, and should thus be applied with due criticism, these standards have attained semi-official status also outside the U.S.A.

Eleven international symposia on reactor dosimetry have been held, the first in Petten, the Netherlands, 1975 and the eleventh in Brussels 2002. The proceedings from these symposia provide comprehensive coverage of the national and international research efforts and practical applications in the field. The symposia are jointly organised by the European Working Group on Reactor Dosimetry (EWGRD) and ASTM, committee E-10. The symposia are listed in Table 2.

Table 2. List of international symposia on reactor dosimetry (previously ASTM-EURATOM symposia) and their proceedings.

Year	**Location**	**Publication**
1975	Petten, The Netherlands	EUR 5667
1977	Palo Alto, California	NUREG CP 0004
1979	Ispra, Italy	EUR 6813
1982	Washington D.C.	NUREG CP 0029
1984	Geesthacht, Germany	EUR 9869
1987	Jackson Hole, Wyoming	ASTM STP 1001
1990	Strasbourg, France	EUR 14356
1993	Vail, Colorado	ASTM STP 1228
1996	Prague, Czech Republic	World Scientific
1999	Osaka, Japan	ASTM STP 1398
2002	Brussels, Belgium	World Scientific

2. Surveillance irradiations in the Loviisa reactors

The VVER-440 reactors in Loviisa are equipped with six pairs of channels for irradiating steel capsules containing test specimens, dosimeters and temperature monitors (see Fig. 1). As can be seen from Fig. 2, they are suspended in the form of chains from above and attached to special locks. This design has the disadvantage of allowing some degree of rotation, which causes the orientation to be effectively random. In combination with a fairly large radial flux gradient this leads to differences in the fluence between specimens in the same container capsule, which cannot be calculated since the orientation is unknown.

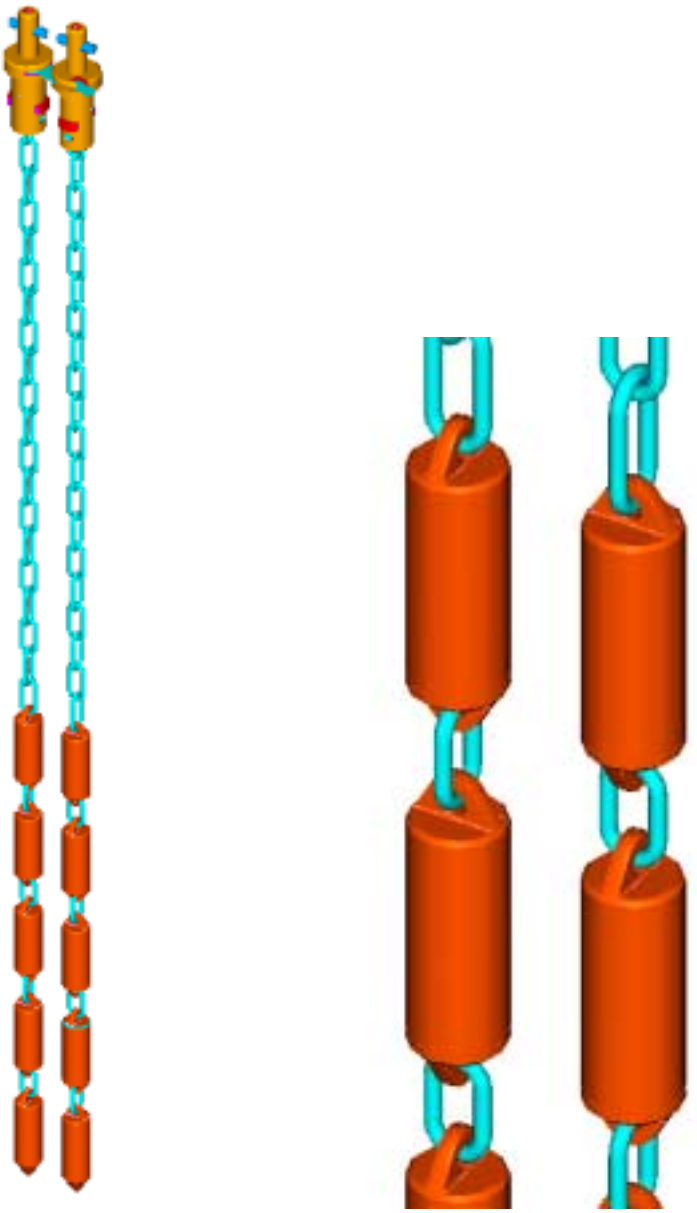

Figure 2. Arrangement of irradiation capsules in chains.

The first chains were rather long, containing 39 capsules per chain pair and extending beyond the core region. Thus the specimens in the highest capsules received fluences less than 1/10 of those in the mid-core region. The more recent chains are, as a rule, shorter, covering only the core region with fairly uniform axial flux distribution.

3. The first steps

Both units were equipped with surveillance chains by the reactor supplier right from the start and the first chain was extracted after one year in 1978. The dosimeter sets in the original chains were somewhat incomplete (Fe, Cu, Co, Nb, not all in the same capsules). The first chain manufactured by VTT was irradiated during the second cycle in Loviisa 1. Hot cell facilities for mechanical testing of irradiated steel specimens were completed at VTT at about the same time (now operated by VTT Industrial Systems).

The container capsules in the first chains typically contained two Charpy or COD specimens with dosimeter sets in a few capsules. The dosimeter capsules were situated in the side fillings of the containers at a position different from the steel specimens. Thus they were not useful for determining the fluences for the individual specimens. This problem was solved by using the specimens themselves as dosimeters, measuring the relative ^{54}Mn activities in various collimated geometries and fixing to absolute activity measurements of small corner samples taken from the specimens. Nowadays this problem is handled by irradiating Fe or Fe/Ni plates directly above and below the specimens (typically three Charpy-size specimens per capsule).

The first information available on the neutron spectrum shape was scarce and in inconvenient form (mainly as graphs). The situation improved in the 80's when the capability for performing transport calculations at VTT (at that time the Nuclear Engineering Laboratory) was built up (e.g. the REPVICS calculation system [3]).

The situation regarding dosimetry cross section data and, in some cases, even basic decay data was also unsatisfactory with large (and unspecified) uncertainties and inconsistencies between different libraries. The first "consensus" library for dosimetry purposes was published by the IAEA in 1982 (IRDF-82, mainly based on ENDF/B-V).

After the first surveillance specimens had been extracted and analysed it turned out that the embrittlement of the pressure vessel material had proceeded considerably faster than in the original evaluations. This prompted some quick and fairly drastic actions. Thus the peripheral fuel assembles were replaced by steel dummy assemblies (see Fig. 1), in Loviisa 1 in 1980 after three cycles and in Loviisa 2 in 1981 after one cycle.

Naturally, these findings also gave the impetus for a large investment in improving surveillance testing and also neutron dosimetry. A summary of VTT's activities in the field of neutron dosimetry up to 1987 is given in Ref. [4].

4. Some highlights

4.1. RPV samples

In order to verify the fluence evaluations for the pressure vessel samples have been milled from both the inner (cladding) and outer surfaces of the pressure vessel walls: 1980 in Loviisa 1 (cladding) and 1986 in both Loviisa 1 (outer surface) and Loviisa 2 (cladding and outer surface).

Iron is, of course, the obvious element in steel to use for dosimetric purposes. In addition, the cladding material contains several useful elements, such as Ni and especially Nb. The utilisation of Nb requires tedious chemical separation and purification procedures, but the favourable response region and long half-life otherwise make it an ideal fluence monitor.

Generally, the agreement between calculations and measurements was very good [4].

4.2. Ex-vessel dosimetry

The ex-vessel cavity in VVER-440 reactors provides ample space for various measurements. Activation measurements can be fairly easily carried out, and are indeed performed on a yearly basis e.g. at the Dukovany reactors in the Czech Republic [5]. Since the activation is modest the detectors can be quickly extracted and counted without need for a hot cell. The problem is that access is provided only through a man-hatch below the cavity.

The first cavity measurements in Loviisa were carried out in 1984-85 in unit 1. The dosimeters (various wires and capsules containing several dosimeters) were attached to a rack with folding ”wings”, which was in turn fastened to the walls using an ordinary car jack. At the end of the irradiation the rack was found at the bottom of the cavity, but the measurements revealed that it had probably fallen down after shut-down. However, the measurements of the axial flux profile also indicated that it had been situated about 20 cm below the planned position during the irradiation. Thus the results from this first attempt must be taken with a grain of salt.

Another attempt was made in 1998–1999 in unit 1 using a specially made reusable holder rack designed and made by Škoda JS, Czech Republic. The holder can be assembled during installation and rests on a support attached to the edges of the man-hatch. This irradiation, which was highly successful, was carried out as an international exercise together with Škoda and NRG Petten [6]. As can be seen from Fig. 3, the agreement between calculations and measurements was excellent.

The reaction $^{58}Fe(n,\gamma)^{59}Fe$ revealed that the azimuthal thermal flux distribution is almost flat. However, the calculations indicate some degree of azimuthal variation. Obviously most thermal neutrons in the cavity are backscattered from the concrete outside the cavity, which has apparently not been properly modelled.

This irradiation took place after a power increase from 1375 MWth to 1500 MWth and simultaneously with a surveillance chain situated at the same azimuthal angle.

Right now a similar one-year irradiation is taking place in Loviisa 2. This will reveal individual differences between the two units, if any.

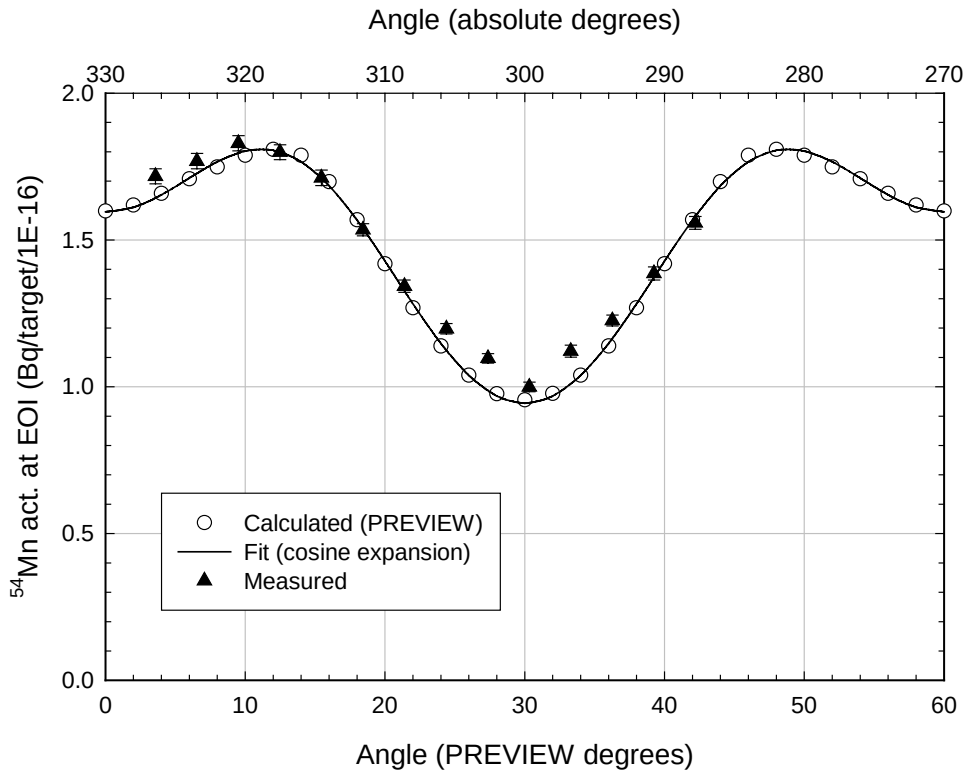

Figure 3. Measured and calculated ^{54}Mn azimuthal activity distribution in the Loviisa 1 ex-vessel cavity.

4.3. Niobium dosimetry

Starting in the mid-80's a major effort, especially by Dr Bruno Bärs, was devoted to the utilisation of the reaction ^{93}Nb(n,n')^{93m}Nb [7]. The chemical separation and purification methods were refined and the Liquid Scintillation Counting (LSC) technique was developed and adapted to ^{93m}Nb measurements, including calibrations with standard liquids. Mass determination techniques using ICP-MS were also developed. The high efficiency of LSC (close to 1) makes it possible to measure very weak activities typically found in small Nb concentrations in pressure vessel materials (down to a few ppm, about 1 % in the VVER-440 cladding material).

The interest in Nb dosimetry has recently been revived within the context of "retrospective dosimetry", i.e. dosimetry using structural reactor materials not originally intended for dosimetric purposes, either from operating ("biopsy") or shut-down ("autopsy") units. To this end VTT

Processes participates together with NRG Petten and SCK●CEN (Belgium) in the RETROSPEC project (EC 5th Framework Programme), which will be finalised during spring 2003.

4.4. The kernel-based PREVIEW program

The original purpose of the PREVIEW code, developed by F. Wasastjerna at VTT Energy for the IVO (Fortum) utility, was to create a fast and easy-to-use tool for determination of neutron fluences at a limited number of important out-of-core locations in VVER-440 reactors, with the capability of taking into account the detailed local flux history, i.e. the changes in the flux distribution (mainly axial) and neutron spectrum over an operating cycle. PREVIEW uses a pre-calculated kernel library based on a large number of transport theory calculations for unit neutron sources distributed over the core.

However, it has also proved to be a very convenient tool in experimental neutron dosimetry. Indeed, its most extensive use has been the comprehensive revision and unification of all dosimetry results for the Loviisa VVER-440 reactors [8]. The detailed description of the local flux history is important for the correct interpretation of activation measurements, especially for relatively short-lived reaction products.

The method employed in PREVIEW and its operating principles have been described in detail by F. Wasastjerna [9]. PREVIEW considers a 60-degree VVER-440 symmetry sector (see Fig. 1) with either full or reduced core loading configuration. It calculates the neutron flux or fluence and various reaction rates, reaction probabilities and activities at a limited number of chosen out-of-core locations (called detector points). This is accomplished by multiplying the nodewise source distribution in the reactor core (calculated using HEXBU-3D [10]) by pre-calculated kernels. The kernels were calculated with the ANISN and DOT 3.5E codes using the 47-group BUGLE-80 library (based on ENDF/B-IV). Each fuel bundle in the core sector is divided into 10 nodes of 25 cm length (22 cm for the outermost nodes). The pre-calculated kernels represent the contribution of a unit source of fission neutrons (^{235}U and ^{239}Pu) at the detector locations. The possible radial locations are: 162.5 cm (surveillance chain), 177.3 cm (RPV cladding), 181.5 cm (RPV ¼ thickness) and 207.5 cm (middle of cavity outside RPV).

One section of the kernel library contains damage and dosimetry cross sections, which makes it possible to directly calculate damage parameters (such as dpa or fluence >1 MeV) and activities, reaction rates and reaction probabilities. These cross sections are mainly based on the IRDF-90 library [11] with a few additions from RRDF-98 [12], condensed to the BUGLE group structure using typical weighting spectra.

One inconvenience in the present version is that the whole large kernel library has to be edited if changes are made to the damage and dosimetry cross sections. Thus a new version of PREVIEW is under development, where the cross sections are read in from a separate file. This would make it easier to use position-specific and/or modified (e.g. for Cd or Gd cover) cross section sets. Also, the cross sections will be updated to conform with the new IRDF-2002 library [13] to be released

this year. The new version will also accommodate a larger number of possible degrees of fuel enrichment being used after the recent power increase.

4.5. Adjustment library for PREVIEW

The vast amount of experimental data accumulated over the years has been utilised in the development of an adjustment library for PREVIEW [14], [15]. Several spectrum adjustments using the generalised least-squares code LSL-M2 [16] have been performed. A special advantage of this code is the capability to adjust the spectrum simultaneously at several locations linked by correlation coefficients.

The results of the adjustments have been collected into an adjustment library containing both axial scaling coefficients and groupwise spectral adjustment coefficients.

The analysis of several recent surveillance chains has revealed that using PREVIEW together with the adjustment library produces excellent agreement between calculations and measurement. However, the already mentioned random orientation of the surveillance capsules still makes it necessary to always perform dosimetric measurements if accurate individual fluences are needed for the specimens.

The adjustment coefficients for the ex-vessel cavity will be revised based on the new more accurate measurements (see Section 4.2.) and the IRDF-2002 cross section library.

5. Some current trends

The much improved accuracy attainable in transport calculations (both Monte Carlo and deterministic) makes it necessary to constantly refine and improve the data and methods used in experimental reactor dosimetry if they are to be of real use. The new IRDF-2002 library is an attempt to address these needs. It will contain the best available dosimetry cross sections accompanied by carefully evaluated uncertainty information. It will also contain recommended basic physical data such as half-lives, emission probabilities, atomic masses etc.

”Retrospective dosimetry” is another important issue in the dosimetry community. It will become especially important as the nuclear power plants approach the end of their lifetime. There will be a vast amount of material from shut-down reactors available for analysis. A proper utilisation of this data will provide a sound basis for possible future lifetime extension decisions.

The pressure vessel of Loviisa 1 was annealed by heat treatment in 1996. After that a new surveillance programme was initialised with several different irradiation-annealing sequences in order to investigate the post-annealing re-irradiation behaviour of pressure vessel steels. This has imposed special requirements on the neutron dosimetry. The orientation of the capsules during re-irradiation is most likely different from the pre-annealing orientation (as has indeed been the case).

Thus the usual ^{54}Fe(n,p) reaction cannot be used since there will be considerable residual activity left from the pre-annealing irradiation (half-life 312.3 d). As a solution to this problem plates of a special Fe70/Ni30 alloy (Goodfellow, UK) are now used by VTT instead of Fe plates as dosimeters. The ^{54}Mn activity will then carry information from both before and after the annealing, while ^{58}Co (70.8 d) ”remembers” only the post-annealing period.

References

1. Neutron Fluence Measurements. IAEA Technical Reports Series No 107, Vienna 1970.

2. Annual Book of ASTM Standards, Section 12, Volume 12.02, Nuclear (II), Solar, and Geothermal Energy (Revision issued annually), American Society for Testing and Materials, West Conshohocken, PA 19428, U.S.A.

3. I. Lux and F. Wasastjerna, ”Development of Pressure Vessel Irradiation Calculation Methods in Finland”, 6th International Conference on Reactor Shielding, Tokyo 1983.

4. B. Bärs, T. Serén & F. Wasastjerna, Experimental and Theoretical Neutron Flux Estimations at the Surveillance Chain, at the Pressure Vessel Inner Surface, and in the Cavity of a VVER-440 PWR. Proceedings of the 6th ASTM-EURATOM Symposium on Reactor Dosimetry, Jackson Hole, Wyoming, May 31 – June 5, 1987. ASTM STP 1001, Philadelphia 1989.

5. J. Hógel and M. Hort, “Ex-Vessel Fast Neutron Fluence Monitoring at NPP Dukovany”, in Reactor Dosimetry, ed. H. Aït Abderrahim et al. (World Scientific Publishing Co., Singapore, 1998), pp. 834–840.

6. T. Serén, J. Hógel and W. P. Voorbraak, ”Post-Annealing Ex-Vessel Dosimetry at Loviisa 1 – an International Exercise”, 11th International Symposium on Reactor Dosimetry, Brussels, Belgium, Aug. 18–23, 2002 (to be published by World Scientific).

7. B. Bärs and E. Häsänen, ”Neutron Flux Estimations Based on Niobium Impurities in Reactor Pressure Vessel Steel”, Proceedings of the 8th ASTM-EURATOM Symposium on Reactor Dosimetry, Vail, Colorado, Aug. 29 – Sept. 3, 1993. ASTM STP 1228, Philadelphia 1994.

8. B. Bärs and T. Serén, ”Revision of Neutron Dosimetry for the Loviisa VVER-440 Reactors: Principles and Application”, Proceedings of the 8th ASTM-EURATOM Symposium on Reactor Dosimetry, Vail, Colorado, Aug. 29 – Sept. 3, 1993. ASTM STP 1228, Philadelphia 1994.

9. F. Wasastjerna, PREVIEW, a Program for Calculation of Pressure Vessel Irradiation in the Loviisa Reactors. VTT Research Report YDI110/91, Espoo 1991.

10. E. Kaloinen *et al.*, HEXBU-3D, A Three-Dimensional PWR Simulator Program for Hexagonal Fuel Assemblies. VTT Nuclear Engineering Laboratory, Report 7/1981.

11. N. P. Kocherov and P. K. McLaughlin, The International Reactor Dosimetry File (IRDF-90). IAEA-NDS-141, Rev. 2, Oct. 1993.

12. K. I. Zolotarev *et al.*, RRDF-98, Russian Reactor Dosimetry File, IAEA-NDS-193, Rev. 0, March 1999.

13. R. Paviotti-Corcuera *et al.*, "International Reactor Dosimetry File: IRDF-2002", 11th International Symposium on Reactor Dosimetry, Brussels, Belgium, Aug. 18–23, 2002 (to be published by World Scientific).

14. T. Serén, Development of an Adjustment Library for the Kernel-Based PREVIEW Program. Proceedings of the 9th International Symposium on Reactor Dosimetry, Prague September 2–6, 1996. World Scientific, Singapore 1998.

15. T. Serén, An Optimised Adjustment Library for the Kernel-Based PREVIEW Program, Licentiate's Thesis, Helsinki University of Technology, Department of Engineering Physics and Mathematics, November 2001.

16. F. W. Stallmann, LSL-M2: A Computer Program for Least-Squares Logarithmic Adjustment of Neutron Spectra, NUREG/CR-4349, ORNL/TM-9933, Oak Ridge 1986. (Additional unpublished manual provided with version 2.0, September 1994).

Program

XI MEETING ON "REACTOR PHYSICS CALCULATIONS IN THE NORDIC COUNTRIES"

Espoo/Helsinki/Tallinn/Gulf of Finland, April 9–10, 2003

Wednesday, April 9 *(Chairman: Randolph Höglund)*

Session1: 10:30–12:00

1
Introduction
Randolph Höglund, VTT Processes

2
VTT Nuclear
Lasse Mattila, VTT Processes

3
The Finland-5 project
Tapio Saarenpää, Teollisuuden Voima Oy

4
On the average chord length
Nils G. Sjöstrand, Chalmers University of Technology

Lunch: 12:00–13:30

Session 2: 13:30–15:00

5
Reactor physics calculations and core analysis at the Nuclear Power Safety Division, KTH
Audrius Jasiulevicius, KTH

6
Comprehensive rehomogenisation
Sten-Örjan Lindahl, Studsvik Scandpower

7
CASMO-4E and fuel storage rack calculations
Joel Rhodes, Nicholas Gheorghiu, Kord Smith & Malte Edenius, Studsvik Scandpower (presented by Malte Edenius)

8
Development of the new deterministic 3-D radiation transport code MultiTrans
Petri Kotiluoto, VTT Processes

Coffee break: 15:00–15:30

Session 3: 15:30–17:00

9
ARES – a new BWR simulator
Riku Mattila, VTT Processes

10
POLCA-T – 3D safety and core analysis tool
Lars Paulsson, Westinghouse

11
Something cuckoo in the Oskarshamn-1 core model
Christer Netterbrant, OKG AB

Bus transport to the harbour: 17:30

M/s Romantika leaves for Tallinn: 18:45

Session 4: 19:15–20:15
Welcome aboard drink

12
Loading pattern search by branching and bounding batch patterns enumerated under constraints
Brian Beebe, Westinghouse

13
Supporting the SVEA-96 Optima designs with reliable methods
Juan Casal & Maria Petersson, Westinghouse (presented by Maria Petersson)

Dinner: 20:45

Midnight show

Thursday, April 10 *(Chairman: Nils G. Sjöstrand)*

Breakfast

Sightseeing in Tallinn: 09:00–11:00

Session 5: 11:30–13:00

14
BWR fuel development at Framatome
Dieter Bender & Peter Urban, Framatome ANP (presented by Dieter Bender)

15
Direct heating in a BWR assembly – investigations with the HELIOS lattice code
Waldemar Lipiec, Westinghouse

16
Gamma scanning evaluation with PHOENIX4/POLCA7 on fuel rods in Barsebäck 1
Per-Olov Andersson, Westinghouse

17
Simulation of reactor scram experiments in the Loviisa and Mochovce VVER reactors
Pertti Siltanen, Fortum Nuclear Services, Elja Kaloinen & Frej Wasastjerna, VTT Processes (presented by Pertti Siltanen)

Coffee break: 13:00–13:30

Session 6: 13:30–15:00

18
Validation of PHOENIX4 against critical measurements at the PROTEUS facility
Petri Forslund & Morgan Johansson, Westinghouse (presented by Sture Helmersson)

19
Transmutation of nuclear waste in accelerator driven reactors
Janne Wallenius, KTH

20
Calculation of energy deposition in the moderator tank of the Forsmark 1 BWR
C. F. Højerup & Erik Nonbøl, Risø National Laboratory (presented by Erik Nonbøl)

21
25 years of surveillance dosimetry for the Loviisa reactors – highlights and trends
Tom Serén, VTT Processes

Late lunch: 15:30

End of cruise and meeting: 17:00

Appendix B

Participants

XI MEETING ON "REACTOR PHYSICS CALCULATIONS IN THE NORDIC COUNTRIES"

Espoo/Helsinki/Tallinn/Gulf of Finland, April 9–10, 2003

Chalmers University of Technology

Nils G. Sjöstrand

Fortum Nuclear Services Ltd

Pertti Siltanen

Framatome ANP

Dieter Bender
Robert Koch
Dieter Kreuter
Lucie Plathner
Peter Urban
Roger Velten

OKG AB

Christer Netterbrant
Göran Wiksell

Radiation and Nuclear Safety Authority of Finland (STUK)

Nina Lahtinen

Ringhals AB (Ringhals & Barsebäck)

Catarina Harde
Urban Sandberg
Fredrik Winge

Risø National Laboratory

Erik Nonbøl

Stockholm Royal Institute of Technology (KTH)

Audrius Jasiulevicius
Janne Wallenius

Studsvik Scandpower

Malte Edenius
Christian Jönsson
Sten-Örjan Lindahl
Lars Moberg

Teollisuuden Voima Oy

Kim Dahlbacka
Saku Latokartano
Tapio Saarenpää

Vattenfall Bränsle AB

Marek Kosinski
Andreas Lidén
Erik Nordström

VTT Processes (Technical Research Centre of Finland)

Markku Anttila
Antti Daavittila
Randolph Höglund
Elja Kaloinen
Petri Kotiluoto
Jaakko Leppänen
Lasse Mattila
Riku Mattila
Anssu Ranta-Aho
Hanna Räty
Tom Serén
Timo Vanttola

Westinghouse

Per-Olov Andersson
Brian Beebe
Ulf Bredolt
Sture Helmersson
Waldemar Lipiec
Lars Paulsson
Maria Petersson

Published by

Series title, number and report code of publication

VTT Symposium 230
VTT–SYMP–230

Author(s)
Randolph Höglund (ed.)

Title

Reactor physics calculations in the Nordic countries

Proceedings of the 11th Nordic Reactor Physics Meeting

Abstract

The eleventh biennial meeting on reactor physics calculations in the Nordic countries was arranged by VTT Processes in Otaniemi, Espoo and on board Tallink's m/s Romantika on April 9–10, 2003. The previous meetings in this series were held in Göteborg 1983, Roskilde 1985, Espoo 1987, Oslo 1989, Stockholm 1991, Roskilde 1993, Espoo 1995, Kjeller 1997, Göteborg 1999 and Roskilde 2001. 18 technical papers on very different subjects in the field of reactor physics were presented by the 46 participants of 8 nationalities representing 13 organizations in 6 countries: research establishments, technical universities, utilities, consultants and suppliers. Thus, some participants from outside the Nordic countries were also present this time. Additionally, VTT's activities in the nuclear field and the "Finland-5" project were described.

General reactor physics, calculational methods, a code system adapted for RBMK reactor analyses, and transmutation of nuclear waste were presented by representatives of universities and programme developers (Royal Institute of Technology, Chalmers University of Technology, Studsvik Scandpower).

Computer programmes are the most important tools of reactor physics and new versions of old ones as well as entirely new ones based upon better and more accurate, alternatively faster and more efficient, methods and models are still evolving. At the meeting there were presentations of VTT Processes' new deterministic 3-dimensional radiation transport code MultiTrans and BWR simulator ARES based upon the AFEN (Analytic Function Expansion Nodal) model, and also of new features in internationally wellknown codes like CASMO-4E and POLCA (POLCA-T) together with results obtained by these programmes. A code for PWR loading pattern search, called LP-fun (Loading Patterns – for user´s need) is being developed by Westinghouse and others.

Experiments and measurements are necessary for the validation of the computer codes. Measurements on SVEA-96+ fuel bundles in the PROTEUS facility had been analyzed with the PHOENIX4 code, reactor scram experiments in the Loviisa and Mochovce VVER reactors using CASMO-4, MCNP4B and HEXTRAN, results of gamma scanning on fuel bundles by the PHOENIX4/POLCA7 combination. Some difficulties in predicting the power distribution in the reactor core with sufficiently good accuracy using any of the available code systems were reported by OKG.

The importance of direct heating, i.e. transfer of fission energy to non-fuel regions by gamma radiation and neutrons had been investigated using the HELIOS lattice code. Calculational results for heat deposition from gamma radiation in the moderator tank of the Forsmark-1 reactor were reported by Risø. Measurements and calculations of the pressure vessel exposure to neutrons have been performed by VTT during the whole life of the Loviisa reactors.

New and more efficient nuclear fuels are continuously being developed. Successful introduction of a new fuel type requires extensive numerical analyses as well as experimental measurements and feedback from users' experiences. Framatome ANP and Westinghouse described the development and characteristics of the SVEA-96 Optima and ATRIUM 10 fuels.

The twelfth meeting in the series is preliminary scheduled to be arranged by Institutt for energiteknikk and Studsvik Scandpower AS in Norway in 2005.

Keywords
nuclear waste transmutation, nuclear power safety, reactor analyses, nuclear fuels, calculational methods

Activity unit
VTT Processes, Tekniikantie 4 C, P.O.Box 1604, FIN–02044 VTT, Finland

ISBN			Project number
951–38–6286–0 (URL: http://www.vtt.fi/inf/pdf/)			
Date	Language	Pages	Price
June 2003	English	175 p. + app. 5 p.	D
Name of project		Commissioned by	
Series title and ISSN VTT Symposium 1455–0873 (URL: http://www.vtt.fi/inf/pdf/)		Sold by	

The eleventh biennial meeting on reactor physics calculations in the Nordic countries was arranged by VTT Processes in Otaniemi, Espoo and on board Tallink´s m/s Romantika on April 9–10, 2003.

General reactor physics, calculational methods, a code system adapted for RBMK reactor analyses, and transmutation of nuclear waste were presented by representatives of universities and programme developers.

Computer programmes are the most important tools of reactor physics. At the meeting there were presentations of VTT Processes' new deterministic 3-dimensional radiation transport code MultiTrans and BWR simulator ARES based upon the AFEN model, and also of new features in internationally wellknown codes like CASMO-4E and POLCA (POLCA-T) together with results obtained by these programmes. A code for PWR loading pattern search, called LP-fun, is being developed by Westinghouse and others.

On the subject of code validation, measurements on SVEA-96+ fuel bundles in the PROTEUS facility had been analyzed with the PHOENIX4 code, reactor scram experiments in the Loviisa and Mochovce VVER reactors using CASMO-4, MCNP4B and HEXTRAN, results of gamma scanning by the PHOENIX4/POLCA7 combination. Some difficulties in predicting the power distribution in the reactor core with sufficiently good accuracy using any of the available code systems were reported by OKG. Heating of non-fuel regions by gamma radiation and neutrons had been investigated using the HELIOS lattice code. Calculational results for heat deposition from gamma radiation in the moderator tank of the Forsmark-1 reactor were reported by Risø. Measurements and calculations of the pressure vessel exposure to neutrons have been performed by VTT during the whole life of the Loviisa reactors.

Successful introduction of a new fuel type requires extensive numerical analyses as well as experimental measurements and feedback from users' experiences. Framatome ANP and Westinghouse described the development and characteristics of the SVEA-96 Optima and ATRIUM 10 fuels.

Tätä julkaisua myy
VTT TIETOPALVELU
PL 2000
02044 VTT
Puh. (09) 456 4404
Faksi (09) 456 4374

Denna publikation säljs av
VTT INFORMATIONSTJÄNST
PB 2000
02044 VTT
Tel. (09) 456 4404
Fax (09) 456 4374

This publication is available from
VTT INFORMATION SERVICE
P.O.Box 2000
FIN–02044 VTT, Finland
Phone internat. + 358 9 456 4404
Fax + 358 9 456 4374

ISBN 951–38–6286–0 (URL: http://www.vtt.fi/inf/pdf/)
ISSN 1455–0873 (URL: http://www.vtt.fi/inf/pdf/)